INVESTIGATION OF THE DRAG REDUCTION BEHAVIOR OF POLYACRYLAMIDE/POLYSACCHARIDE BINARY POLYMER SOLUTIONS

By

MEHDI HABIBPOUR

Bachelor of Science in Chemical Engineering
University of Science & Technology
Tehran, Iran
2006

Master of Science in Chemical Engineering
University of Science & Technology
Tehran, Iran
2009

Submitted to the Faculty of the
Graduate College of the
Oklahoma State University
in partial fulfillment of
the requirements for
the Degree of
DOCTOR OF PHILOSOPHY
May 2017

INVESTIGATION OF THE DRAG REDUCTION BEHAVIOR OF

POLYACRYLAMIDE/POLYSACCHARIDE BINARY POLYMER SOLUTIONS

Dissertation Approved:

Dr. Peter E. Clark

Dissertation Adviser

Dr. Geir Hareland

Dr. Clint Aichele

Dr. Jack Pashin

I would like to express my deepest appreciation to my adviser **Dr. Peter Clark**, who has continually and convincingly conveyed a spirit of adventure in regard to research and scholarship.

I would also like to thank my lovely wife **Maryam**, who has been with me and supported me in this journey.

Name: MEHDI HABIBPOUR

Date of Degree: MAY, 2017

Title of Study: INVESTIGATION OF THE DRAG REDUCTION BEHAVIOR OF POLYACRYLAMIDE/POLYSACCHARIDE BINARY POLYMER SOLUTIONS

Major Field: CHEMICAL ENGINEERING

Abstract:

In this study, rheological behavior and drag reduction (DR) efficiency of various polymer solutions were investigated. The studied polymer solutions included anionic polyacrylamide (HPAM), xanthan gum (XG), guar gum (GG) and binary polyacrylamide/polysaccharide mixtures. Polyacrylamide is a long-chain flexible molecule, which acts as an efficient drag reducer in the solution. Mechanical degradation at turbulent flow is a drawback associated with polyacrylamide, which results in DR decline. Guar gum and xanthan gum are known to exhibit DR properties and high resistance to shear degradation. In this research, the DR behavior of polymer solutions were investigated in closed flow loop and rheological characterization was utilized to assess the flow properties of the solutions. Initially, the DR behaviors of single polymer solutions were determined. It was found that concentration directly effected viscosity and DR efficiency of the polymer solutions. Among the studied HPAM solutions, the greatest efficiency belonged to 1000 wppm solution (68%). All HPAM solutions suffered from mechanical degradation and loss DR efficiency. On the other hand, both XG and GG solutions exhibited good resistance to shear degradation (< 5% decline). DR efficiency of the solutions were in the following order: HPAM > XG > GG. In order to benefit from the advantages of both polymer types, binary polyacrylamide/polysaccharide solutions were prepared and tested. No synergism was observed in HPAM/GG solutions even at high concentration (C = 1150 wppm). Dilute HPAM/XG solutions (C < 300 wppm) initially exhibited greater DR efficiency (40% and 55%) than XG solutions, but due to shear degradation, DR% declined. Increasing the concentration of XG in binary HPAM/XG solutions (C > 300 wppm), improved both DR efficiency and shear stability (6-8% decline after shearing for 2 hours) of the solutions. Another issue associated with HPAM is the sensitivity to the presence of salt ions in the solution. Addition of 2% KCl in the solution reduced the DR% of 1000 wppm solution from 68% to10%. The effect of salt on concentrated HPAM/XG solutions was verified. It was found that presence of XG in binary solutions reduced the negative effect of salt ions on HPAM molecules.

TABLE OF CONTENTS

Chapter Page

LIST OF TABLES

Table Page

LIST OF FIGURES

Figure Page

CHAPTER I

INTRODUCTION

1.1 Review of literature

1.1.1 Hydraulic fracturing fluids

Oil and gas production from unconventional resources has played an important role in supplying the energy of the United State in recent years [1-3]. Hydraulic fracturing has released the potential of hydrocarbon production from unconventional reservoirs, such as coal-bed methane, tight gas, and shale gas formations [4]. Shale formations are complicated resources with natural fractures. It is believed that the existing natural fractures are blocked by the settlement of minerals over time, which is the reason for ultra-low permeability of such reservoirs [1]. In hydraulic fracturing treatment of shale formations a network of highly conductive flow paths connecting the reservoir to wellbore is created and naturally existing fractures in the rock are connected during the operation [5]. The generated fractures enhance the conductivity of the reservoir by increasing hydrocarbon production surface area [6]. Achieving an economic rate of hydrocarbon production is only possible when micro-fractures are connected and created through effective stimulation treatments such as horizontal well fracturing in multiple stages [7, 8]. High production rate and low cost make multistage fracturing of horizontal wells a suitable method for stimulating reservoirs with low permeability. Using one well to contact and produce large portions of the reservoir is a significant benefit that horizontal drilling offers [9]. Another of

the advantages of horizontal drilling over traditional vertical drilling is the drastically different contact between the un-stimulated wellbore and the formation [10].

Creation of openings in the reservoir rock involves pumping fracturing fluids into the wellbore at high flow rate and pressure. The fracturing fluid is usually a complex viscous material that carries tiny granular solid particle, called proppant, into the generated fractures to prevent them from closing and provide resistance against the stresses from earth's above layers [6]. Viscosity of a fracturing fluid has a remarkable effect on the fracture initiation and the final size of the fracture [11]. Based on their viscosities, fracturing fluids can be categorized into two groups. Less viscous fluid or "slickwater", which was the main fluid of 50's and 60's. The main component of low viscosity fracturing fluid is water and very low concentrations of polymer. The second type is highly viscous gel-based fluid, which is typically 50 - 1000 times more viscous than water [12]. Guar gum, in its linear and cross-linked forms, is the oldest water-soluble fracturing fluid. Guar-based fluids form a filter cake on the faces of the fractures, which is advantageous in preventing the fluid leak-off to the adjacent formation. But, in the last decade, an amazing shift towards using slickwater has occurred. As an example, outside of the Bakken shale, in more than 80 % of fracturing treatments, water and friction reducer is applied as fracturing fluid [5].

Because of the relatively low viscosity of slickwater, clean-up problems and damage associated with using viscous fluids are minimized, which makes slickwater suitable for fracturing low permeability reservoirs [4, 7]. As a result of low viscosity, slickwater cannot suspend and transport proppant as effectively as gelled fluids [13]. To overcome poor proppant transport, high pumping rate is applied. High flow rate, in turn, leads to significant energy loss due to friction and turbulence in the tubular pipeline [4, 14]. In slickwater treatment, friction reducer is an important component of the fluid. Polymeric additives are known to achieve friction reduction efficiencies up to 80%, even at very low concentrations [15]. Among various friction

reducers, long chain, flexible polyacrylamide is considered as the most efficient drag reduction polymer [7].

1.1.2 Drag reduction induced by polymers

Since its discovery, polymer induced drag reduction phenomenon has found numerous applications [15-17]. Some of the important applications of drag reduction include: oil transfer pipelines (trans-Alaska pipeline), oil well operations, fire fighting, field irrigation, and transport of slurries and suspensions [18]. Lowering pressure drop in pipe flow is a major outcome of polymer addition (even at low concentrations) compared to a pure liquid at the same flow conditions. The length of the polymer chain, radius of gyration, hydrodynamic volume, concentration, and molecular weight are the main properties that influence the drag reduction induced by a polymer, with the latter being the most important actor [19].

The type of the drag reducing agent is important in determining the extent of drag reduction, as well. Polymer drag reducers are categorized into flexible and rod-like molecules, regarding their molecular structure and mechanical strength. Flexible polymers are high molar mass linear molecules like polyacrylamide and polyethylene oxide. These polymer chains undergo mechanical degradation at high shear rates such as high pumping rates experienced in slick water hydraulic fracturing, which is a significant drawback for practical applications [15]. The second group of drag reducers includes rod-like polymers, which are more resistant to shear degradation. Naturally occurring polymers such as xanthan gum and guar gum are examples of rod-like polymers, which have been used in variety of applications [15].

Xanthan gum is a high molar mass charged polymer, or polyelectrolyte, which has found many industrial applications due to its thickening and friction reduction characteristics [20-23]. The molecular structure of xanthan is comprised of a β-1-4-linked glucan backbone with negatively charged tri-saccharide side chains (Fig. 1) [24]. Based on the ionic strength of the

solution xanthan molecule takes two conformations: the first state is disordered and highly stretched (due to the repulsive forces) exerted by charges on the side chains), which occurs at salt free solution and the second state occurs in the presence of salt and the conformation is helical. In the latter conformation polymer chains are more rigid than the disordered conformation [25-27].

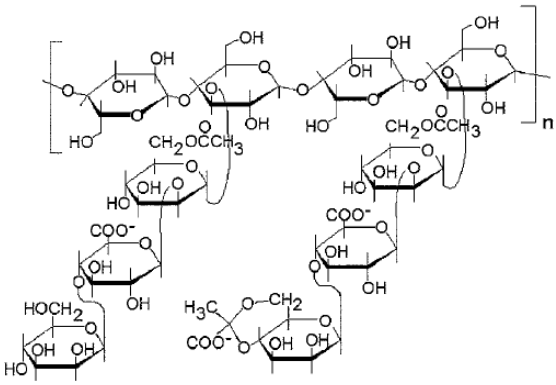

Fig. 1. Molecular structure of xanthan gum [24]

Guar gum is another water-soluble polysaccharide and in produced from guar seeds. The structure of guar gum consists of linear chains of 1,4-linked β-D-mannopyranosyl units with α-D-galactopyrannosyl units attached by 1,6-links in a ratio of 2:1 (Fig. 2). Similar to xanthan, guar solution shows good drag reduction properties [24, 28-32]. Kim et al. [33] suggested that drag reduction induced by guar gum is not as effective as polyethylene oxide, but solutions containing guar gum exhibit much superior shear stability than polyethylene oxide solutions. Similar results have been obtained by other researchers who also suggest that guar gum induces lower drag reduction than either xanthan gum or polyacrylamide, but promises greater resistance to mechanical degradation [34, 35].

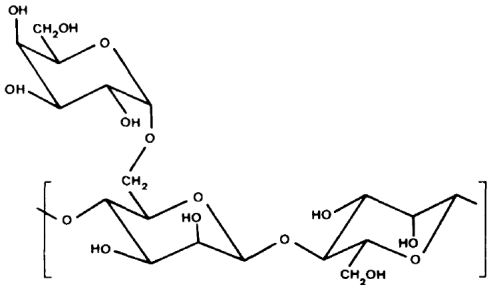

Fig. 2. Molecular structure of guar gum [28]

A common method for demonstrating drag reduction is Prandtl – Karman coordinates [36], which is a plot of $1/\sqrt{f}$ versus $log(Re\sqrt{f})$, where f is the fanning friction factor. There are three solid lines in the Prandtl-Karman coordinates (Fig. 3) each representing a boundary for drag reduction behavior. The first line represents the Poiseuille's law for laminar flow of Newtonian fluids:

$$\frac{1}{\sqrt{f}} = \frac{Re\sqrt{f}}{16} \qquad \textbf{(1)}$$

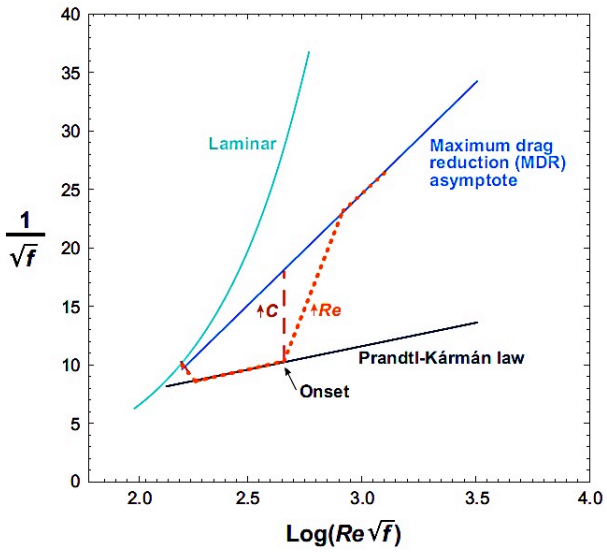

Fig. 3. Prandtl-Karman coordinates [29]

The second line is Prandtl – Karman law for Newtonian turbulent flow, which describes the onset of drag reduction:

$$\frac{1}{\sqrt{f}} = 4.0\ log_{10}\left(Re\sqrt{f}\right) - 0.4 \quad (2)$$

The upper limit for drag reduction is called "maximum drag reduction asymptote" (MDR) which is independent of polymer properties [37]. VirK et al. developed an empirical correlation, which defines the MDR as:

$$\frac{1}{\sqrt{f}} = 19.0\ \log_{10}\left(Re\sqrt{f}\right) - 32.4 \quad or \quad f = 0.58\, N_{Re}^{-0.58} \quad (3)$$

The area bound between the Prandtl-Karman and MDR lines is where drag reduction phenomenon is observed [36, 38].

The extent of drag reduction in flexible polymers depends on concentration, molecular weight of the polymer, and the Reynolds Number [15]. Virk et al. [38] suggested two mechanisms for drag reduction induced by polymers. The first mechanism occurs in polymers that are in coiled conformation (flexible chains) when they are at rest. As the level of shear force reaches a certain level, polymer molecules begin to stretch and hence drag is reduced [39]. Ptasinski et al. [40] suggested that as the effective viscosity increased, the thickness of the buffer layer also increased, and consequently the flow rate was enhanced. It should be noted that drag reduction phenomenon only occurs in turbulent flow regime [39, 41-43].

The effect of molar mass on drag reduction is displayed in Fig. 4. It can be observed that as the molar mass increases, the onset of drag reduction shifts to lower Reynolds Numbers. Also, it is observed that the degree of drag reduction is higher for high molar mass polymers. It is

believed that higher molar mass molecules absorb turbulent forces through interaction with large vortexes [15].

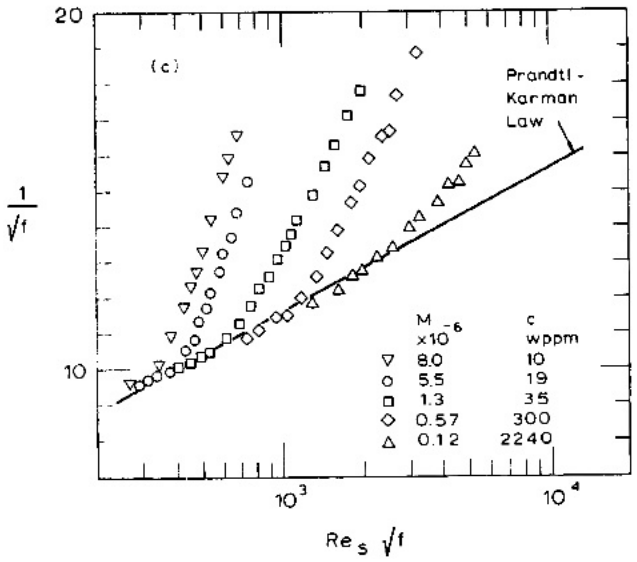

Fig. 4. Effect of molar mass on drag reduction

In the second mechanism, which is typical for rigid polymers, the molecules are already stretched and with application of shear force, further stretching or change in the molecular conformation does not occur, therefore the onset of drag reduction emerges quickly [15]. Polymer concentration has a direct effect on the extent of drag reduction. Although, increasing polymer concentration above a certain limit will not result in drag reduction increase (MDR).

According to the criterion proposed by Hershey et al. [44], the onset of drag reduction occurs when the flow time scale of near wall turbulence is shorter than the polymer relaxation time. Two theories have been proposed to explain the onset of drag reduction; viscous and elastic [36]. According to the viscous theory, the strain rate in the turbulent buffer layer is large enough to fully stretch the polymer molecules, which results in an increase in the effective viscosity [45]. The increase in effective viscosity dissipates the energy of turbulent fluctuations and thickens the turbulent buffer layer and consequently reduces friction [46]. But based on the elastic theory, molecules are only partially stretched, therefore the increase in effective viscosity is negligible

[47]. As a result of partial stretching elastic energy is stored and when the cumulative elastic energy equals the energy of turbulent fluctuations in the buffer layer, the onset of drag reduction occurs [48].

Biopolymers such as high molecular weight polysaccharides exhibit good degrees of drag reduction. Rod-like polymers induce smaller drag reduction compared to flexible molecules [49], but some industrially used biopolymers such as xanthan gum and guar gum are known to posses considerable mechanical stability both in deionized water and ionic solutions [15, 34, 50]. Previous studies (Sohn et al. [51]; Kim et al. [34]; Berman et al. [52]) also suggested that drag reduction induced by xanthan and other biopolymers depended on concentration and molar mass and the effect of Reynolds Number on drag reduction was negligible. It was also observed that biopolymers were shear resistant and maintained good level of drag reduction in the presences of salt at certain concentrations.

Flexible and rod-like polymers approach maximum drag reduction differently (Fig. 5). At large Re, the mean velocity profile of flexible polymers (open triangles) pursues the MDR line until a certain point where the velocity profile deviates and becomes parallel with the Prandtl-Karman line. For rod-like polymers (solid triangles and open squares), the velocity profile is always bound between the two asymptotes and is a function of polymer concentration [53].

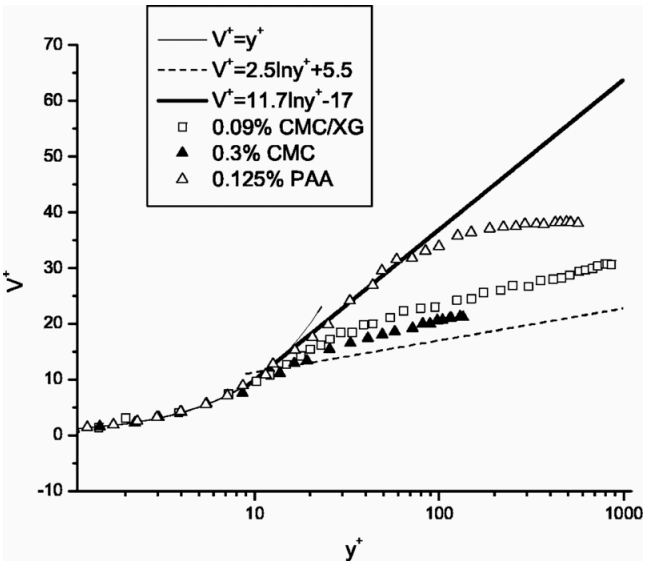

Fig. 5. Comparison of mean velocity profiles of flexible and rod-like polymers

According to the literature, binary polymer solutions give rise to DR efficiency and shear stability. Dingilian et al. [54] investigated the DR behavior of PAM, PEO, and carboxymethylcellulose (CMC) single and binary solutions. They observed negative deviation from additivity for binary solutions of two flexible polymer molecules (PEO/PAM) and positive deviation for PAM/CMC and PEO/CMC binary solutions, where flexible and rigid molecules coexisted in the solution. Dschagarowa et al. [55] also observed synergism in the DR behavior of poly-isobutylene and l,4-cis-isoprene rubber binary solutions. They also concluded that flow conditions could affect the degree of deviation from additivity. Malhorta et al. [56] verified DR performance of PAM/GG, GG/XG, and PAM/XG binary solutions and concluded that the degree of DR and synergism depended on polymer concentration and flow rate. They also concluded that positive deviation in additivity occurred when both polymers were rigid. But, they mentioned that their conclusions were limited to their experimental conditions and synergism might be observed in many other binary mixtures at higher concentrations. Reddy and Singh [57] verified the same binary solutions at higher concentrations (C > 200 wppm) and in a larger experimental setup. Contrary to previous authors, they observed negative deviation for PAM/polysaccharide binary

solutions. They also verified the shear stability of the polymer solutions and concluded that the solutions showing synergism in DR were more shear resistant. Recently Sandoval and Soares [58] verified the DR behavior of PAM/XG and PEO/XG binary solutions in a pressure driven flow loop. The authors reported clear synergism between polymers. They concluded that the improvement observed in the mixed solutions was related to the change of the polymeric conformation from coiled to elongated form. Compared to single polymer solutions, limited information is found on the drag reduction behavior of binary polymer solutions in the literature. On the other hand the existing published research is limited to certain conditions such as small-scale experimental setups (capillary tube), low flow rates and Reynolds numbers, and certain concentrations or molecular weights. Also, some of the available data contradict each other. As mentioned above, Reddy and Singh reported a different observation from Sandoval and Soares regarding the DR behavior of PAM/XG binary solution, which we believe is due to the differences in the experimental setup and the molecular weights of the polymers.

1.1.3 Shear degradation of polymer molecules

Mechanical degradation is one of the main drawbacks of using polymers as drag reduction agents. In oil-field operations such as treatments of shale formations, the irreversible mechanical degradation occurs when molecules pass through pumps, valves, and perforations [50]. Polyethylene oxide and polyacrylamide based solutions have been the focus of large number of studies and have found many applications due to their low cost and abundance. On the other hand, their lower mechanical stability at elevated shear rates limits the scope of their application [19].

According to Den Toonder et al. [59] when shear force is applied to a solution in a pump or a pipe, molecules break, which results in a decline in molecular weight and drag reduction. In a turbulent flow regime, due to the interaction with flow vortexes, molecules have to deal with extension and rotation. If extensional forces increase to a certain limit, molecular scission occurs.

Breakdown of polymer aggregates is another phenomenon that results in drag reduction decline [19]. Based on the observations of Liberatore et al. [60] the existence of aggregates in a solution could contribute to drag reduction, particularly at low shear rates where chain scission is of less significance. Khan et al. [61] found that aggregates formation only occurs for low molar mass polymer solutions, however Kim et al. [62] suggested that in the case of high molecular weight polymers macromolecular structures only form at very high concentrations (above 3000 ppm), which leads to significant enhancement of drag reduction. Hence it can be concluded that destruction of macromolecular structures can have an important effect in drag reduction decline at high polymer concentrations.

Polymer degradation can be described by exponential models as suggested by Brostow [63] and Bello et al. [64]. The empirical model proposed by Brostow, which has been adapted by many research groups, is based on polymer chain scission at midpoint:

$$\frac{DR(t)}{DR(0)} = \frac{1}{1+W(1-e^{-ht})} \quad \textbf{(4)}$$

where DR(t) and DR(0) stand for drag reduction at time t and initial drag reduction, respectively. Parameter h is a constant and accounts for the magnitude of the rate of degradation and W stands for degree of shear stability [63]. Also a single-relaxation exponential decay function has been proposed [64], which is found to describe the degradation of the shear resistant polysaccharides and PAM very well.

$$\frac{DR(t)}{DR(0)} = \exp\left(\frac{-t}{\lambda_s}\right) \quad \textbf{(5)}$$

This model deviates from experimental data for drag reducers such as polyethylene oxide, so Choi et al. [64] concluded that the single decay function is not a universal model and also is not applicable for short periods of drag reduction.

1.1.4 Effect of salt on the drag reduction behavior of polymer molecules

Another issue associated with drag reducing additives is sensitivity to the presence of ions in the solution [19]. Produced water from underground sources is often used in slickwater treatments, which has high concentrations of mono and divalent salts. Therefore, produced water should be treated before use, which is a costly process. Also, the use of fresh water is prohibited in most states. One strategy to overcome water shortage problem is to recycle water. But during each recycle more salt is dissolved and the hardness of the flowback water increases and since common friction reducers are sensitive to salt, recycling cannot always be utilized. The second strategy is to use polymers that are resistant to high brine content of produced water [65]. This can be achieved by chemically manipulating the polymer chains, which increases the production costs of such polymers.

Salinity and the ionic strength of a solution have great influence on the hydration of polymer molecules and consequently their drag reduction performance [65]. It is believed that addition of salt results in reduction in the size of polyacrylamide macromolecule and the viscosity of the solution [66]. Friction reducers are more sensitive to di and trivalent salts, as they increase the ionic strength several times more than monovalent salts [65].

The behavior of biopolymers in ionic solutions is different from flexible polymers. Depending on the concentration of the polymer in the solution, different rheological behaviors can be observed. Critical overlap concentrations C* and C** define the transition points from dilute to semi-dilute and semi-dilute to concentrated regimes, respectively [67]. Wyatt et al. [68] observed that above C** addition of salt increases the viscosity of the xanthan solution significantly. At C

> C**, the repulsive forces between salt ions and anions of xanthan molecule resulted in an expansion in the entangled chains and formation of a large elastic network. They also concluded that changes in viscosity also depended on the size and type of the salt ions [69]. But in dilute (C < C*) and semi-dilute (C* < C < C**) solutions of xanthan gum, the presence of salt affected the rheological properties of the solution in a different way and resulted in viscosity reduction. Previous research showed that, presence of salt increased the rigidity of the molecule and hence viscosity was reduced [69]. Wyatt et al. [20] suggested that salinity of the solution did not alter the drag reduction capability of xanthan gum at concentrations above its second critical concentration, C**. At dilute concentrations presence of salt negatively affected the drag reduction capability of xanthan solutions. Gittings et al. [31], investigated the properties of guar solutions in the presence of different salts. They concluded that salt did not have a significant influence on the rheological behavior of guar solution.

1.2 Objective and specific aims

This work was focused on investigation of the drag reduction behavior of HPAM/polysaccharide binary solutions, emphasizing on improving some of the drawbacks of using HPAM in drag reduction applications. In this regard, we followed two main goals: Improving the shear stability of HPAM solutions and modifying the drag reduction efficiency of HPAM solutions in ionic environments. According to the literature and our preliminary experiments naturally occurring polysaccharides displayed promising drag reduction capabilities, as well as, high shear stability and low sensitivity to ionic environments. In the present study, we proposed to prepare and characterize HPAM/XG and HPAM/GG binary mixtures and assessed their drag reduction behavior, in order to increase the shear stability of the solutions, as well as, to decrease the sensitivity of the friction reducers to the presence of salt ions in the medium. On the other hand, there was a concern about the low drag reduction efficiency of XG and GG compared to HPAM. Simultaneous presence of flexible and semi-rigid/rigid polymer molecules in a solution could

improve the drag reduction efficiency of XG and GG due to synergic effects. In order to achieve improved friction reduction capability via mixed polymer fluids, it was important to study their rheological characteristics and compare them with individual polymer solutions. The proposed work enabled us to understand the properties of mixed solution and design more efficient friction reducers that are used in applications such as hydraulic fracturing. In the proposed study, we pursued three specific aims:

Specific aim I: Preparation and rheological characterization of HPAM/XG and HPAM/GG binary mixtures in ionic and non-ionic environments

In this part of the project, samples of mixed solutions were prepared at different ratios and concentrations. Then a full rheological characterization including steady shear test, oscillation experiments were carried out and the results were compared to samples of individual polymers.

Specific aim II: Investigation of the drag reduction behavior of HPAM/XG and HPAM/GG binary mixtures

In specific aim II, we focused on measuring the drag reduction extent of the solutions. Both individual and binary solutions at various concentrations were prepared at large quantities. The shearing experiments were carried out on the prepared solutions. These experiments included shearing friction reduction solutions at different flow rates for short intervals. The data obtained were used in determining the friction factor and Prandtl-Karman graphs. Also, the solutions were sheared for a 2 hours period at maximum flow rate, in order to verify the shear degradation in polymer solutions. During the shearing period, samples were taken from the flowing fluid. Those samples were characterized by a rheometer and the results were compared to the results prior to shearing

Specific aim III: Investigation of the drag reduction models for the prepared binary mixtures

In order to predict the drag reduction behavior of the mixed polymer solutions finding a suitable model was necessary. Therefore, the data gathered from the drag reduction experiments were fit to the existing drag reduction models, including Brostow's model [63] and exponential decay function [64], in order to predict the drag reduction behavior of polyacrylamide/polysaccharide mixed solutions.

CHAPTER II

RHEOLOGICAL CHARACTERIZATION OF POLYMER SOLUTIONS

2.1 Introduction

Rheological characterization is an important step in understanding the flow and drag reduction behavior of non-Newtonian fluids such as polymer solutions. Chapter II is focused on an introduction to rheological characterization methods as well as characterization of the materials used in drag reduction experiments. Rheological characterization experiments included flow ramp and oscillatory experiments, which were carried out in a rheometer. The specifications of rheological characterization instrument and details of the experiments can be found in the materials and methods section (2.2). Information regarding the chemical structures and physical properties of the polymers is reported in section 2.2.1. The results from the rheological experiments include shear stress and viscosity vs. shear rate profiles as well as the degree of viscoelasticity of the polymer solutions, which were used throughout this research in determining the critical overlap concentrations, parameters of the viscosity models and etc. Section 2.2.2 of this chapter includes an introduction to various rheological characterization methods and their importance. In section 2.2.3, the most common viscosity models and their parameters are explained. Finally, section 2.3 discusses the results from rheological experiments, correlation of the viscosity data, and calculations of critical overlap concentrations.

2.2 Materials and methods

2.2.1 Materials and preparation of polymer solutions

Anionic polyacrylamide, XG, and GG as linear flexible and rod-like polymer molecules were chosen for this investigation. The molecular weights of HPAM (Kemira Co.), XG, and GG (PFP Technology) were 6-8×10^6 kg.mol^{-1}, 4-5×10^6 kg.mol^{-1}, and 1-2×10^6 kg.mol^{-1}, respectively (as reported by the vendors). The accurate values for molar mass were measured using light scattering (for HPAM) and viscometry (for XG and GG) methods. In the light scattering method, the solvent was filtered through 0.02 μm cellulose acetate Millipore filters. The HPAM solutions were prepared by dissolution of a known amount of polymer in the 0.5 mol L^{-1} NaCl solvent. The solutions were filtered through a 0.45 μm cellulose acetate Millipore filters. The concentration range of the polymer solutions (0.2-2.0 g L^{-1}) were analyzed using the batch-mode (without size separation) of a MALS detector (DAWN-HELEOS II, Wyatt Technology) with a laser wavelength of 658 nm. The specific refractive index increments (dn/dc) value of the HPAM in 0.5 mol L^{-1} NaCl solution, which was determined by OPTILAB T-reX differential refractometer (Wyatt Technology) at 633 nm and 25 °C, was 0.162 mL/g. Viscosity averaged molecular weight of XG was measured using the method described in [70]. In this method the intrinsic viscosity [η] was measured via Ubbelodhe capillary viscometer (diameter capillary 0.46 mm, Schott-Gerate), immersed in a water bath maintained at 25.0 ± 0.1 °C. First, the specific viscosity η_{sp} was calculated from the relative viscosity, which is the ratio of the viscosity of polymer solution at a certain concentration to that of the solvent. Each concentration was measured five times. The plot of η_{sp}/C versus C gave a straight line, the intercept of which was [η]. Then, using the Mark-Houwink equation the molar mass was calculated:

$$[\eta] = \lim_{c\to 0} \frac{\eta_{sp}}{c} = 6.6\times10^{-6}(\overline{M_v})^{1.35} \qquad [ml/g] \qquad \textbf{(6)}$$

The measured values for the molecular weights of the polymers, HPAM, XG, and GG were 7.2×10^6 kg.mol^{-1}, 3.9×10^6 kg.mol^{-1}, and 1.8×10^6 kg.mol^{-1} respectively. To establish a baseline for further studies, deionized water was used throughout. Using an analytical balance polymer powders were weighed with an accuracy of ±1 mg (Mettler Toledo XS603s). The preparation of the polymer solutions took place in a separate tank. The polymer powders were gradually sprinkled into the solvent and slowly agitated at 30 rpm, in order to prevent particles from clumping on the surface. Then, the prepared solutions were stored overnight for complete hydration.

2.2.2 Viscosity models and rheological characterization methods

Rheology is the science of flow and deformation of matter and flow is a special case of deformation. The relationship between stress and deformation is a material property. Therefore, rheology is defined as the study of stress – deformation relationship. These fundamental relations are called constitutive relations. The simplest relation between force and deformation is called the Hooke's law:

$$\boldsymbol{\tau = G\gamma} \qquad \textbf{(7)}$$

where τ is stress, γ is strain, and G is called the elastic modulus. For liquids, the simplest constitutive equation is called Newton's law of viscosity; the stress is proportional to the rate of straining:

$$\boldsymbol{\tau = \eta\dot{\gamma}} \qquad \textbf{(8)}$$

where $\dot{\gamma}$ shear rate and η, the Newtonian viscosity, is the constant of proportionality. Many materials obey ideal laws. For example, most metals or ceramics are Hookean or ideally elastic. Gases and most simple molecule liquids like water and oils are Newtonian. But many important materials such as polymers, paint, and blood lie between ideal elastic solid and ideal viscous

fluid. For these materials (including polymer solutions, emulsions, and concentrated suspensions) viscosity can be a strong function of the rate of deformation.

A large number of models have been developed that are based on strain rate, but all of them originate from the general viscous fluid model. The power-law model is the most commonly used form of the general viscous constitutive relation:

$$\boldsymbol{\eta_a = K(\dot{\gamma})^{n-1}} \quad \textbf{(9)}$$

where, n (behavior index) is a measure of deviation from Newtonian behavior and K (consistency index) is a measure of average viscosity. For Newtonian fluids the value of n is 1 and for shear-thinning fluids such as polymer solutions n is less than 1. As the value of n deviates from 1, the degree of non-Newtonian behavior increases. Nearly all polymer solutions and melts show shear thinning behavior. The power-law model provides a good estimate to data from viscosity vs. shear rate in the processing range of many polymeric liquids and dispersions. At high shear rates, $\dot{\gamma} > 1$, the power-law fits the data well [71].

One of the disadvantages of the power-law model is that it fails to describe the low shear rate region. Since n is usually less than one, at low shear rates η goes to infinity rather than to a constant η_0 (zero shear viscosity), as is experimentally observed. Also, at high shear rates Newtonian viscosity behavior is observed for many dilute polymer solutions [71].

In order to predict Newtonian regions at both low and high shear rates, Cross [72] proposed a new model:

$$\frac{\boldsymbol{\eta-\eta_\infty}}{\boldsymbol{\eta_0-\eta_\infty}} = \frac{\mathbf{1}}{\mathbf{1+(K\dot{\gamma})^{\frac{1-n}{2}}}} \quad \textbf{(10)}$$

where η is the shear viscosity, and η_0 and η_∞ are viscosities at zero-shear and infinite-shear plateaus and K is a time constant related to the relaxation time the polymer solution.

To fit data even better, Yasuda et al. [73] proposed:

$$\frac{\eta-\eta_\infty}{\eta_0-\eta_\infty} = [1 + (\lambda\dot{\gamma})]^{\frac{n-1}{a}} \quad (11)$$

In Carreau-Yasuda model, λ, n, and a represent the inverse shear rate at the onset of shear thinning, power-law index, and transition index, respectively.

Other viscosity models are found throughout the literature, but the power-law, cross and Carreau-Yasuda models have been used in most of the studies. Throughout the present work, non-linear fitting method was used in order to calculate the viscosity model parameters and to correlate the viscosity-shear rate data. The best model was chosen based on the statistical analysis of the data fits.

Viscosity measurements were carried out in a DHR Controlled Stress Rheometer. The instrument is equipped with a Peltier system to control sample temperature. In our experiments, sample temperature was maintained at 25±0.01 °C and the geometry used in the apparent viscosity measurements was cone and plate. The cone diameter and angle were 60 mm and 2°, respectively. Approximately, 2 mL of the solution was placed between the cone (rotating plate) and the fixed plate and the instrument was set to the strain control mode. In this mode, shear rate ($\dot{\gamma}$) was logarithmically increased from 0.01 to 1000 s^{-1} and shear stress was measured simultaneously, and then apparent viscosity was calculated using $\eta_a = \sigma/\dot{\gamma}$ correlation, where σ and η_a were shear stress and apparent viscosity, respectively.

Two types of rheological experiments were carried out on polymer solutions: Dynamic oscillatory, steady shear tests. Oscillatory shear tests were conducted in order to study the viscoelastic response of the materials. The oscillatory tests included strain sweep and frequency sweep tests. Strain sweep tests were conducted prior to dynamic frequency sweep tests to find the linear viscoelastic region, where the dynamic modulus is independent of frequency.

Frequency sweep tests were performed in the linear viscoelastic region as determined by the strain sweep test. The angular frequency range for the dynamic frequency sweep tests was 0.01 to 100 rad/s. The measurement temperature for all samples was 25°C (±0.01°C). Steady shear tests were used to verify the flow behavior or deformation of a fluid under steady shear condition. The data for evaluation of rheological properties was obtained by logarithmically increasing shear rate, $\dot{\gamma}$, from 0.001 to 1000 s^{-1}. All measurements were carried out at 25ºC (±0.01ºC).

For all of the experiments, samples were prepared in triplicate and evaluated on three separate sets of experiments. The reported values were averages of the measurements performed on all samples, and the errors associated with the measurement were represented as the standard deviation of the measurements.

2.3 Results and discussion

2.3.1 Steady shear test

In this section the effect of polymer concentration on the rheological behavior of the solutions was verified. Therefore, various concentrations of individual and binary polymer solutions were prepared and their viscosity profiles were measured via steady shear test. The viscosity profiles of various concentrations of HPAM solutions are displayed in Fig. 6. As expected for polymer solutions, a shear thinning behavior was observed for all of the HPAM solutions, even at very dilute concentrations. Both the zero and infinite rate viscosity plateaus were detected for HPAM solutions at $\dot{\gamma} < 0.2$ s^{-1} and $\dot{\gamma} > 1000$ s^{-1}, respectively. It was found that the concentration of the HPAM in the solution had a direct influence on the viscosity of the solutions. The largest and smallest measured apparent viscosity belonged to 1000 wppm and 80 wppm solutions, respectively.

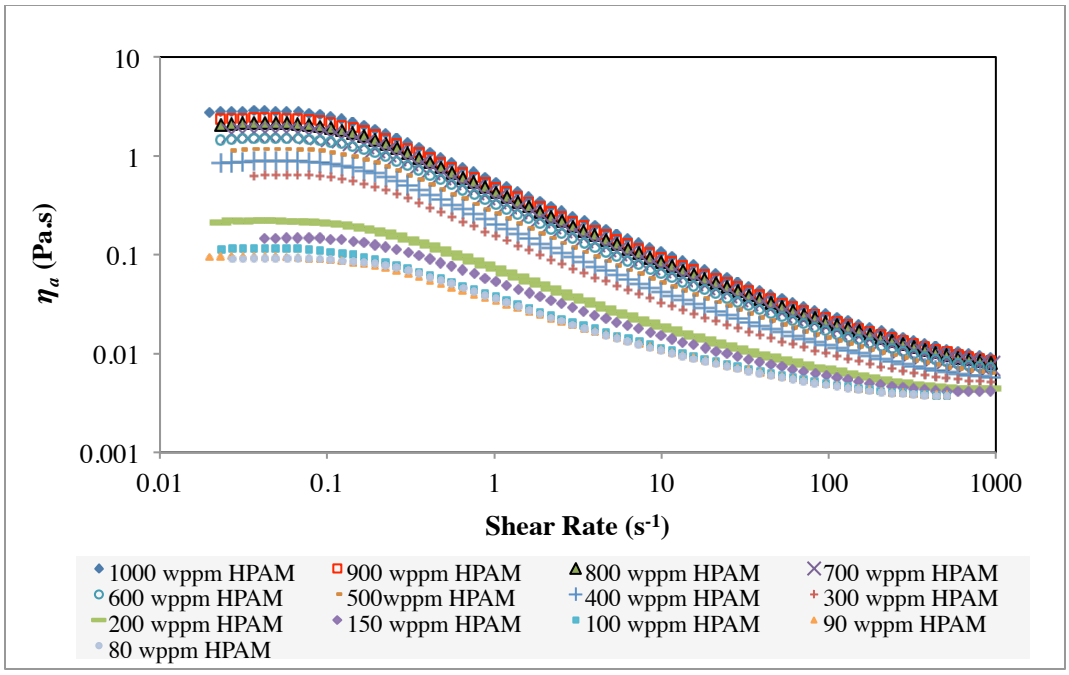

Fig. 6. Apparent viscosity profiles of HPAM solutions

In order to obtain more information from viscosity measurements, various viscosity models were fit to the measured data. Throughout this work, only Carreau-Yasuda and power-law models were reported, beacuse Carreau-Yasuda model gave best predictions and power-law model was simple and applicable in the mid-range shear rates. The parameters calculated from curve fitting of the viscosity data of HPAM solutions is displayed in Table 1.

It was observed that as concentration increased the η_0 and K values tended to increase, indicating that solutions got more viscous. The largest and smallest η_0 values belonged to 1000 wppm and 80 wppm solutions, respectively. Comparison of the viscosity profiles of HPAM solutions showed that by increasing concentration from 200 wppm to 300 wppm, a large increase in the apparent viscosity of the solutions occurred (from 0.2223 Pa.s to 0.6390 Pa.s). It is believed that the observed increase in viscosity was due to the entanglement of the polymer chains.

Table 1: Carreau-Yasuda and power-law parameters of HPAM solutions

	Carreau-Yasuda						Power-law		
Concentration (wppm)	η_0 **(Pa·s)**	η_∞ **(Pa·s)**	λ **(s)**	***a***	***n***	R^2	***K*** ***(Pa.s^n)***	***n***	R^2
80	0.09145	0.0030	4.69	2.94	0.36	0.99	0.041	0.47	0.99
90	0.09712	0.0029	6.20	2.36	0.40	0.99	0.042	0.47	0.99
100	0.1170	0.0029	6.89	2.52	0.38	0.99	0.040	0.42	0.99
150	0.1492	0.0032	5.16	2.68	0.36	0.99	0.051	0.41	0.99
200	0.2223	0.0034	5.79	2.36	0.35	0.99	0.073	0.39	0.99
300	0.6390	0.0040	7.28	2.32	0.28	0.99	0.16	0.27	0.99
400	0.8741	0.0044	7.47	4.65	0.28	0.99	0.21	0.25	0.99
500	1.164	0.0047	7.86	4.55	0.27	0.99	0.26	0.25	0.99
600	1.485	0.0051	8.03	4.46	0.27	0.99	0.33	0.25	0.99
700	1.712	0.0051	8.46	4.34	0.27	0.99	0.37	0.25	0.99
800	2.121	0.0054	8.76	4.34	0.27	0.99	0.44	0.24	0.99
900	2.406	0.0055	8.85	4.35	0.27	0.99	0.49	0.24	0.99
1000	2.815	0.0056	9.22	4.39	0.26	0.99	0.55	0.24	0.99

Polymer solutions are categorized into three concentration regimes; dilute, semi-dilute, and concentrated. In the dilute regime, polymer chains are so distant that they do not interact with each other. As the concentration increases (semi-dilute regime), polymer chains begin to overlap and become entangled, which results in more interaction. As the concentration further increases, a transition to the concentrated regime occurs. In this regime, molecules cannot move freely and due to the lack of space significant interpenetration occurs. All of the above changes are reflected in the rheology of the solution. Critical overlap concentrations C* and C** define the transition points from dilute to semi-dilute and semi-dilute to concentrated regimes, respectively [67]. Several methods have been utilized to determine the critical concentrations, among which rheological measurement is the most popular method due to its simplicity. The quantities of C*

and C** are determined by plotting specific viscosity, η_{sp}, versus concentration in a double-log plot (the points where slope changes). The specific viscosity is calculated using the following equation:

$$\boldsymbol{\eta_{sp} = \frac{\eta_0 - \eta_s}{\eta_s}} \quad \textbf{(12)}$$

where η_0 and η_s are zero shear and solution viscosities, respectively.

The concentration regimes and critical overlap concentrations of HPAM solutions were determined using the parameters calculated from viscosity data (Fig. 7). The values of C* and C** for HPAM solutions were determined to be 160 wppm and 4950 wppm, respectively.

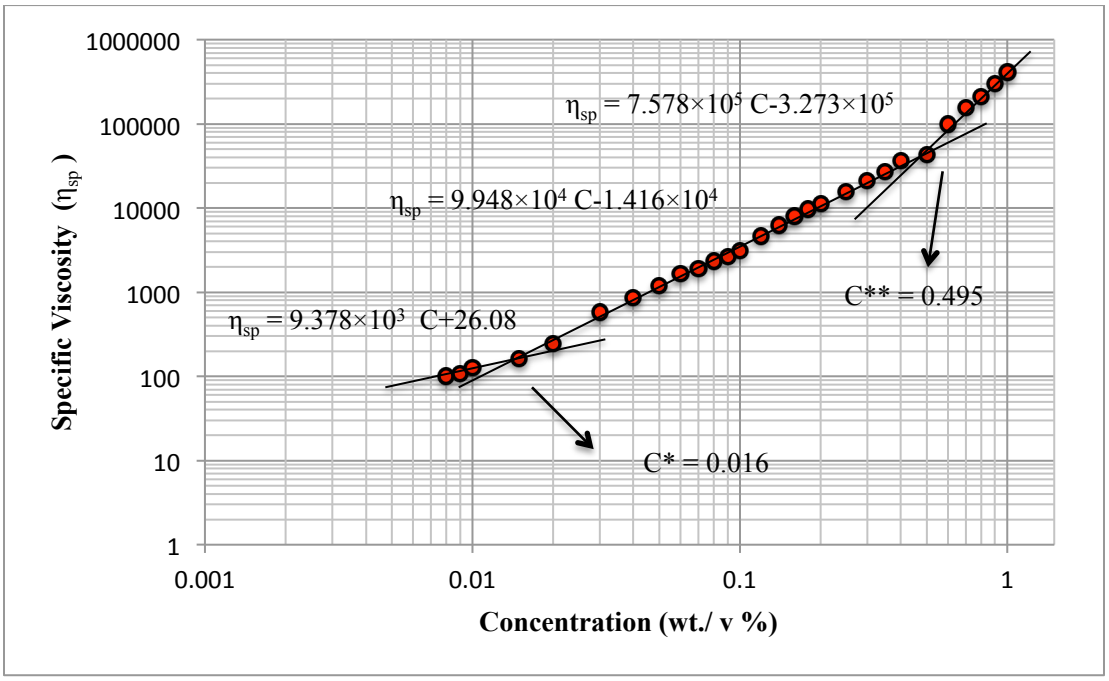

Fig. 7. Critical overlap concentrations of HPAM solutions

Viscosity profiles of various concentrations of XG solutions are displayed in Fig. 8. Similar to HPAM solutions, XG solutions exhibited shear thinning behavior. The zero shear plateau was clearly observed for all of the polymer solutions. But infinite shear plateau was only observed at low concentrations (C < 600 wppm). The zero shear plateaus of XG solutions were not identical and occurred at different shear rates. For example, the upper shear rate boundary of 10000 wppm

solution was ~ 0.01 s^{-1}, whereas for 100 wppm solution the upper boundary was ~ 1 s^{-1}. Contrary to HPAM solutions, dilute solutions of XG (C <160 wppm) behaved almost like Newtonian fluids. But similar to HPAM solution, increasing XG concentration resulted in an increase in the viscosity of the solutions. The largest and smallest measured apparent viscosities belonged to 10000 wppm and 100 wppm solutions, respectively.

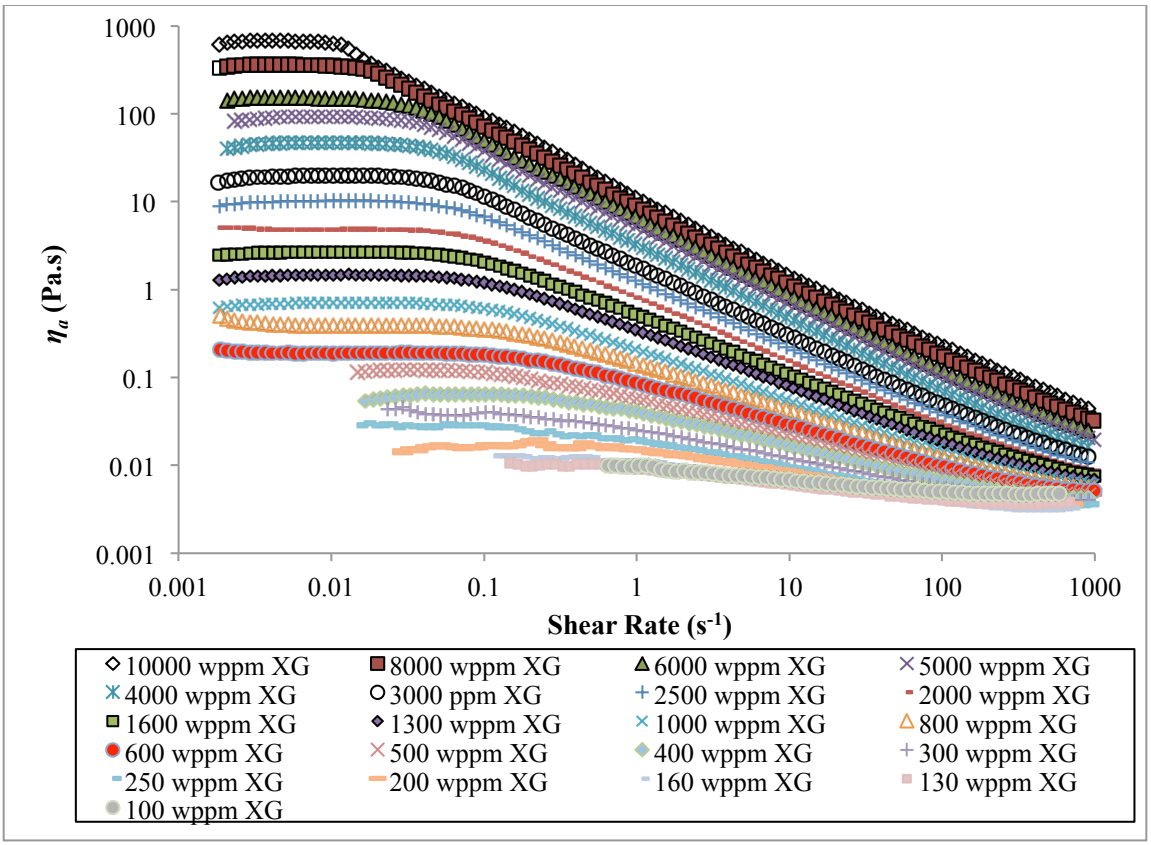

Fig. 8. Viscosity profiles of XG solutions

Similar to HPAM solutions, the concentration regimes and critical overlap concentrations of the HPAM solutions were determined using the parameters calculated from viscosity data (Fig. 9). The values of C* and C** for XG solutions were determined to be 260 wppm and 3400 wppm. Comparison of the C* values of HPAM and XG solutions indicated that HPAM polymer chains began to interact with each other at lower concentrations. Also, comparison of the viscosities profiles of XG and HPAM solutions revealed that HPAM solutions were more viscous

solutions. The lower C* values associated with HPAM solutions could be due to the large molecular weight (large polymer chains) of HPAM compared to XG.

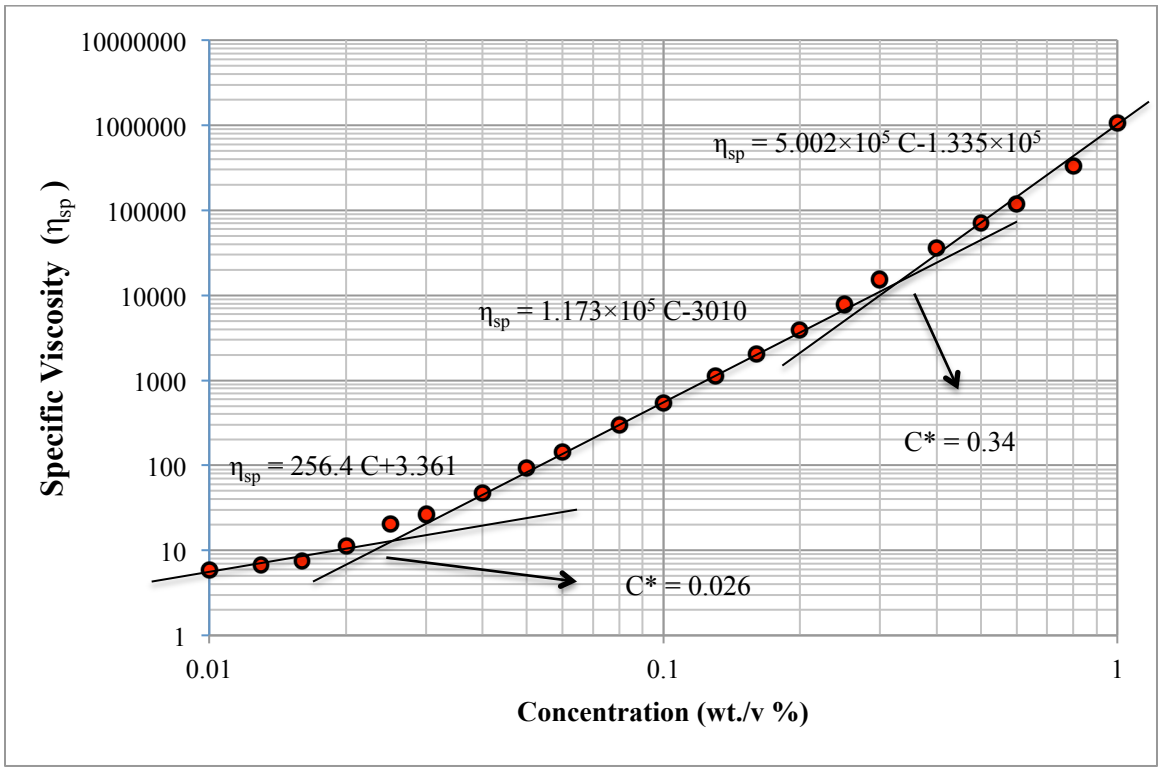

Fig. 9. Critical overlap concentrations of XG solutions

Viscosity profiles of various concentrations of GG solutions are displayed in Fig. 10. Like other polymer solutions, GG solutions exhibited shear thinning behavior and similar to XG solutions the infinite shear plateaus were only observed for dilute GG solutions and zero shear plateaus boundaries moved to lower shear rates by increasing concentration (for example 10 s^{-1} for 1000 wppm and 0.1 s^{-1} for 10000 wppm). The zero shear plateaus of GG solutions were wider compared to XG and HPAM solutions. Similarly, viscosity of the solutions were directly proportional to polymer concentration, 10000 wppm GG and 100 wppm GG solutions were the most and the least viscous solutions, respectively. GG solutions were less viscous than both XG and HPAM solutions and the solutions began to behave like Newtonian fluids at C < 600 wppm.

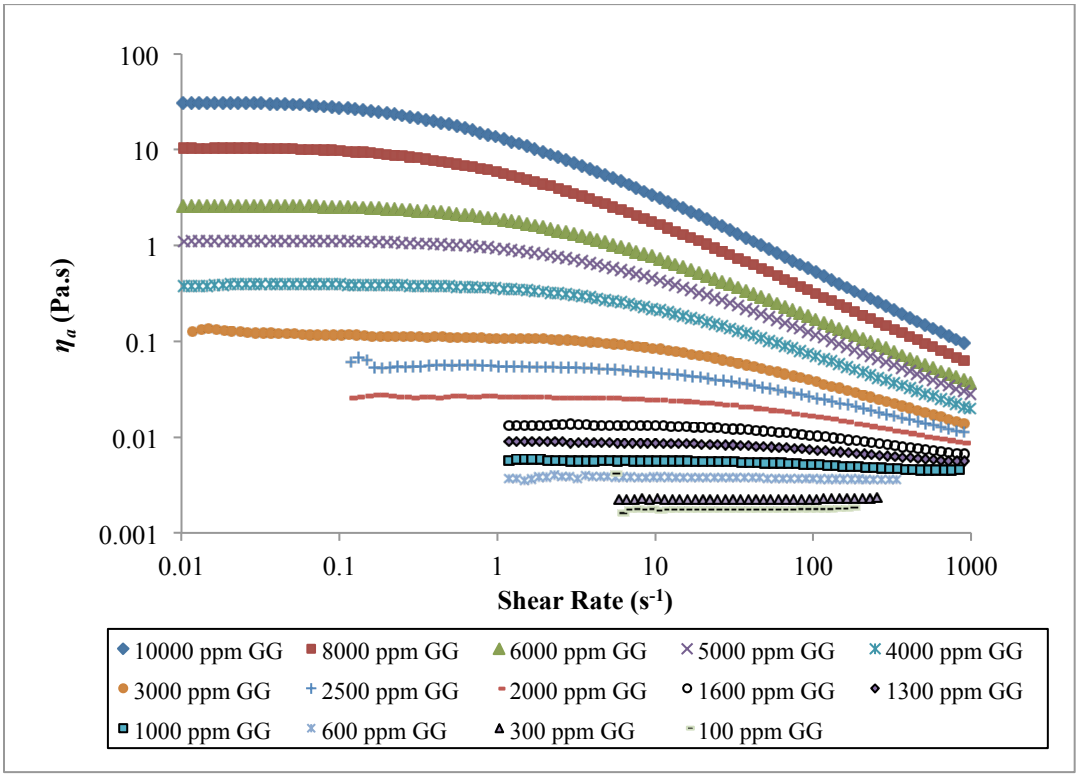

Fig. 10. Viscosity profiles of GG solutions

Critical overlap concentrations of GG solutions were calculated using viscosity data (Fig. 11). The values of C* and C** for GG solutions were 720 wppm and 2400 wppm, respectively. The critical overlap concentrations of HPAM, XG, and GG solutions are reported in Table 2. Among the three polymer solutions, the smallest C* vales belonged to HPAM solutions, indicating that HPAM polymer chains began to interact at lower concentration than XG and GG molecules. The reason for this phenomenon is attributed to the large molecular weight of HPAM molecule. The largest C* vales belonged to GG solutions, indicating that GG polymer chains began to interact at a greater concentration than XG and HPAM molecules.

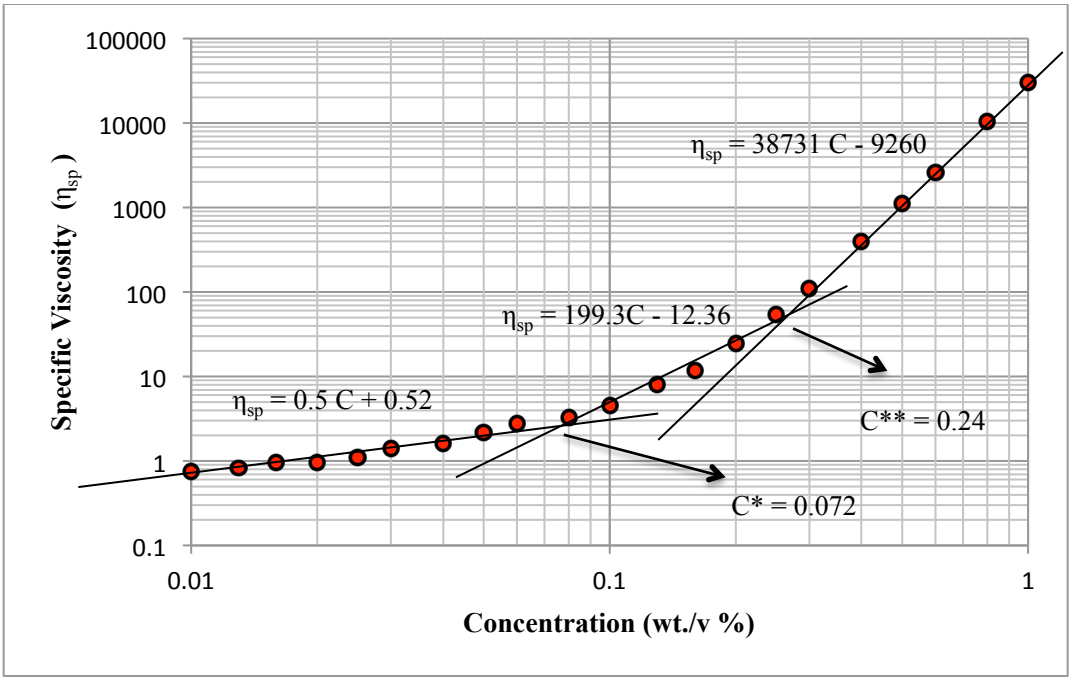

Fig. 11. Critical overlap concentrations of GG solutions

The second critical overlap concentration was in HPAM > XG > GG order, indicating that the second jump in the viscosity of HPAM solutions occurred at a higher concentration than XG and GG. This kind of behavior could be as a result of high flexibility of HPAM molecules. We know that as polymer concentration increases, the polymer chains get more entangled and form agglomerates. So due to the flexibility of HPAM molecules, the polymer networks are loose compared to the networks formed by less flexible polymer molecule such as GG. As a result, we observed that the C** was inversely proportional to the rigidity of polymer molecules.

Table: Critical overlap concentrations of HPAM, XG, and GG solutions

Polymer	C* (wppm)	C** (wppm)
HPAM	160	4950
XG	260	3400
GG	720	2400

2.3.2 Oscillation experiments

In order to verify the viscoelastic behavior of polymer solutions, dynamic oscillatory experiments were carried out. One of the important oscillatory experiments is frequency sweep test. In a frequency sweep test, measurements are made over a range of oscillation frequencies at a constant oscillation amplitude and temperature [74]. The parameters that can be measured and calculated include complex (G*), storage (G') and loss (G") moduli, and phase angle (δ). Complex modulus (G*) is a measure of material's overall resistance to deformation and is determined as:

$$G^* = G' + iG'' \quad (13)$$

Storage modulus (G') is a measure of elasticity of the material and the ability of the material to store energy. Loss modulus (G") is the ability of the material to dissipate energy in the form of heat. Phase angle (δ) is the measured shift between input and output waves and is a measure of material's damping. For a Hookean solid δ is equal to zero, whereas for a Newtonian fluid δ is 90 degrees [74, 75]. For all viscoelastic materials $0 < \delta < 90$,

$$\tan \delta = \frac{G''}{G'} \quad (14)$$

Frequency sweep experiments were carries out on HPAM solutions. The storage and loss moduli for various concentrations of HPAM are displayed in Fig.12 and Fig. 13, respectively. It was observed that both G' and G" increased by increasing concentration (which means G* increased), indicating that the resistance of the solutions to deformation increased by increasing polymer concentration. The observations were consistent with the literature data [76]. Also, a jump in both G' and G'' values was observed as the concentration increased from 200 wppm to 500 wppm.

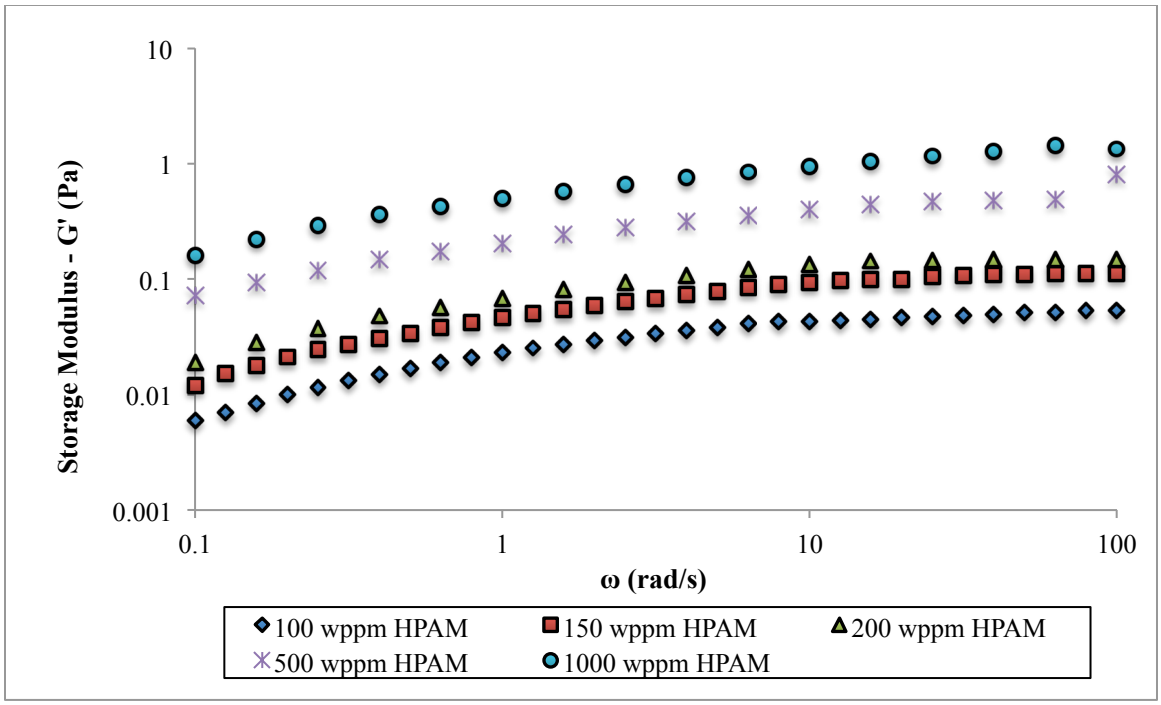

Fig. 12. Storage modulus (G') for various concentrations of HPAM solutions

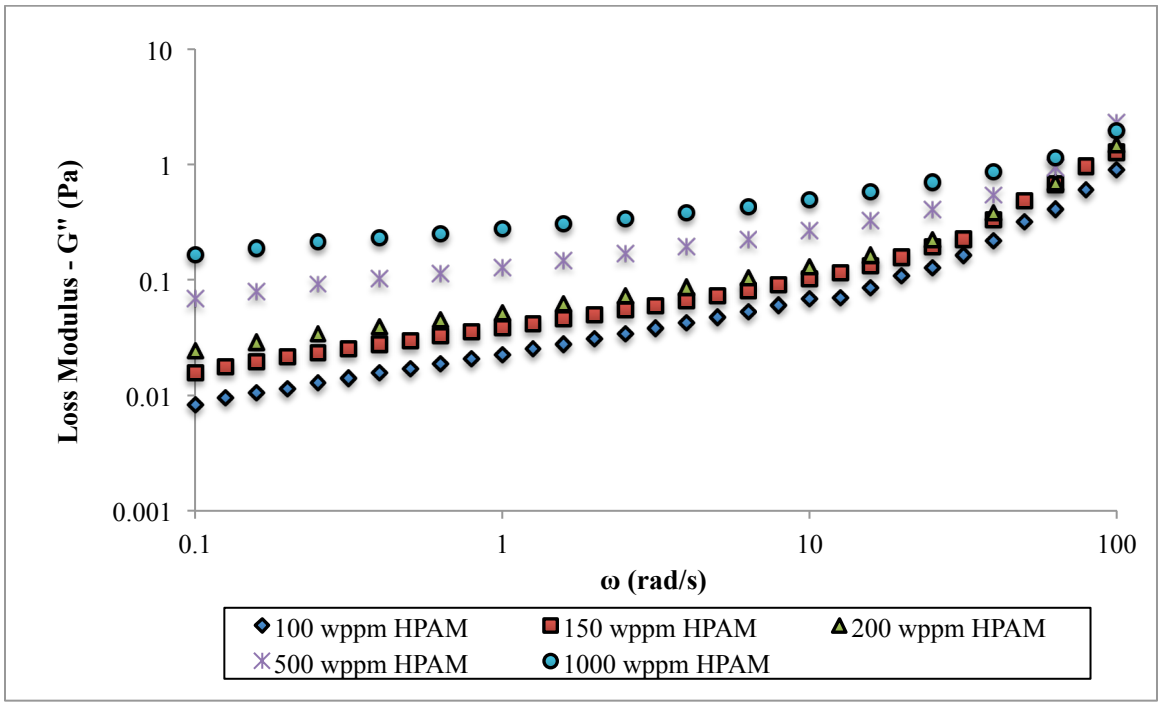

Fig. 13. Loss modulus (G") for various concentrations of HPAM solutions

The relative magnitude of G" to G' (tan δ) for various concentrations of HPAM in the 0.1-100 rad/s frequency range is displayed in Fig. 14. The values of tan δ decreased with increasing concentration suggesting that polymer concentration increased the elasticity of the solutions. It was observed that for C ≤ 200 wppm at low frequencies (ω < 0.3 rad/s), tan δ was greater than 1, indicating that the solutions were more behaved more like a viscous fluid. For C ≥ 500 wppm, tan δ values were close to 1 (or δ = °45). As angular frequency increased, tan δ values decreased and a minimum was observed in 0.3 < ω < 10 range for all of the HPAM solutions. For example, the minimum tan δ for 100 wppm solution was 0.98 at ω = 1 rad/s, whereas for 1000 wppm the minimum value of tan δ was 0.5 at ω = 2.5 rad/s. The minimum value of tan δ = 1 were the crossover points of G' and G" curves. The crossover points marked the transition from elastic region to viscous region and vise versa. Finally, it was observed that at high frequencies ω > 10 rad/s, tan δ values increased quickly. In ω > 10 rad/s frequency range, the viscous behavior of the solutions dominated their elastic behavior.

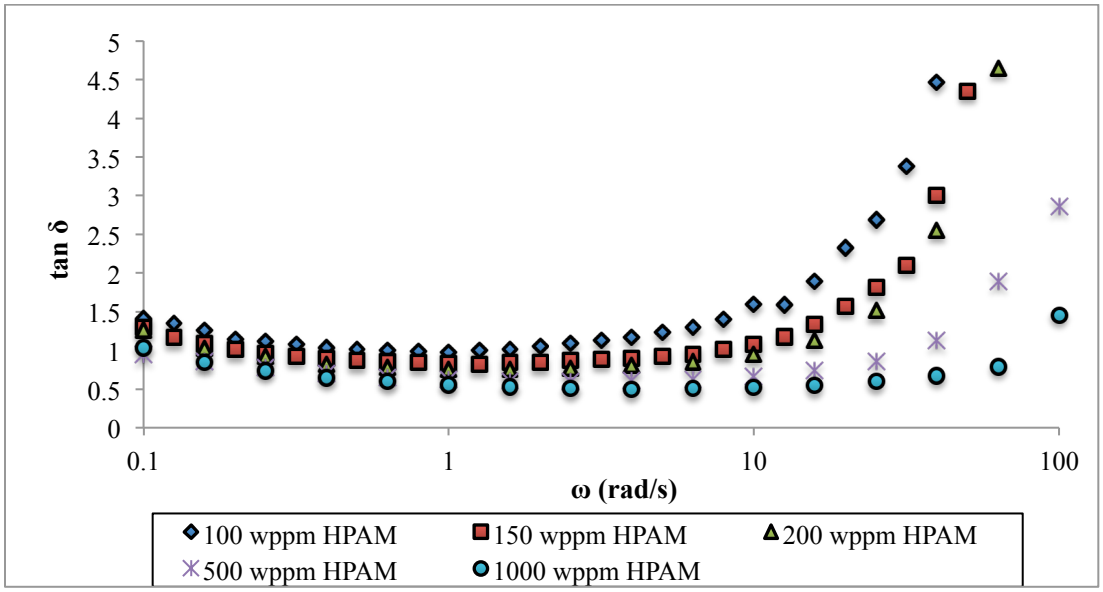

Fig. 14. Calculated phase angle for various concentrations of HPAM solutions

The results of dynamic oscillatory experiment for XG solutions are displayed in Figs. 15 through 17. Similar to HPAM solutions, both G' and G" increased by increasing XG concentration, indicating that the resistance of the solutions to deformation increased by increasing polymer concentration. Both G' and G" were dependent on frequency suggesting that the solutions (at the studied concentrations) were not structured (were fluid-like). The calculated values of relative G" to G' are shown in Fig. 17. Results showed that values of tan δ decreased with increasing concentration, suggesting that polymer concentration increased the elasticity of the solutions. Similar to HPAM solutions, a minimum was observed in tan δ values of all XG solutions. The values of tan δ remained smaller than 1 for 1000 wppm XG solution within $0.1 < \omega < 100$ rad/s range. On the other hand tan δ vales of 200 and 300 wppm XG solutions remained above 1 within the same frequency range. But for 600 and 800 wppm solutions, tan δ values were both above and below 1, indicating that G' and G" curves crossed over.

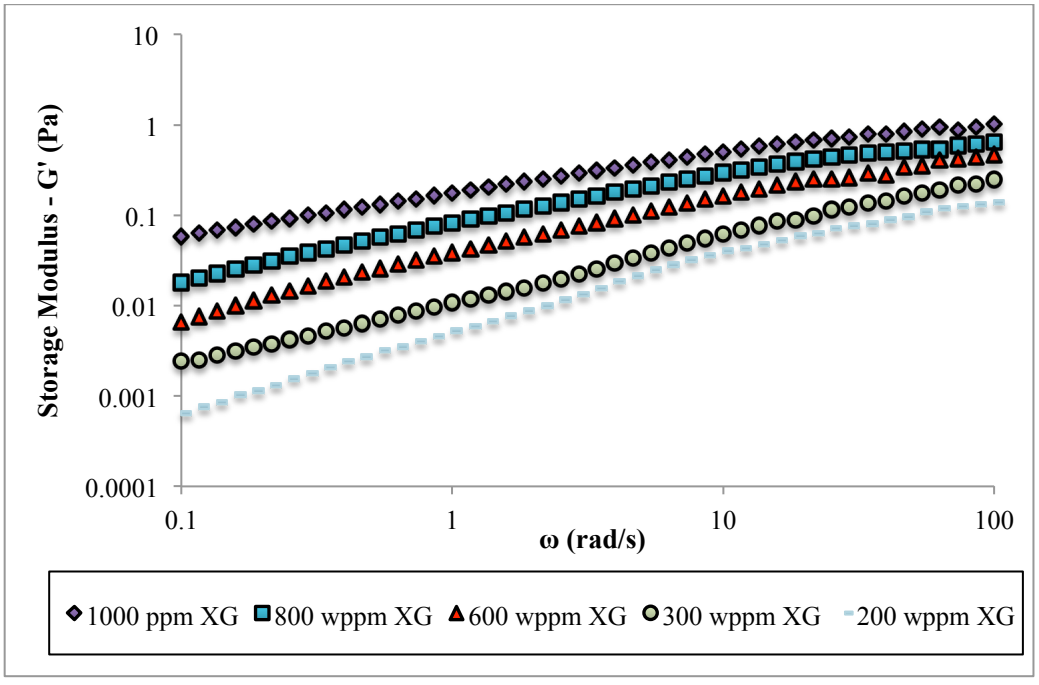

Fig. 15. Storage modulus (G') for various concentrations of XG solutions

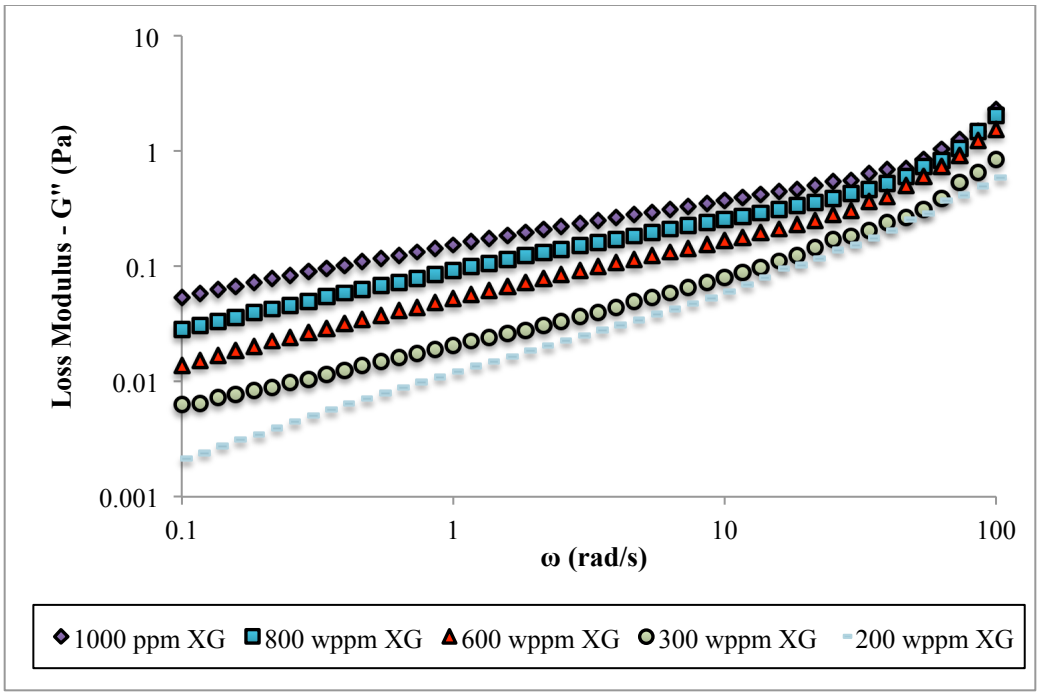

Fig. 16. Loss modulus (G") for various concentrations of XG solutions

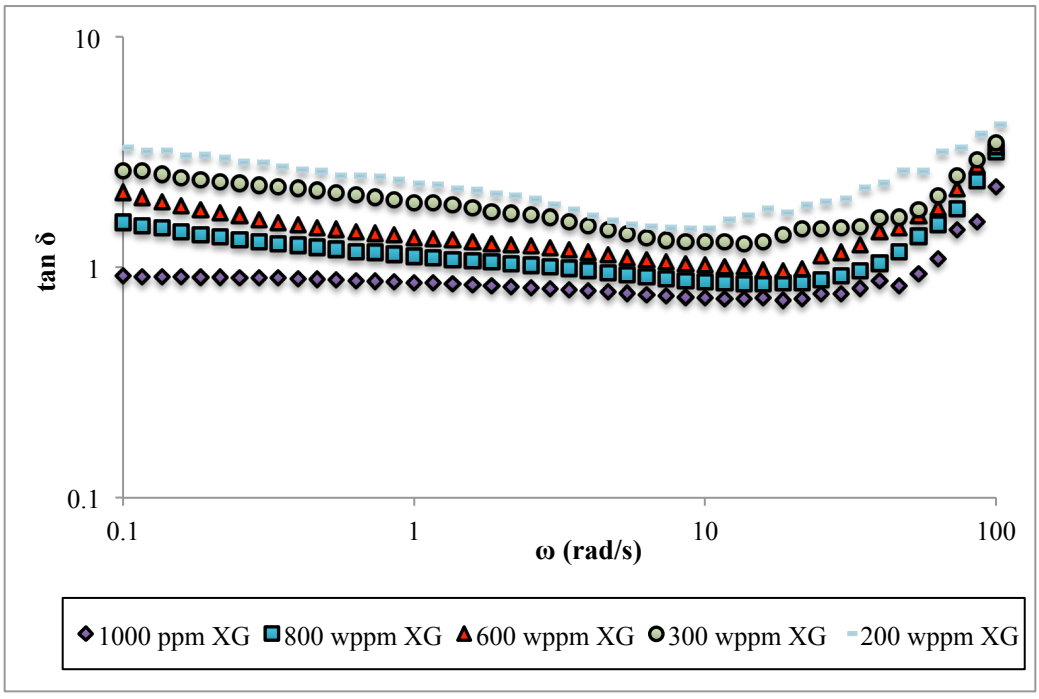

Fig. 17. Calculated phase angle for various concentrations of XG solutions

Frequency sweep experiments were carried out on GG solutions as well. But, the measured values of G' and G" for GG solutions were very small (or zero) compared to HPAM and XG solutions, indicating that the resistance of GG solutions to deformation was low. In order to obtain reasonable results, the experiments were carried out at high concentrations. The G' data is displayed in Fig. 18. It was observed that even for the shown concentrations, the G' values were very small or the measured data was unstable, particularly at low frequencies ($\omega < 1$ rad/s) Therefore, since the studied concentrations are too high for friction reduction application, the results were not discussed further and other relevant data was reported in Appendix A.

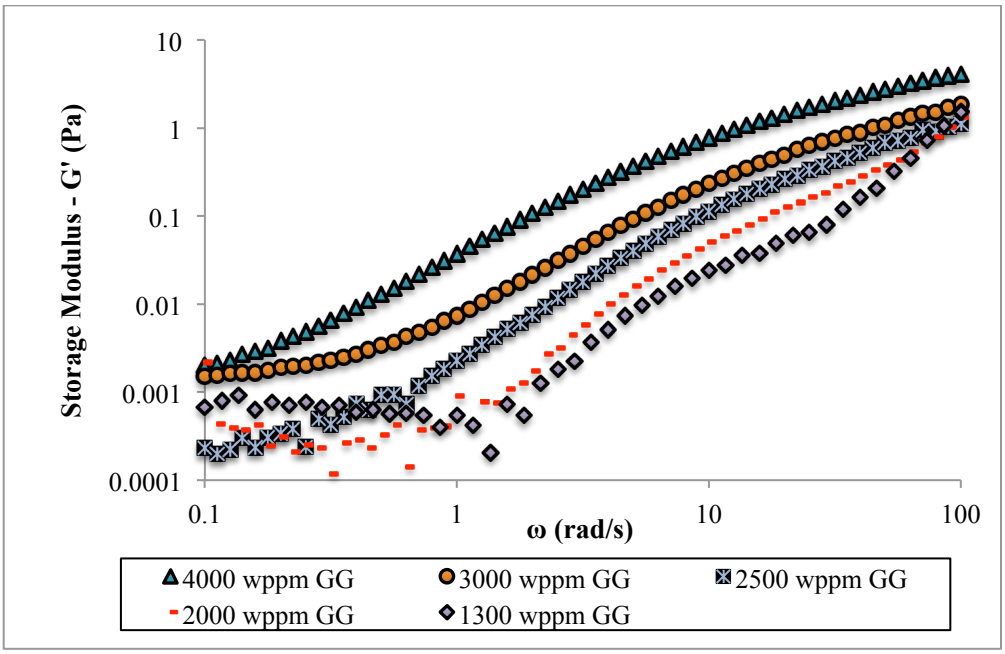

Fig. 18. Storage modulus (G') for various concentrations of GG solutions

According to the dynamic oscillatory results, the resistance of the polymer solutions (at the same concentration) to deformation was in HPAM > XG > GG order, indicating that the degree of elasticity for HPAM solutions was greater than XG and GG solutions.

CHAPTER III

DRAG REDUCTION BEHAVIOR OF SINGLE AND BINARY SOLUTIONS

3.1 Introduction

In this chapter, drag behavior (DR) and resistance to mechanical degradation of single and binary HPAM, XG, and GG solutions are verified. Anionic PAM is the partially hydrolyzed form of polyacrylamide that has a relatively large molar mass and exhibits greater flexibility than regular PAM molecule. All of the polymers are widely used in industrial applications such as hydraulic fracturing treatments. There has been little or no work regarding the DR behavior of anionic HPAM, XG, and GG and mixtures. We believe that it would be interesting to verify the DR behavior of two negatively charged molecules coexisting in a solution (HPAM/XG), as well as the drag reduction behavior of HPAM/GG mixtures. Since various HPAM, XG, and GG molecules with different molecular weights are available in the market, we also study the behavior of single polymer solutions, so that we can compare with binary solutions and assess the degree of improvement in drag reduction efficiency and shear stability. The drag reduction experiments were carried out in a closed flow loop system, which is explained in section 3.2. The results and discussion regarding the DR behavior of single and binary polymer solutions are reported in section 3.3. Finally, the DR behavior of HPAM and HPAM/XG solutions are discussed in section 3.4.

3.2 Materials and Methods

In this work, drag reduction behaviors of HPAM, XG and GG single polymer solution, as well as HPAM/XG and HPAM/GG binary solutions were studied (Table 2). In order to verify the effect of salt, initially 2% KCl was dissolved in deionized water and then following the procedure explained in section 2.2.1, polymer powders were dissolved in the solution. The studied solutions were 1000 wppm HPAM/2% KCl, 150 wppm HPAM+300 wppm XG/2% KCl, and 150 wppm HPAM+300 wppm XG/ 2% KCl.

A closed loop flow system was utilized for drag reduction and turbulent flow measurements (Fig.19). The system was comprised of a 60 liter supply tank connected to a progressive cavity pump (SEEPEX BN 10-12) with a pumping capacity of 30 GPM (113.56 l/min), and a seamless stainless steel horizontal pipe test section of L = 8 ft. (2.438 m) and inner diameter of 1 inch (2.54cm). The flow rate of the system was measured using a mass flow meter (OPTIMASS 1000, KROHNE) with an accuracy of ±0.15% and a repeatability of ±0.05% as stated by the manufacturer. The pressure drop data along the measuring length of the pipe was gathered using a membrane differential pressure transducer (PX409, OMEGA). At each flow rate Fanning friction factor is calculated by:

$$\boldsymbol{f = \frac{D}{2\rho U^2}\left(\frac{\Delta P}{L}\right)} \qquad \textbf{(15)}$$

Here, f is the Fanning friction factor, ρ is the fluid density, U is the average velocity, ΔP is pressure drop in the measurement length of L, and D is the internal diameter of the pipe. In the flow experiments, drag reduction efficiency of the polymer solutions was defined as:

$$\boldsymbol{DR = \left(\frac{f_w - f_s}{f_w}\right)_{Re=const}} \qquad \textbf{(16)}$$

where subscripts "*w*" and "*s*" stand for water and polymer solution, respectively, and "*Re* = const." signifies the fact that the comparison between the flows is made at the same Reynolds numbers. Here $Re = \rho UD/\eta_a$, and η_a is fluid viscosity. In drag reduction experiments the flow rate was increased stepwise (and kept constant for 1 minute at each flow rate) and then the polymer solutions were sheared in the flow loop at maximum flow of 30 GPM for 2 hours and sampling was performed 8 times at shearing periods of t = 0, 15, 30, 45, 60, 80, 100, and 120 min. After the shearing process, flow rate was decreased stepwise in the same manner as it was increased.

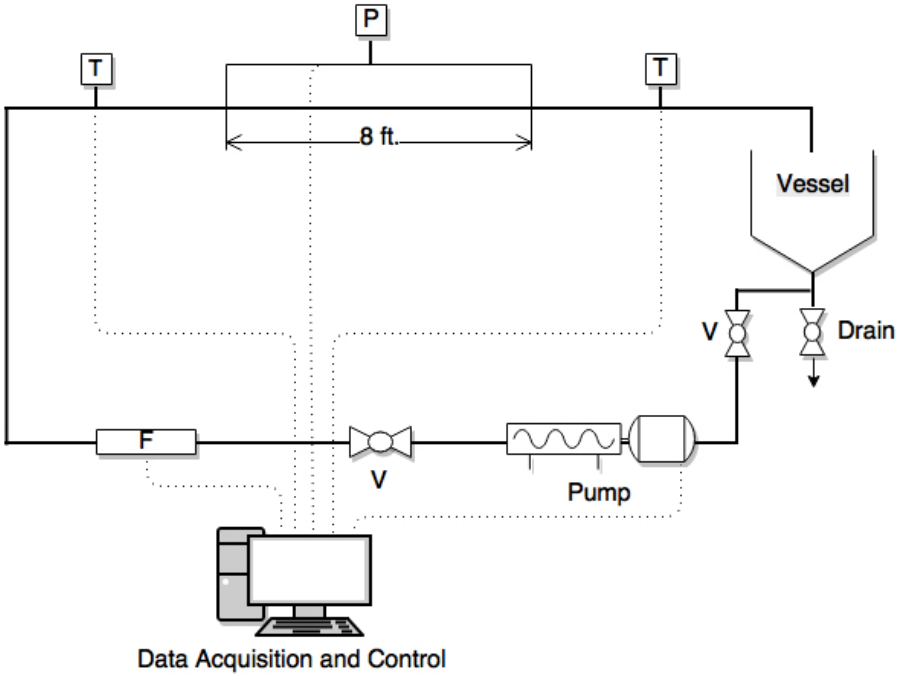

Fig. 19. Schematic illustration of the flow loop; Instrumentation consists of a digital flow meter (*F*), differential pressure transducer (*P*), valves (*V*), and temperature sensors (*T*).

3.3 Drag reduction behavior of polymer solutions

3.3.1 Polyacrylamide solutions

In order to assess the degree of drag reduction and polymer degradation, several samples were taken at specified intervals over the shearing process. Shear stress and apparent viscosity of the samples were measured in the rheometer and power-law and Carreau-Yasuda, parameters were calculated. For Newtonian fluids the value of n is 1 and for shear-thinning fluids, such as polymer solutions, n is less than 1. As the value of n deviates from 1, the degree of non-Newtonian behavior increases. The Carreau-Yasuda and power-law parameters calculated for different concentrations of the anionic polyacrylamide are shown in Table 2 and Figs. 20a,b, respectively.

Table 2. Calculated parameters of Carreau-Yasuda model for HPAM, XG and HPAM/XG solutions

Concentration, wppm	η_0 (Pa·s)	η_∞ (Pa·s)	λ (s)	a	n
100 ppm HPAM	0.08351	0.0035	4.96	1.37	0.37
150 ppm HPAM	0.2668	0.0041	5.46	3.15	0.26
200 ppm HPAM	0.3717	0.0042	5.80	3.14	0.27
500 ppm HPAM	1.211	0.0052	8.70	3.74	0.26
1000 ppm HPAM	3.507	0.0067	10.1	3.52	0.21
600 ppm XG	0.2689	0.0040	5.34	1.92	0.43
100 ppm HPAM + 100 ppm XG	0.1331	0.0039	4.18	2.51	0.36
150 ppm HPAM +100 ppm XG	0.2873	0.0038	7.20	2.28	0.33

Comparison of power-law parameters of fresh (zero shearing time) HPAM solutions showed that by increasing concentration, values of K increased and n values decreased, indicating increased non-Newtonian behavior. It can also be found that, as the shearing time increased, the

values of power-law parameters changed for all the polymer solutions. Fig. 2a shows that, over the shearing time, *K* values of HPAM solutions decreased and *n* values increased and got close to one (Newtonian behavior). The difference in the *n* values of the solutions before and after the shearing was large (35%-152% increase for various concentrations). The overall change in *n* values (after the shearing period) was 35% for 100 wppm solution, and by increasing concentration, the maximum change in *n* values (152%) appeared at 200 wppm. As the concentration increased above 200 wppm, change in n value drops to 69% for 1000 wppm solution. As a result of shear degradation and consequently viscosity reduction, *K* values decline. By increasing concentration from 100 wppm to 1000 wppm, *K* values reached a maximum decline of 64% at 200 wppm, but with further concentration increase a 33% decline in *K* value was found for 1000 wppm HPAM solution.

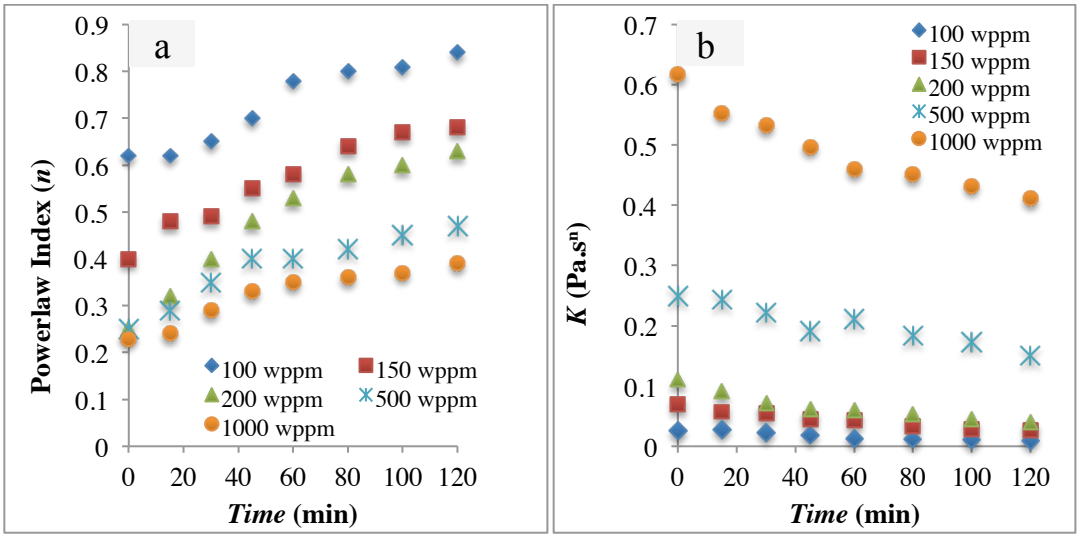

Fig. 20. Power-law model parameters variation over shearing time for HPAM solutions

Another indication of shear degradation is shown in Fig. 21, where the apparent viscosity of the 200 wppm HPAM solution, at shear rates under 10 s^{-1}, undergoes drastic reduction as the circulation time increases. The reason that we only saw changes at lower shear rates might be related to the scission of the molecules that belong to the high tale of the molecular weight

distribution of the polymer [77]. Those molecules contributed to the formation of the zero shear viscosity plateau.

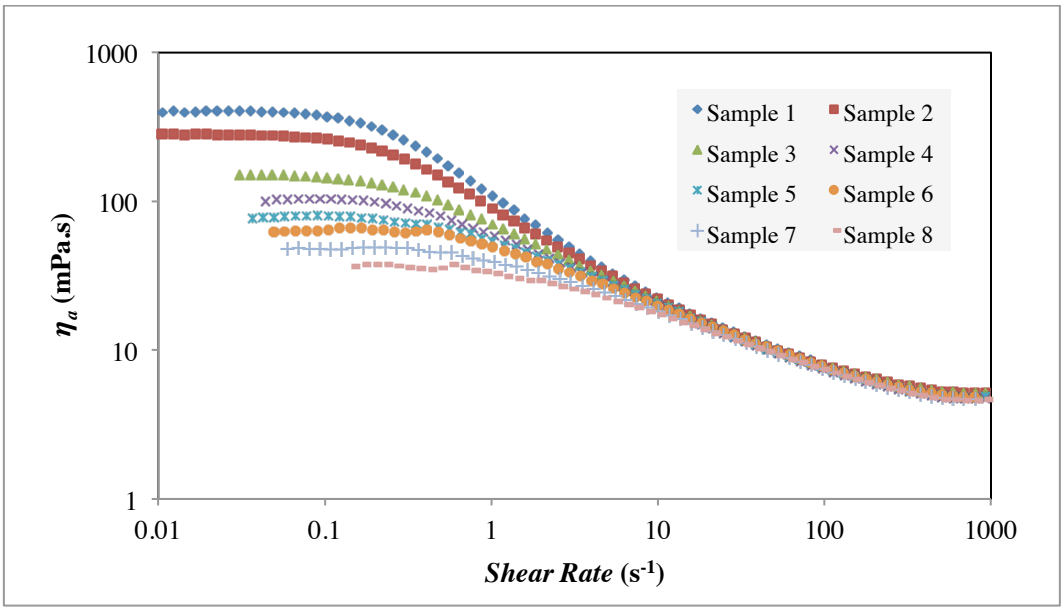

Fig. 21. Apparent viscosity of 200 wppm sheared HPAM samples (Sample 1 to 8: Fresh, 15, 30, 45, 60, 80, 100, and 120 minutes shearing time)

Prandtl-Karman coordinates are a semi-log graph of $f^{-½}$ versus $Re.f^{½}$, where f and Re are Fanning friction factor and Reynolds number, respectively. Using Prandtl-Karman coordinates, the degree of DR of polymer solutions can be compared with respect to the boundaries of drag reduction; the onset of drag reduction as the point of departure from Prandtl-Karman law and maximum drag reduction (MDR) or Virk's asymptote [36, 38]. Prandtl-Karman plot for different concentrations of HPAM is shown in Fig. 4. Three flow regimes can be detected:

a) $Re\sqrt{f} < 200$; laminar flow. All polymer solutions obey Poiseuille's law.

b) $200 < Re\sqrt{f} < 350$; laminar to turbulent transition.

c) $Re\sqrt{f} > 350$; turbulent flow.

It is observed that except for the laminar to turbulent transition region, the turbulent friction factor data for the solutions is bounded in the area between the two universal asymptotes and the data points are linear for all concentrations.

Table 3. Linear fit results of DR data in the turbulent regime for HPAM solutions

Concentration	Linear fit equation	R^2	Slope increment (δ)
100 wppm	$1/\sqrt{f} = 6.0 \log Re\sqrt{f} - 4.1$	0.99	2.05
150 wppm	$1/\sqrt{f} = 7.1 \log Re\sqrt{f} - 4.4$	0.99	3.09
200 wppm	$1/\sqrt{f} = 9.3 \log Re\sqrt{f} - 7.3$	0.99	5.28
500 wppm	$1/\sqrt{f} = 9.6 \log Re\sqrt{f} - 8.2$	0.99	5.60
1000 wppm	$1/\sqrt{f} = 12.8 \log Re\sqrt{f} - 15.9$	0.99	8.81

Results of linear fitting of the data points in the turbulent region (Table 3) revealed that by increasing polymer concentration, the slope of the lines tended to increase. According to the literature the slope increment with respect to the Prandtl-Karman law (δ) is proportional to the square root of polymer concentration ($\delta \propto \sqrt{C}$) with a proportionality constant that is the characteristic of the polymer [37]. The slope increment values are reported in Table 2. The proportionality constant for the HPAM is calculated to be 0.27±0.05. Figure 22 shows that by increasing HPAM concentration, the extent of DR increased and the data points approached Virk's asymptote. Among different concentrations, the extent of DR and slope of data points for 100 wppm HPAM solution were closest to the Prandtl-Karman line (the onset of DR). On the other hand, the greatest DR belonged to 1000 wppm solution. For solutions with polymer content greater than 200 wppm, in $200 < Re\sqrt{f} < 500$ range, the data points were nearly tangent to the MDR line, but by increasing the flow rate (Reynolds number), the data points tended to deviate from MDR. Results indicated that further increase of concentration did not have a large effect on the degree of DR in the experimental conditions of this work.

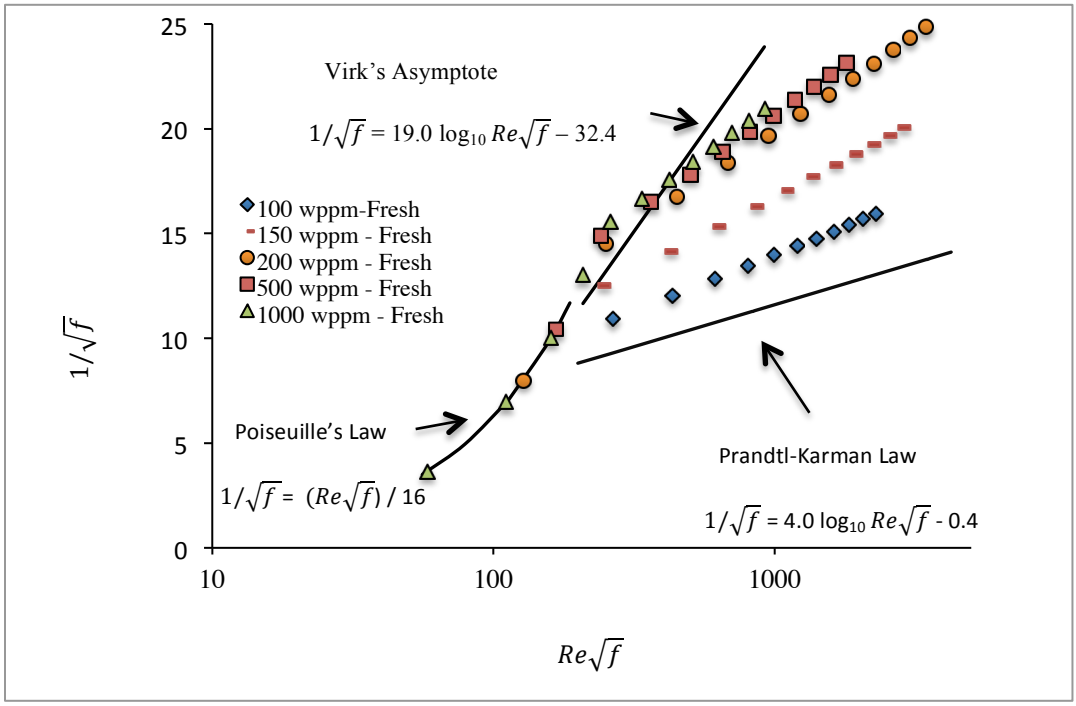

Fig. 22. Prandtl-Karman coordinates for HPAM solutions

The effect of polymer concentration and mechanical degradation on Fanning friction factor of HPAM solutions is shown in Figs. 23a, b, respectively. It was observed that even at low concentrations of polymer (100 wppm), Fanning friction factor values were very small compared to water. Increasing polymer concentration resulted in further reduction in friction factors (data points moved towards maximum drag reduction asymptote) and consequently, drag reduction efficiency increased. The smallest friction factor values at different Reynolds numbers belonged to 1000 wppm solution. It was also observed that the difference between turbulent friction factors of 200, 500, and 1000 wppm solutions was very small, which is in agreement with the results shown in Prandtl-Karman coordinates, indicating that at the studied range of Reynolds numbers DR efficiency was close to its maximum value (MDR). Further concentration increase did not change friction factors. It was also found that as the Reynolds numbers increased, the data points tended to deviate from MDR.

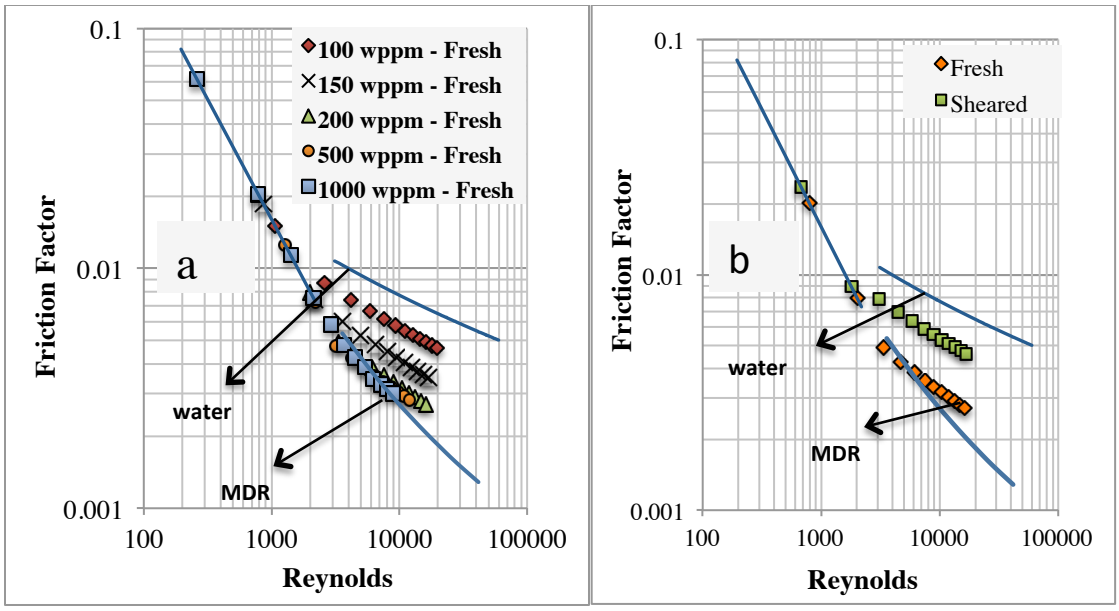

Fig. 23. Friction factor vs. Re: a) Effect of HPAM concentration, b) Effect of shearing on 200 wppm HPAM

Shearing had a large impact on reducing the DR ability of polyacrylamide solutions. Comparison of the friction factors of 200 wppm HPAM solution at different Reynolds numbers (Fig. 23b) showed a 30 - 50 % decline after 2 hours of shearing. It was observed that as a result of shearing, friction factor values moved from MDR line and shifted towards water friction factors in the studies range of Reynolds numbers. In spite of constant flow rate in all of the experiments, a shift in the data points of the sheared samples towards lower Reynolds numbers was observed. The shift was an indication of alteration in the flow regime, which occurred due to the change in the rheological properties of the solutions as a result of shear degradation. Figure 24 shows the changes in the DR% over shearing time for different concentrations of HPAM at constant flow rate. It was observed that, for fresh samples (t = 0), the extent of DR increased from 30% to 67% by increasing polymer concentration from 100 wppm to 1000 wppm. Results also indicated that solutions above 200 wppm produced nearly identical DR at the early stages of shearing (t < 20 minutes), which corresponds to the results shown in Prandtl-Karman coordinates (Fig. 22). But beyond 20 minutes, the DR curves tended to diverge, indicating that the degree of shear

degradation was different for each polymer solution. Ptasinski et al. [40] reported that in flexible polymers such as HPAM, as shear force reached a certain level, molecules stretched and effective viscosity increased, and consequently the turbulent buffer layer thickened, and due to dissipation of the energy from turbulent fluctuations drag was reduced. It is also known that drag is reduced when turbulent flow interacts with polymer networks. When polymer concentration is high enough (above critical overlap concentration, C^*), polymer chains are packed closer and begin to interact with each other and form entangled networks [21].

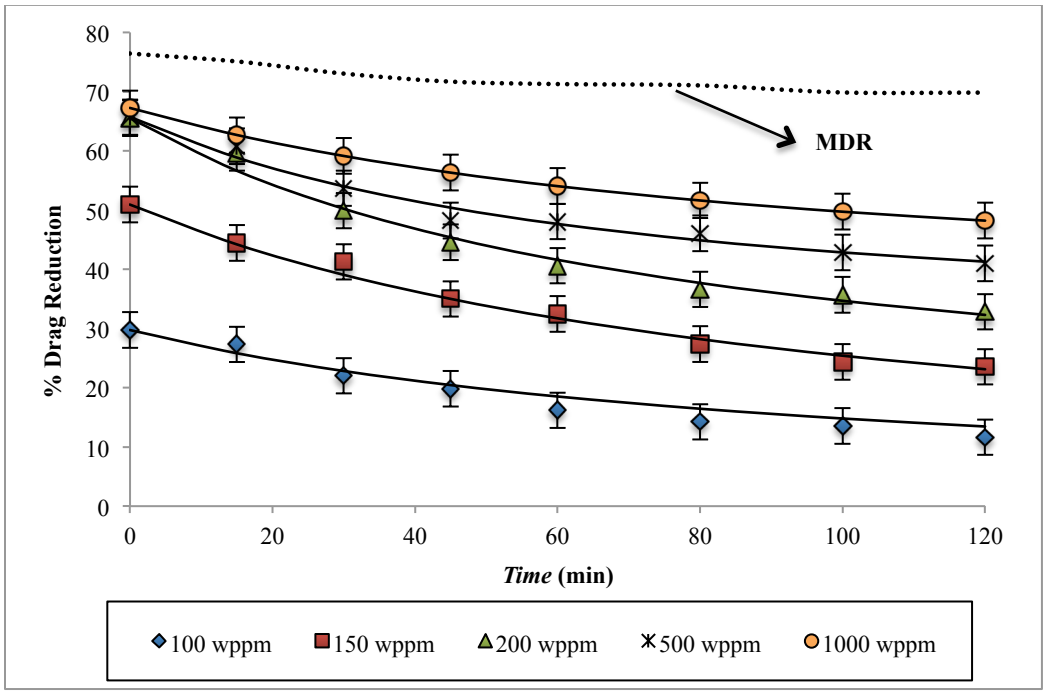

Fig. 24. Drag reduction behavior of different concentrations of HPAM at 30 GPM (113.56 l/min)

A decline was observed in the degree of DR of all concentrations of HPAM solution. Resistance to mechanical degradation over the shearing period is shown in Fig. 25.

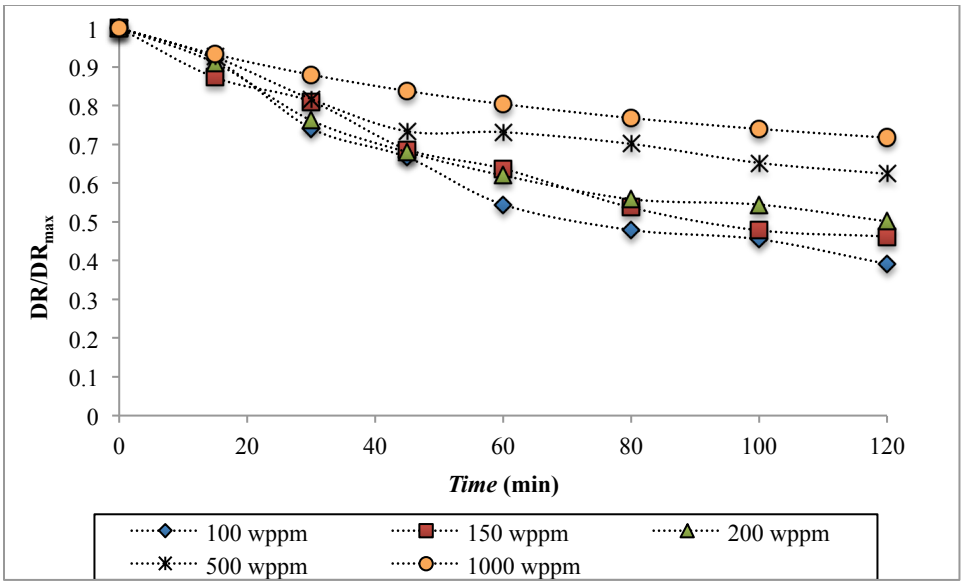

Fig. 25. Resistance to mechanical degradation (DR/DR_{max}) for HPAM Solutions at 30 GPM (113.56 l/min)

Results showed that, as concentration increased, resistance to mechanical degradation increased. This made the 100 wppm solution the least resistant and 1000 wppm solution the most resistant to mechanical degradation among HPAM solutions. These results agreed with those reported by Soares et al. (2015), who reported that increasing polymer concentration (PAM or PEO) in the solution increased resistance to mechanical degradation. It was also observed that the shear stabilities of 100, 150, and 200 wppm solutions were very close and followed the same trends. In other words, the 200 wppm solution was only slightly more resistant to degradation ($DR_{t=120}/DR_{max} = 0.5$) than 100 wppm solution ($DR_{t=120}/DR_{max} = 0.39$). But above 200 wppm, a sudden rise in the shear resistance of the solutions was observed. Both 500 and 1000 wppm solutions showed superior shear stability compared to other solutions. We found that although 200 wppm HPAM solution had similar initial DR% to 500 and 1000 wppm solutions (Fig. 24), it had a larger decline in DR (Fig. 25). The values of $DR_{t=120}/DR_{max}$ for 500 and 1000 wppm solutions were 0.62 and 0.72 at the end of 2-hour shearing period, respectively. It is also interesting to note that the DR/DR_{max} declined at a slower rate after $t = 60$ min. For example, the

reduction in DR/DR_{max} value for 1000 wppm solution from t = 60 min to t = 120 min was only 0.06.

From viscosity measurements, critical overlap concentration (the concentration that marks the beginning of polymer-polymer interaction) of the HPAM solution was determined to be 160 wppm. At C < 200 wppm, there was no polymer network, so there was no decline due to polymer network breakup, but at C > 200 wppm, the networks were more entangled and upon deformation could recover quickly. Also, it seemed that at higher concentrations (C > 200 wppm), the extensional force from the turbulent flow was distributed among larger number of molecules, which resulted in lower number of chain scissions and higher DR stability. But at C < 200 wppm polymer networks just began to form and were weak. Therefore, at the beginning of the shearing process DR efficiency increased, but gradually as shear forces acted, unstable polymer networks, as well as individual polymer molecules broke up, which resulted in a large decline in the DR efficiency of C < 200 wppm HPAM solutions compared to higher concentrations.

It was found that the rate of DR decline was fast in the first 60 to 80 minutes of the shearing process. This is probably due to the presence of longer polymer chains in the fresh solutions, which were more susceptible to chain scission (required less energy to break). After 60 minutes, the gap between DR lines (Fig. 24) remained nearly constant, which indicated that polymer chains were broken up at similar rate in all of the solutions.

Several models for correlating the DR behavior of polymer solutions is found in the literature. Two of the most common models are exponential decay model [78] and Brostow's model [63]. Based on the exponential decay model proposed by Bello et al. (1996), DR follows an exponential decline with time for polyacrylamide and polysaccharide solutions:

$$\boldsymbol{DR\%(t)/DR\%(0) = e^{(-t/\lambda)}} \quad \textbf{(17)}$$

where DR%(t) and DR%(0) (or DR_{max}) are percent drag reduction at times t and t = 0, respectively, and λ is an adjustable parameter. Brostow's equation is a more general model, which has been applied to various shear degradation applications [79] and has been developed to quantitatively describe DR and its changes with time:

$$\boldsymbol{DR\%(t)/DR\%(0) = [1 + W(1 - e^{(-ht)})]^{-1}} \quad \textbf{(18)}$$

Here W is the average number of vulnerability points per chain and h is called rate constant.

Both models were used to correlate the DR data of HPAM and HPAM/XG solutions. Calculated model parameters and goodness of fitting (R^2) for both models are reported in Table 4. The solid lines in Fig. 24 represent the fitting results. It was found that for the studied concentrations of HPAM solutions, both models described the degradation behavior well. Though, Brostow's model gave better fits and the predicted values of it were more accurate.

Table 4. Calculated parameters of Brostow and exponential decay models for HPAM solutions

Concentration (wppm)	**Exponential Decay Model**		**Brostow's Model**		
	λ (min)	**R^2**	**W**	**h (min^{-1})**	**R^2**
100	87.32	0.96	374.2	32.7 e-5	0.94
150	146.7	0.97	43.43	2.31 e-4	0.98
200	162.3	0.95	2.723	3.90 e-3	0.99
500	245.0	0.90	0.8628	9.63 e-3	0.98
1000	312.1	0.88	0.6351	8.12 e-3	0.96

3.3.2 Xanthan gum solutions

The extent of drag reduction in rigid polymers depends on concentration and molecular weight of the polymer [15]. In order to verify the effect of XG concentration on the extent of drag reduction, various concentrations of XG solutions were prepared, characterized, and sheared in the flow loop at maximum flow rate. Several samples were taken at specified intervals over the shearing process, and shear stress and apparent viscosity of the samples were measured in the rheometer, and Carreau-Yasuda parameters were calculated. The calculated Carreau-Yasuda parameters for the studied polymer solutions are shown in Table 5.

Table 5. Calculated parameters of Carreau-Yasuda model for GG, XG, HPAM/XG and HPAM/GG solutions

Concentration (wppm)	η_0 (pa.s)	η_∞ (Pa.s)	λ (s)	a	n
300 ppm XG	0.039	0.0031	1.98	2.47	0.54
600 ppm XG	0.269	0.0040	5.34	1.92	0.43
1000 ppm XG	0.829	0.0042	5.89	1.30	0.38
150 ppm HPAM + 300 ppm XG	0.376	0.0046	4.42	2.10	0.38
150 ppm HPAM +500 ppm XG	0.252	0.0044	4.52	2.33	0.38
500 ppm GG	0.004	0.0028	0.64	0.71	0.89
1000 ppm GG	0.006	0.0042	1.46	0.81	0.78
2000 ppm GG	0.024	0.0044	2.81	0.56	0.64
150 ppm HPAM +1000 ppm GG	0.122	0.0045	4.23	3.65	0.53

Prandtl-Karman coordinates are a semi-log graph of $f^{-1/2}$ versus $Re.f^{1/2}$, where f and Re are Fanning friction factor and Reynolds number, respectively. By plotting the Prandtl-Karman coordinates, the degree of DR of polymer solutions can be compared with respect to the boundaries of drag reduction; the onset of drag reduction as the point of departure from Prandtl-Karman law and maximum drag reduction (MDR) or Virk's asymptote [36, 38]. Prandtl-Karman plot for different concentrations of XG is shown in Fig. 26. Similar to HPAM solutions, three flow regimes was detected:

- $Re\sqrt{f} < 200$; laminar flow. All polymer solutions obey Poiseuille's law.
- $200 < Re\sqrt{f} < 350$; laminar to turbulent transition.
- $Re\sqrt{f} > 350$; turbulent flow

It was observed that as the concentration increased the data point moved towards the MDR (maximum drag reduction asymptote). Among XG solutions, the extent of DR and slope of data points for 300 wppm solution were closest to the Prandtl-Karman line (the onset of DR). On the other hand, the greatest DR belonged to 1000 wppm solution. Results indicated that by increasing the flow rate (Reynolds number), the data points tended to deviate from MDR. It was also observed that the extent of DR of XG solutions was no way near the MDR values. It is expected that with further increase of concentration (above 1000 wppm) DR degree would increase.

Results of linear fitting of the data points in the turbulent region (Table 6) revealed that by increasing polymer concentration, the slope of the lines slightly increased. According to the literature the slope increment with respect to the Prandtl-Karman law (δ) is proportional to the square root of polymer concentration ($\delta \propto \sqrt{C}$) with a proportionality constant that is characteristic of the polymer [37]. The slope increment values are reported in Table 6. The proportionality constant for the studied XG solutions was calculated to be 0.08±0.008.

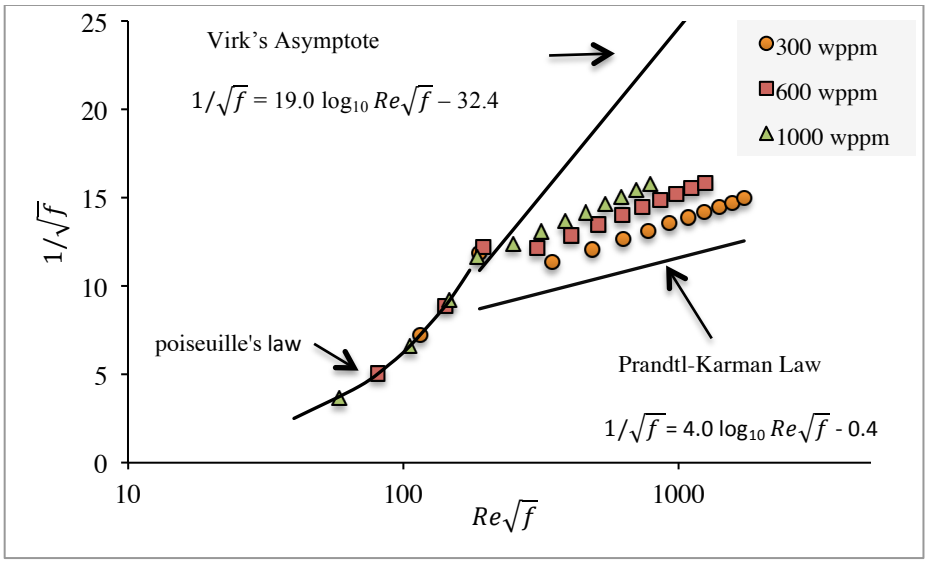

Fig. 26. Prandtl-Karman coordinates for XG solutions

Table 6. Linear fit results of DR data in turbulent regime for XG solutions

Concentration	Linear fit equation	R-Squared	Slope Increment (δ)
300 wppm	$1/\sqrt{f} = 5.18 \log Re\sqrt{f} - 1.82$	0.99	1.18
600 wppm	$1/\sqrt{f} = 6.08 \log Re\sqrt{f} - 2.99$	0.99	2.08
1000 wppm	$1/\sqrt{f} = 6.76 \log Re\sqrt{f} - 3.83$	0.99	2.76

The plot of drag reduction behavior of XG solutions at constant flow rate in a 2-hour flow experiment is shown in Fig. 27. It was observed that, for fresh samples (t = 0), the extent of DR increased from 26% to 45% by increasing XG concentration from 100 wppm to 1000 wppm, which was consistent with the results shown in Fig. 26. The DR results also indicated that at the studied concentrations, the DR efficiencies were well below the MDR.

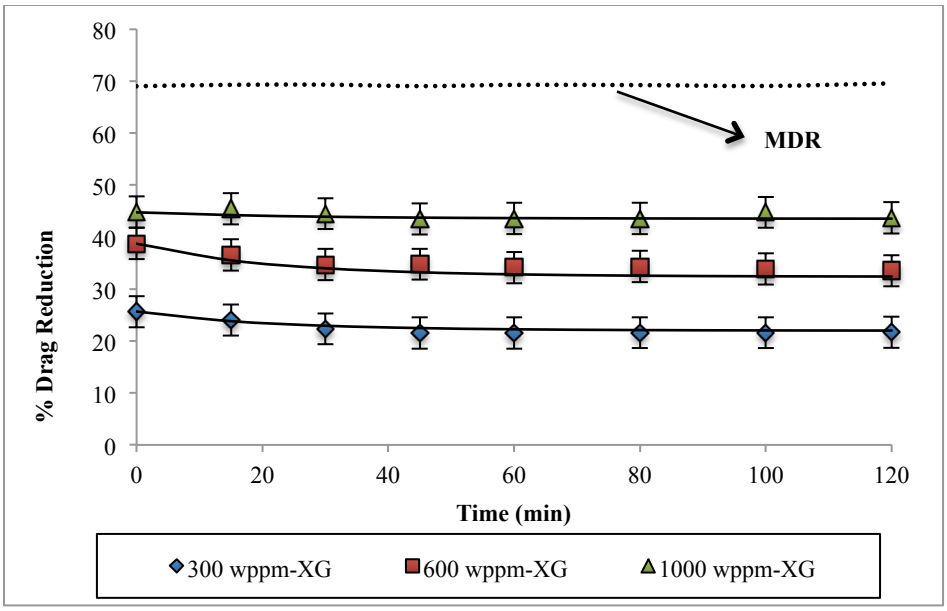

Fig. 27. Drag reduction behavior of XG solutions at 30 GPM (113.56 l/min)

Resistance to mechanical degradation (DR/DR_{max}, where DR_{max} is the extent of DR at t = 0) is shown in Fig. 28. It was observed that all XG solutions exhibited high shear resistance to mechanical degradation. At the end of the shearing period (t = 120 min), $DR_{t=120}/DR_{max}$ values for 300, 600, and 1000 wppm solutions were 0.85, 087, and 0.97, respectively. These values were higher than $DR_{t=120}/DR_{max}$ values of HPAM solutions ($DR_{t=120}/DR_{max}$=0.72 for 1000 wppm HPAM), indicating that XG solutions were more resistant to shear degradation. Increasing concentration resulted in an increase in the shear stability, as well as the DR efficiency of the solutions. The 1000 wppm solution exhibited the highest DR stability among XG solutions. Soares et al. [80] similarly observed that increasing polymer concentration (PAM or PEO) in the solution increased the resistance to mechanical degradation.

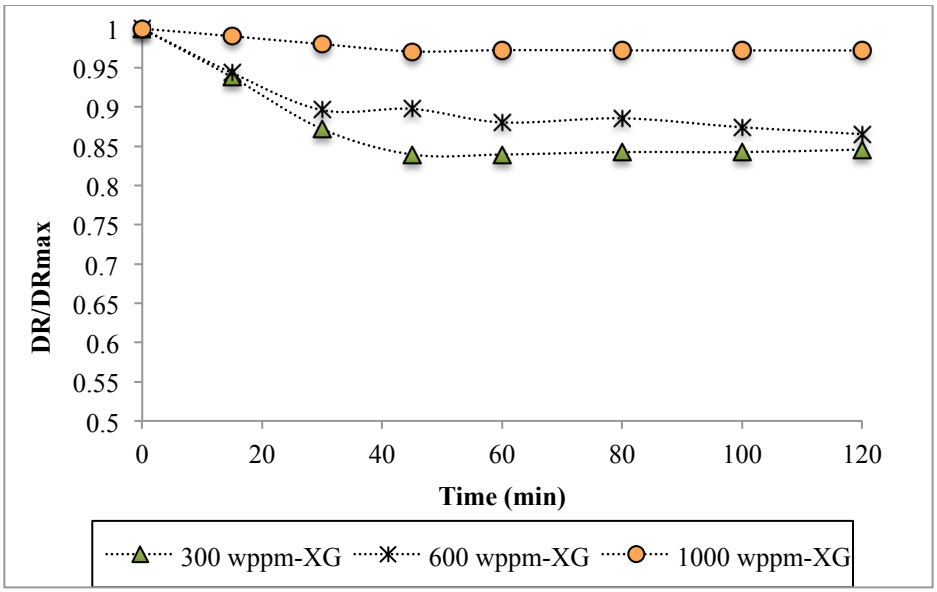

Fig. 28. Shear resistance of XG solutions at 30 GPM (113.56 l/min)

Both exponential decay and Brostow's models were used to correlate the DR behavior of polymer solutions. Calculated model parameters and goodness of fitting values (R^2) for both models are reported in Table 7 and the solid lines in Fig. 27 represent the fitting results from Brostow's model. It was observed that Brostow's model could predict the DR behavior of XG solutions very well. Brostow's model gave better fits and the predicted values were more accurate. On the other hand, the R^2 values for the exponential decay model were small, indicating that Bello's model was not suitable for the studied XG solutions.

Table 7. Calculated parameters of Brostow and exponential decay models for XG solutions

Concentration (wppm)	Exponential Decay Model		Brostow's Model		
	λ (min)	R^2	W	h (min^{-1})	R^2
300	488.47	0.29	0.1971	0.04115	0.95
600	571.40	0.32	0.1664	0.04118	0.91
1000	3037.5	0.34	0.0294	0.03957	0.98

3.3.3 Guar gum solutions

The measured friction factor values for GG solutions at various flow conditions are shown in Prandtle-Karman coordinates (Fig. 29). It was found that the data points for 500 wppm GG solution were very close to the Prandtle-Karman line (onset of DR). As GG concentration increased, the data points moved from the onset of DR line. Overall, it was observed that the data points (even for 2000 wppm solution) were far from reaching the maximum drag reduction asymptote.

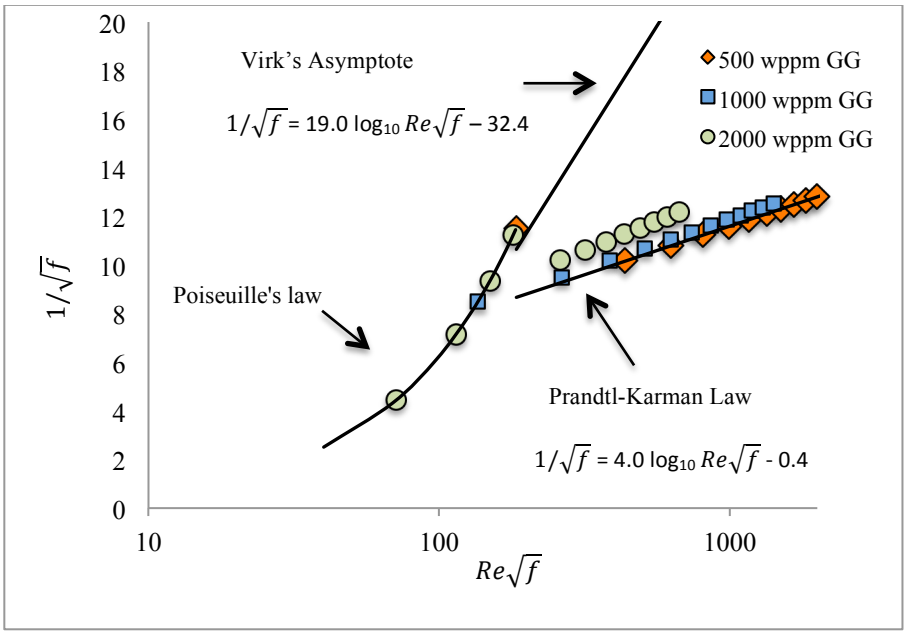

Fig. 29. Prandtl-Karman coordinates for GG solutions

Drag reduction behavior of different concentrations of GG solutions is shown in Fig. 30. The first observation was that the extent of DR was much lower compared to HPAM and XG solutions. At concentrations below 1000 wppm the solutions behaved like Newtonian fluids and the DR approached to very small values (DR < 1% for 500 wppm GG). As mentioned earlier GG is not a flexible molecule and the extent of drag reduction depends only on concentration and molecular weight of the polymer and drag reduction occurs as a result of the interactions of polymer networks with turbulent flow [34, 51, 52]. The first critical overlap concentration for GG

solution was measured to be ~720 wppm, which is greater than that of XG and HPAM (260 and 160 wppm, respectively). This implied that, in order for GG to be an effective friction reducer, the required polymer concentration should be greater than the concentration required for XG or HPAM. Our results indicated that due to polymer chain entanglement, the degree of DR began to increase at C > 1000 wppm. The DR efficiencies of 1000 and 2000 wppm solutions were measured to be 5% and 18%, respectively. It was also found that GG solutions were excellent at resisting the shear forces and mechanical degradation was zero.

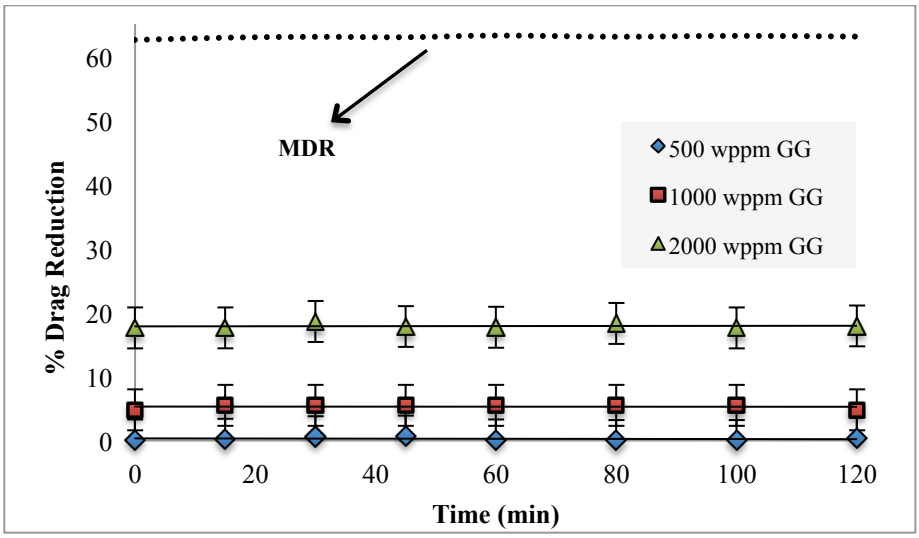

Fig. 30. Drag reduction behavior of GG solutions at 30 GPM (113.56 l/min)

3.3.4 HPAM/GG binary solutions

The drag reduction behavior of a HPAM/GG, HPAM, and GG solutions is shown in Fig. 31. Comparison of the DR efficiency of the solutions, before shearing (t = 0), showed that the efficiency of the binary solution (41%) was 10% below the value of 150 wppm HPAM. After shearing, DR efficiency of HPAM solution was still greater than that of the HPAM/GG solution (until t = 100 min), indicating that addition of GG did not have a positive effect on the DR efficiency of binary solutions.

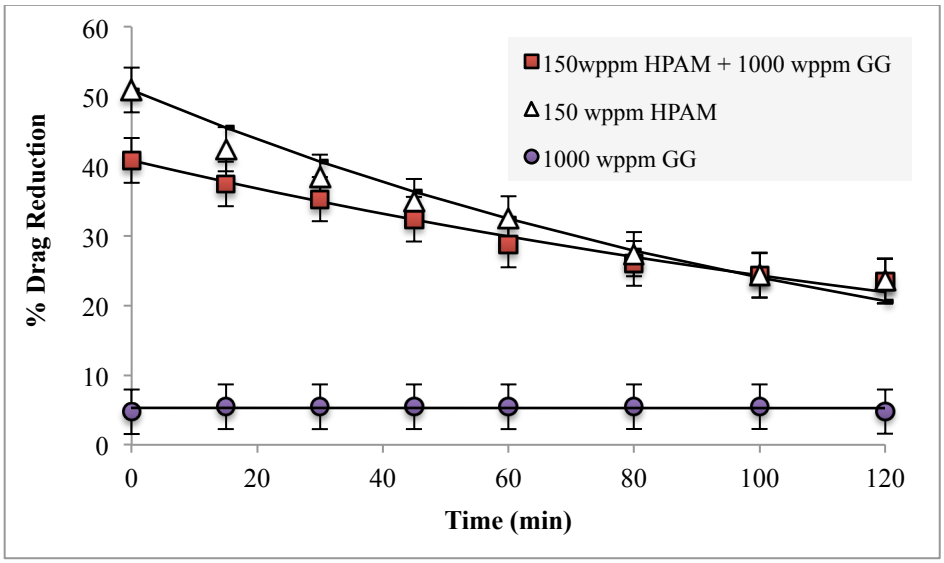

Fig. 31. Drag reduction behavior of HPAM/GG mixed solution at 30 GPM (113.56 l/min)

Comparison of the shear resistance data of the solutions is displayed in Fig. 32. The results indicated that the shear resistance of 1000 wppm GG solution was excellent (DR/DR_{max}~1). Comparison of DR/DR_{max} of the HPAM/GG and HPAM solutions showed that the binary solution was more resistant to mechanical degradation. The decline in DR of 150 wppm HPAM+ 1000 wppm GG solution after 2 hours was 17%, whereas for HPAM solution 27% decline was observed.

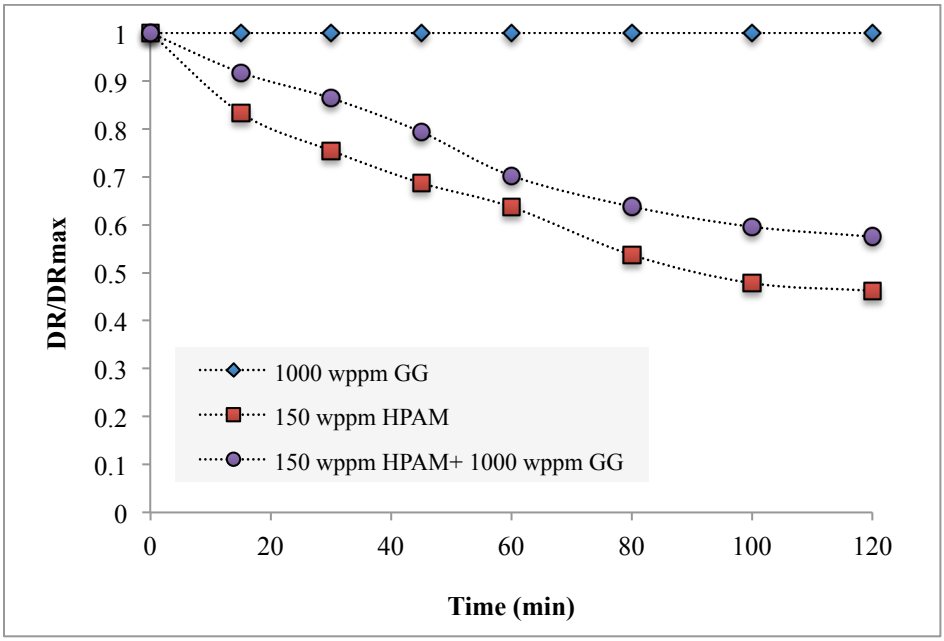

Fig. 32. Shear resistance of GG and HPAM/GG mixed solutions

3.3.5 HPAM/XG – Low concentration (C < 300 wppm)

In order to verify the possibility of stabilizing HPAM with XG, mixed solutions were prepared and sheared in the same manner as single polymer solutions. Based on the results obtained from the previous sections, among HPAM solutions, the 200 wppm solution was the optimum solution regarding DR efficiency and polymer concentration. Several authors have mentioned that the degree of DR in XG solutions depends on the concentration and molar mass of XG [15, 80]. So higher concentrations of XG are required to reach the same level of DR as HPAM. Our preliminary experiments showed that the DR efficiency of 600 wppm XG was close to the DR values of 200 wppm HPAM. Therefore, DR behaviors of binary polymer solutions were compared to those of 200 wppm HPAM and 600 wppm XG solutions.

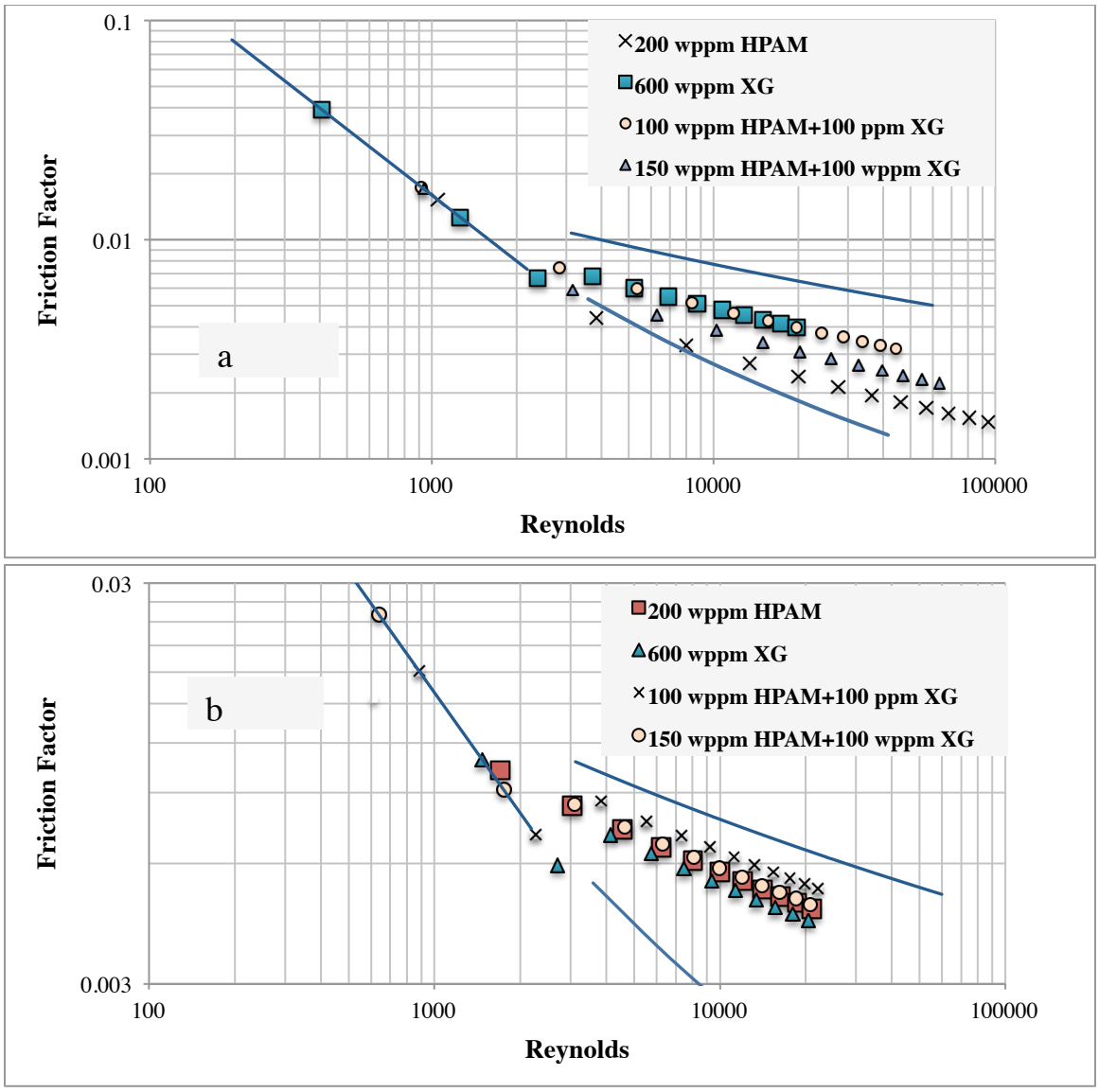

Fig. 33. Fanning friction factor of mixed solutions in a) fresh form and b) after shearing for 120 minutes

The Carreau-Yasuda model fitting results of the mixed solutions, as well as 200 wppm HPAM and 600 wppm XG solutions are included in Table 8. Also, friction factors of the binary and 600 ppm XG and 200 wppm HPAM solutions at various Reynolds numbers are displayed in Fig. 33a. It was found that, although polymer concentration in the 600 wppm XG solution was greater than that of 200 wppm HPAM solution, the 600 wppm XG solution possessed greater friction factors. Higher flexibility of HPAM polymer chains with respect to semi-rigid XG chains

resulted in higher energy adsorption (stretching) due to interaction with dynamic turbulent flow and subsequently, superior drag reduction capability of HPAM. Also, it was found that in the fresh binary solutions, there was no outstanding synergetic effect between HPAM and XG molecules. Even for the 150 wppm HPAM+100 wppm XG solution, which had higher total polymer concentration, the friction factors were greater than 200 wppm HPAM.

Table 8. Parameters of Carreau-Yasuda model for HPAM, XG and HPAM/XG solutions

Concentration, wppm	η_0 (Pa·s)	η_∞ (Pa·s)	λ (s)	a	n
200 ppm HPAM	0.3717	0.0042	5.80	3.14	0.27
600 ppm XG	0.2689	0.0040	5.34	1.92	0.43
100 ppm HPAM + 100 ppm XG	0.1331	0.0039	4.18	2.51	0.36
150 ppm HPAM +100 ppm XG	0.2873	0.0038	7.2	2.28	0.33

Comparison of the friction factors of the solutions after 120 minutes of shearing is displayed Fig. 33b. Because of high shear stability, XG solution maintained its initial friction reduction efficiency, with a relatively small change in friction factor values. But for the mixed HPAM/XG solutions, the friction factor values increased as a result of shearing. It is interesting to note that, 200 wppm HPAM solution had a larger increase in its friction factors than mixed solutions (Fig. 33b). This suggested that addition of XG was beneficial in controlling the shear degradation of HPAM. The decline in the DR efficiency and shear resistance of the solutions over shearing time is shown in Figs. 34 and 35. Also, similar to single polymer solutions, Brostow's and exponential decay models were used to correlate DR with time (solid lines in Fig. 34 and Table 9).

Table 9. Parameters of Brostow and exponential decay models for single and binary HPAM and XG solutions

Concentration (wppm)	Exponential Decay Model		Brostow's Model		
	λ (min)	R^2	W	h (min^{-1})	R^2
200 (HPAM)	145	0.92	1.792	6.8 e-3	0.99
600 (XG)	571	0.94	0.3853	8.8 e-3	0.96
100 (HPAM)+100 (XG)	137	0.92	44.49	2.2 e-4	0.96
150 (HPAM)+100 (XG)	127	0.89	1.768	8.4 e-3	0.99

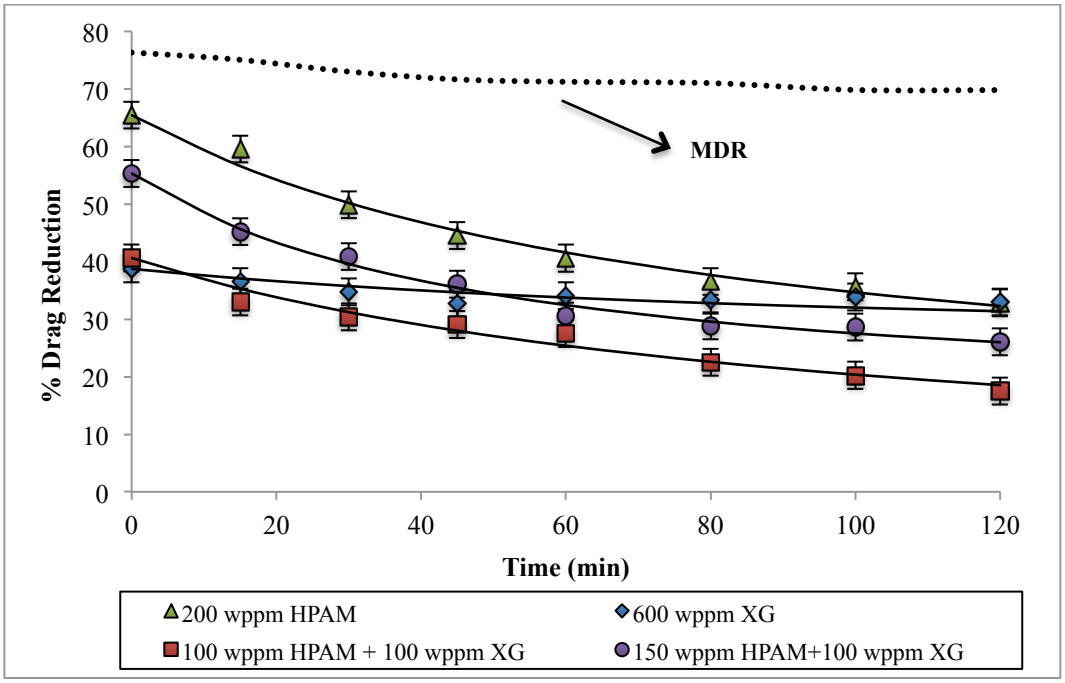

Fig. 34. Drag reduction behavior of mixed HPAM/XG solutions at 30 GPM (113.56 l/min)

The results showed that the DR efficiencies of both HPAM/XG binary solutions were smaller than that of 200 wppm HPAM solution, indicating that partially replacing HPAM with XG in the binary solutions had reduced the DR efficiency of the single HPAM solution. Regarding the DR behavior of HPAM/XG binary mixtures, different views were found in the literature. Sandoval

and Soares recently reported that the DR efficiency of HPAM/XG mixture is close to the DR values of the single HPAM solution at the same total concentration [58]. Though, they confirmed that the synergetic effect in PAM/XG mixture is not as notable as PEO/XG. Reddy and Singh also verified PAM/XG mixtures and reported that the single PAM solution has a higher DR efficiency than binary mixture. Their data was limited to fresh solutions. We believe that the differences in the reported data might be attributed to the differences in the experimental conditions. In our work, since we were dealing with two negatively charged polymers in the solution, we expected to obtain different results. We also believe that due to the higher flexibility (higher molecular weight) of the anionic HPAM used in our experiments, HPAM molecules were more susceptible to scission and the interaction between HPAM and XG was reduced. Compared to 600 wppm XG solution, the DR% of 100 wppm HPAM/150 wppm XG solution was high only in the first 60 minutes of the shearing process and after that, as a result of mechanical degradation the DR values declined. Also, it was found that the 100 wppm HPAM/100 wppm XG solution was less efficient in DR than the 600 wppm XG solution from the beginning till the end of the shearing period. Comparison of the shear resistance (DR/DR_{max}) of the solutions revealed that, as expected, 600 wppm XG solution had the best shear stability among all the solutions and smallest decline in DR over the shearing period (0.15 decline in DR/DR_{max} value). Contrary to XG, 200 wppm HPAM and the binary HPAM/XG solutions suffered from poor shear resistance and a large decline in their DR efficiencies was observed. These results were in agreement with the results reported by Sandoval and Soares [80]. It is interesting to note that the shear resistance of both binary solutions and 200 wppm HPAM solution were nearly identical.

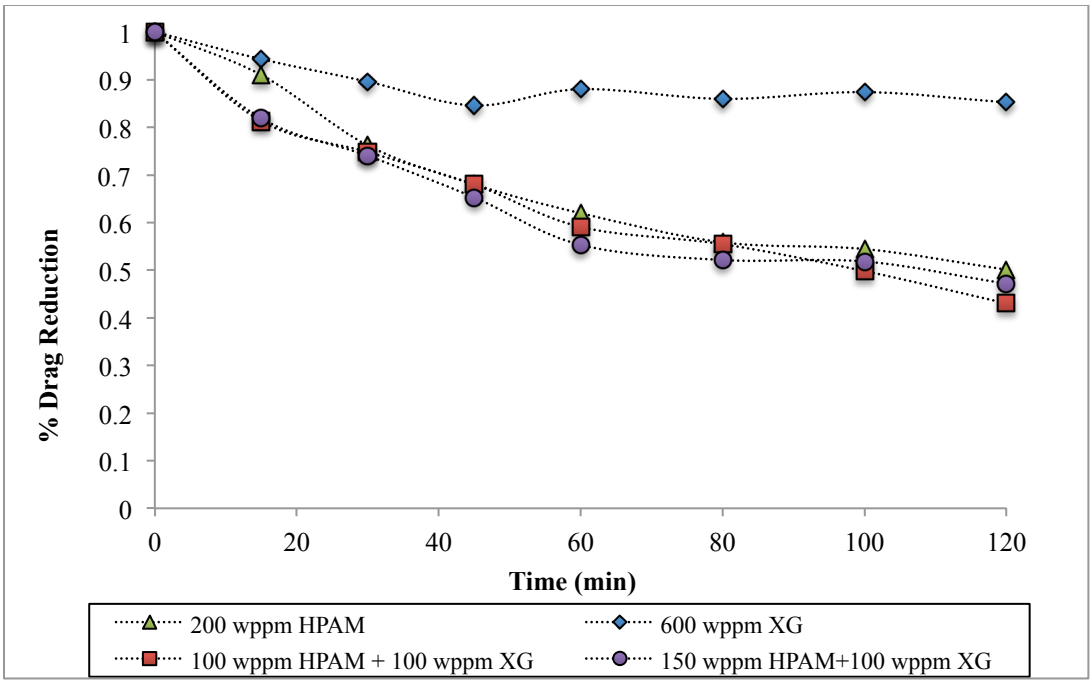

Fig. 35. Effect of shearing on DR decline for HPAM/XG mixed solutions

As concluded from friction factor data, verification of the DR data revealed that addition of XG reduced the DR capability of mixed solutions (DR% = 40% and 55%) with respect to 200 wppm HPAM solution. Also results showed that increasing HPAM concentration in the mixed solutions did not change the DR efficiency decline, significantly. Since there was only a small amount of chain degradation in semi-rigid polymers, the extent of DR depended only on the interaction between polymer chains and entanglements, which was directly related to polymer concentration. It should be considered that the concentration of XG was 100 wppm in the mixed solutions, which was below the critical concentration of XG (260 wppm). Hence, as suggested by other authors [20, 52], mixing HPAM with a higher concentration of XG would be more beneficial in maintaining high DR efficiency and even better control of shear degradation of polyacrylamide solutions, which is the subject of next section. Same as HPAM solutions, Brostow and exponential decay models were used to correlate the drag reduction behavior over time for HPAM/XG mixed solutions. The result is shown in Fig. 34 and Table 9. It was found

that both models could predict the DR behavior and similar to HPAM solutions, the Brostow's model was more suitable for correlating the DR data.

3.3.6 HPAM/XG – High concentration (C > 300 wppm)

Results obtained in the previous section showed that the synergism in binary HPAM/XG solutions having total polymer concentration below 300 wppm (low concentration mixtures) was negligible and addition of XG has slightly improved the shear stability of the HPAM/XG mixed solutions, 23% and 29% decline compared to 33% decline for 200 ppm HPAM solution. The DR behavior of HPAM/XG binary mixtures is not completely understood yet and contradicting reports is found in the literature. Sandoval and Soares recently reported that the DR efficiency of PAM/XG mixture was very close to the DR values of the single PAM solution at the same total concentration [58]. Singh et al. also verified PAM/XG mixtures and reported that the single PAM solution had higher DR efficiency than binary mixture [57]. We believe that the differences in the reported data could be due to the differences in the experimental conditions. In our work, since we were dealing with two negatively charged polymers in the solution, we expected to observe different results.

Due to the high flexibility of PAM molecules, drag reduction occurs as a result of stretching of polymer chains. Therefore, even at a concentration as low as 50 wppm high drag reduction efficiencies is achieved [39]. But, the mechanism of drag reduction is different for XG solutions. XG molecules are not as flexible as PAM molecules and since XG molecules are already in stretched form, application of shear forces does not stretch XG molecules further. Contrary to PAM, in XG solutions the degree of drag reduction depends only on polymer concentration [15]. At high polymer concentrations (greater than the first critical concentration, C*), due to the entanglement of polymer chains, flexible networks of polymer molecules form and interact with turbulent flow, which results in drag reduction. Hence, in order to obtain more efficient binary PAM/XG solutions, the concentration of XG should be greater than C*.

The drag reduction behaviors of binary polymer solutions at C > 300 ppm (total concentration) and individual polymer solutions are shown in Fig. 36. It was observed that compared to binary solutions, 150 ppm HPAM solution initially possessed higher DR (50% at t = 0), but after 10 minutes its DR efficiency declined quickly. Also, it was found that both binary solutions demonstrated higher DR efficiency compared to either 600 wppm XG or 150 wppm HPAM solutions.

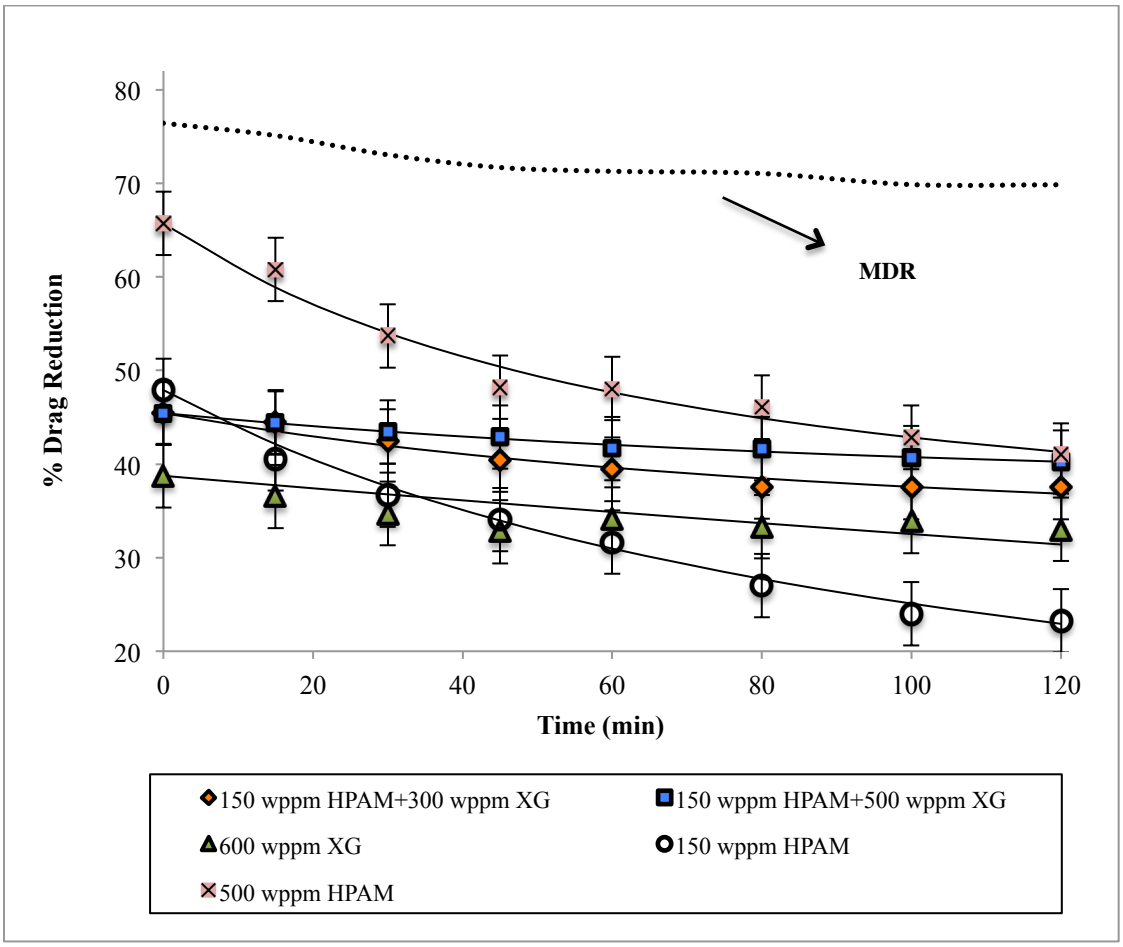

Fig. 36. Drag reduction of mixed HPAM/XG solutions (C > 300 wppm) at 30 GPM (113.56 l/min)

Shear resistance and DR decline of the polymer solutions over the shearing period are displayed in Figs. 37 and 38, respectively. According to the results, both binary solutions and the XG solution exhibited relatively high shear resistance. The $DR_{t=120}/DR_{max}$ values for binary HPAM/XG solutions were 0.88 and 0.82, and 0.85 for 600 wppm XG solution. The greatest shear

resistance belonged to 150 wppm HPAM+500 wppm XG ($DR_{t=120}/DR_{max}$ = 0.88) among polymer solutions. Although the concentrations of XG in HPAM/XG solutions were smaller than in 600 wppm XG solution, both binary solutions exhibited similar or even better shear resistances. These results suggested that addition of XG improved the shear stability of HPAM solutions to a great degree. Also, it was observed that in binary solutions, flexible HPAM molecules contributed to the formation of polymer networks along with XG molecules, which enhanced DR efficiency and mechanical resistance of the solutions. Such a result was not observed at C < 300 wppm.

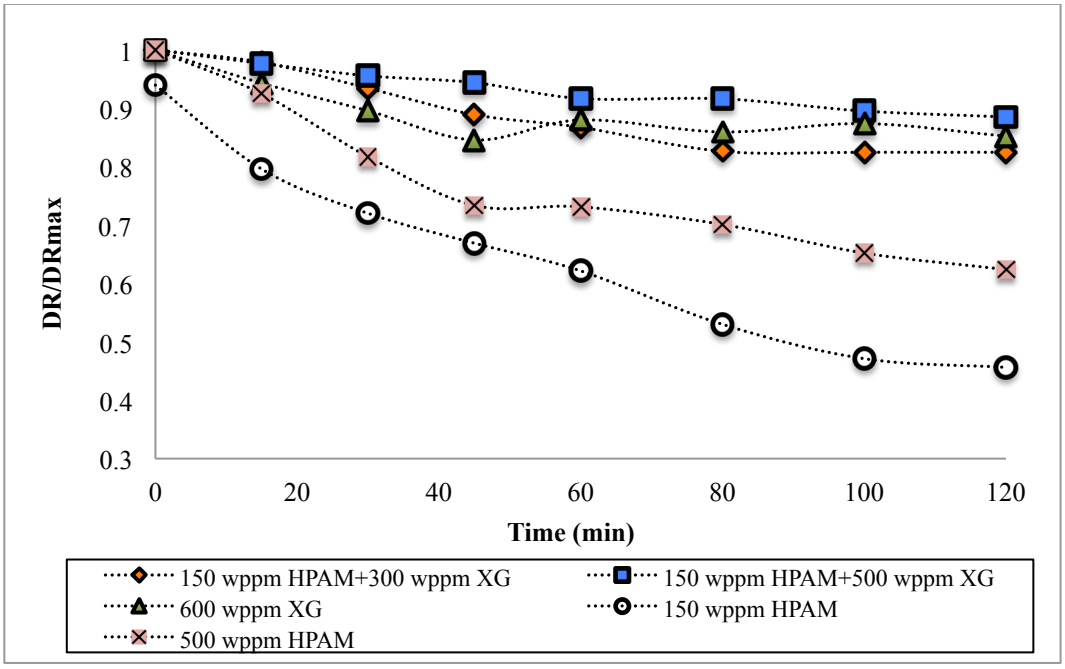

Fig. 37. Shear resistance of HPAM and HPAM/XG mixed solutions at 30 GPM (113.56 l/min)

It was clearly seen that mixed solutions exhibited greater shear stability compared to 150 wppm ($DR_{t=120}/DR_{max}$ = 0.46) and 500 wppm HPAM solutions ($DR_{t=120}/DR_{max}$ = 0.62). According to the results (Fig. 38), the DR decline over the shearing period for the binary solutions were 8% and 6%, which were close to the DR decline of 600 wppm XG solution (6%), whereas in the HPAM solutions DR decline was above 24%. Comparison of the DR behavior of mixed solutions revealed that the solution with higher XG content exhibited slightly greater drag reduction and shear stability.

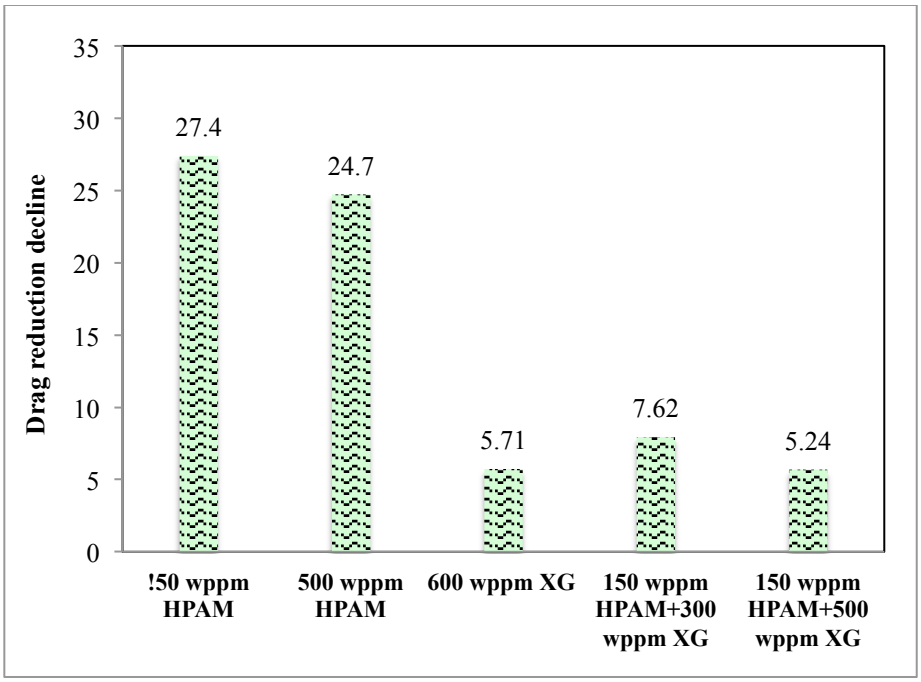

Fig. 38. Decline in DR of polymer solutions after a 2-hour shearing period

The calculated parameters for exponential decay and Brostow's models are reported in table 10 and the solid lines in Fig. 36 represent Brostow's model fits. Both models correlated the DR behavior of binary polymer solutions accurately, though Brostow's model gave more accurate fits.

Table 10. Calculated parameters of Brostow and exponential decay models for HPAM and HPAM/XG solutions

Concentration (wppm)	Exponential Decay Model		Brostow's Model		
	λ (min)	R^2	W	h (min^{-1})	R^2
150 (HPAM)	146.7	0.97	43.43	2.3 e-4	0.98
500 (HPAM)	245.0	0.90	0.8628	9.6 e-3	0.98
150(HPAM)+300(XG)	502.3	0.91	0.3583	8.8 e-3	0.96
150 (HPAM)+500(XG)	907.7	0.94	0.2019	8.5 e-3	0.98

Comparison of the DR behavior of binary solutions and 500 wppm HPAM solution (Fig. 36) showed that the HPAM solution had higher degree of DR during the experiment period. On the other hand, due to weak shear resistance (Fig. 37), DR decline for 500 wppm HPAM solution was so high (~25%) that at the end of the 2-hour shearing process, the DR dropped below the DR efficiency of the 150 wppm HPAM+500 wppm XG solution. Using the Brostow's model, the degree of DR beyond 2 hours was predicted for the polymer solutions (Fig. 39). Due to the excellent shear resistance, DR efficiency of the XG solution was almost constant beyond 2 hours of shearing. Similarly, the decline in the DR efficiency of both binary solutions was very small (~3%). The results also indicated that, as shearing time increased the DR efficiency of 500 wppm HPAM droped below the efficiency of 150 wppm HPAM+500 wppm XG solution. Based on the Brostow's model predictions, it was found that both binary solutions possessed greater DR values than the 600 wppm XG solution even after 6 hours of shearing, indicating that the synergism in mixed polymer solutions resulted in improved shear stability as well as high degree of DR.

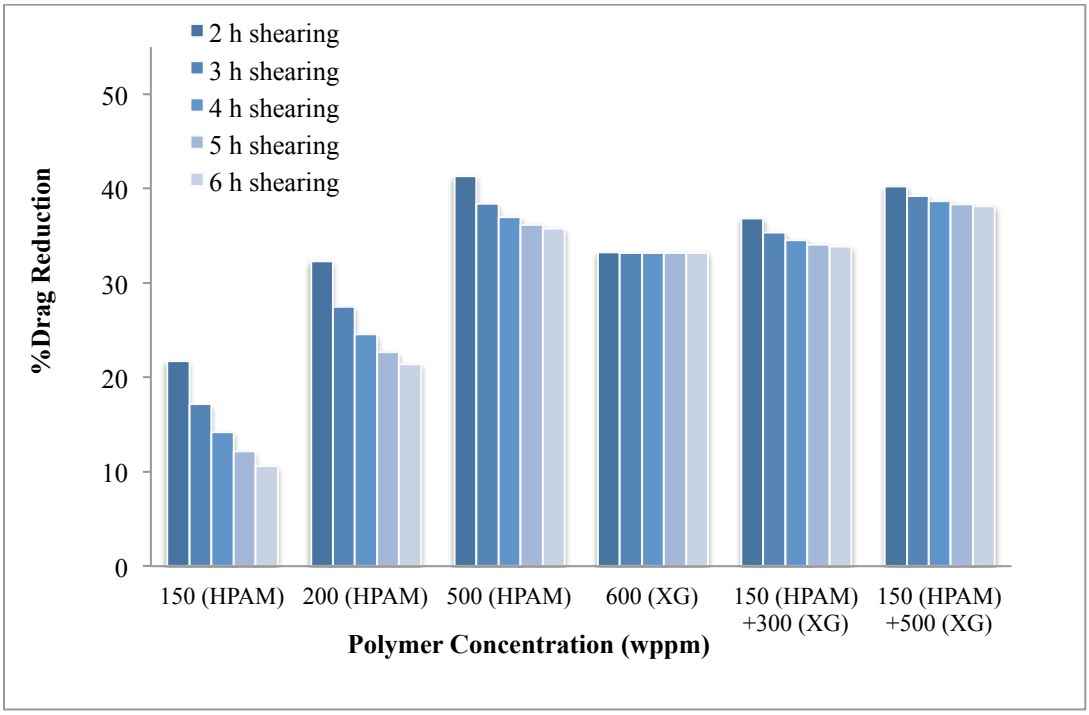

Fig. 39. Predicted drag reduction values of polymer solutions beyond 2 hour shearing period

3.3.7 Effect of solution salinity

As mentioned earlier charged polyacrylamide molecules are very sensitive to the presence of salt ions in the solution. Ionic strength of a solution have great influence on the hydration of polymer molecules and consequently their drag reduction performance [65]. The DR behaviors of 200 wppm HPAM solution in the presence of 2% KCl is shown in Fig. 40 and compared with the same solutions without salt. It was observed that the presence of salt significantly reduced the DR efficiency of the HPAM solution from 65% to 2%. The solution with salt ions in it behaved like a Newtonian fluid with near zero DR efficiency.

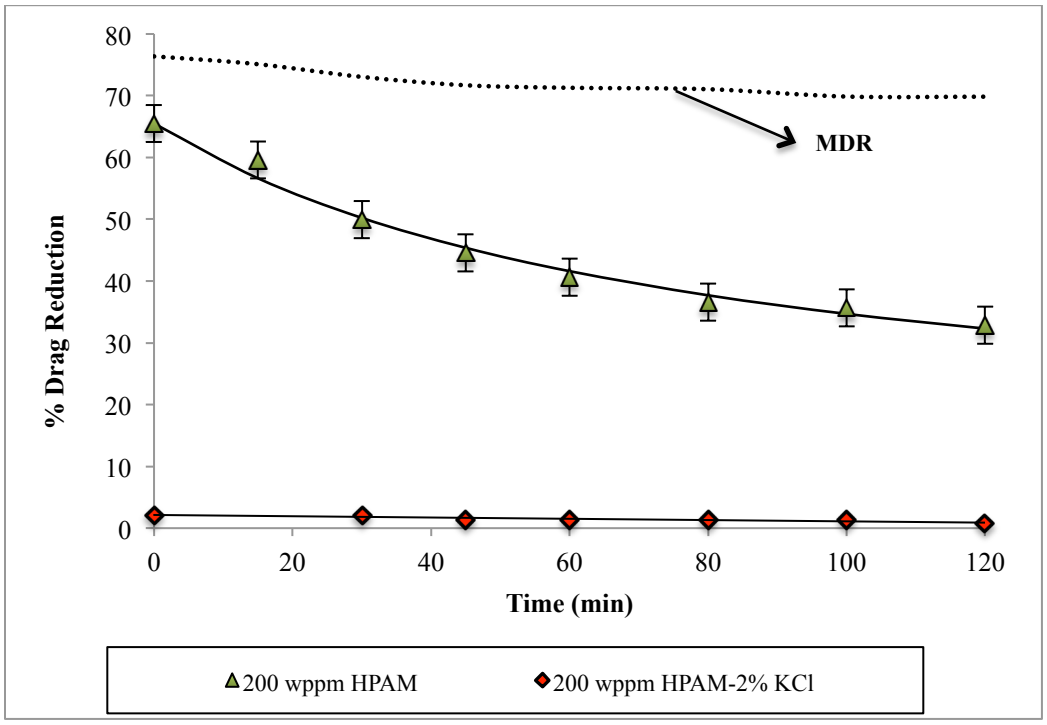

Fig. 40. Drag reduction efficiency of 200 wppm HPAM-2% KCl solution at 30 GPM (113.56 l/min)

The DR behavior of 200 HPAM solution prepared using tab water (instead of deionized water) is displayed in Fig. 41. It was observed that (similar to the 2% KCl solution) the DR efficiency dropped to as low as 7% when the solvent was tab water. These results confirmed that

due to repulsive forces induced by the salt ions, negatively charged HPAM molecules were suppressed and lost their flexibility and consequently their DR efficiency.

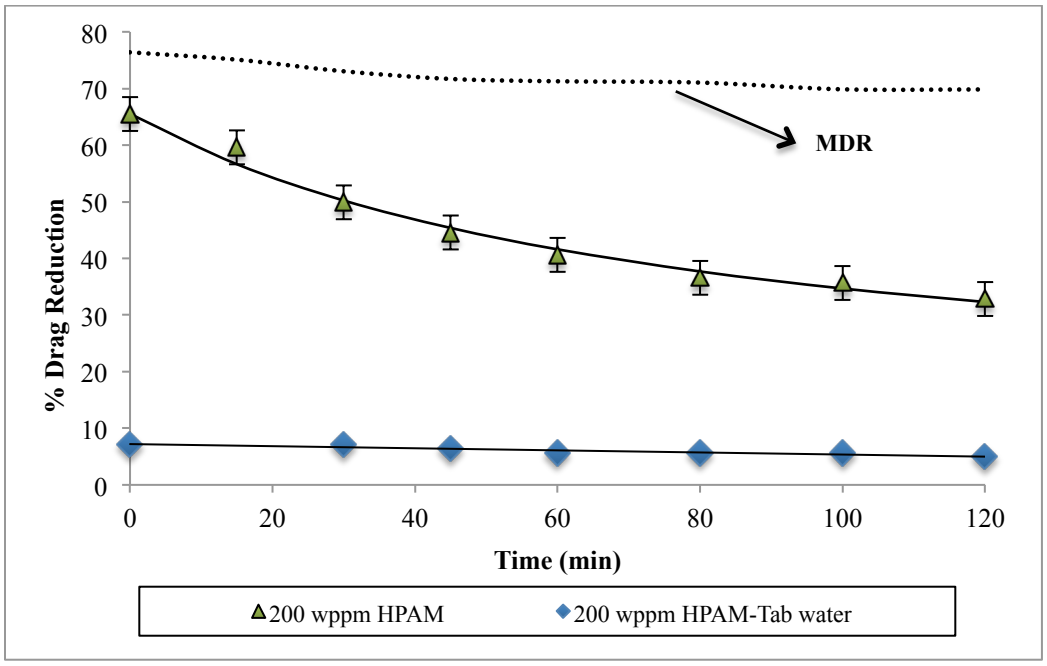

Fig. 41. Drag reduction efficiency of 200 wppm HPAM-Tab water solution at 30 GPM (113.56 l/min)

Since 200 wppm solution did not exhibit good DR efficiency, we decided to increase HPAM concentration in the solution in order to see how HPAM concentration would affect the DR behavior. The results (Fig. 42) indicated that even at a relatively high concentration of HPAM (1000 wppm), presence of salt significantly suppressed the DR efficiency (10% compared to ~68% without salt). It is interesting to note that presence of salt improved the shear resistance of the HPAM solution (~0% decline). It is believed that due to the shielding by salt ions, the size and consequently flexibility of the polymer chains decreased significantly [66]. These results suggested that, in saline environments, increasing HPAM concentration would not be a good choice for improving the DR efficiency.

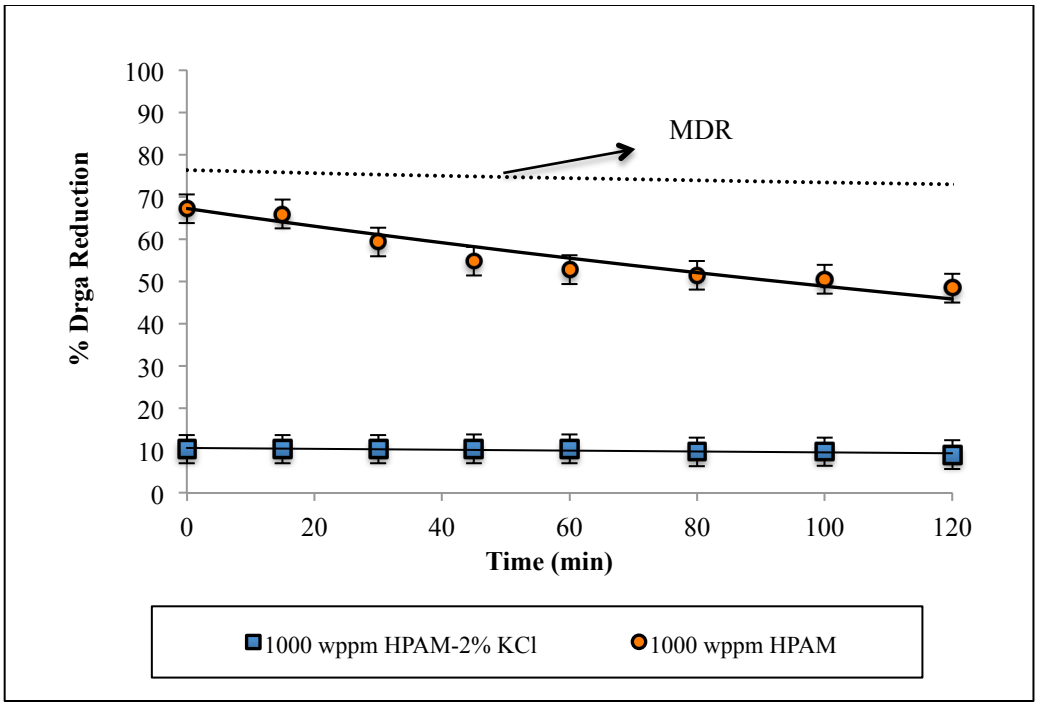

Fig. 42. Effect of salt (2% KCl) on the drag reduction efficiency of 1000 wppm HPAM at 30 GPM (113.56 l/min)

Kim et al. [43] observed that biopolymers maintained a good level of drag reduction in the presences of salt ions at concentrations above 50 ppm. The behavior of biopolymers in ionic solutions is different from flexible polymers. Depending on the concentration of the polymer in the solution, different rheological behaviors can be observed. Wyatt et al. [20] suggested that salinity of the solution did not alter the drag reduction capability of XG at concentrations above its second critical concentration, C**. But at dilute concentrations (C < C*), presence of salt negatively affects the drag reduction capability of XG solutions.

In order to verify the DR behavior of XG in the presence of salt, 600 wppm XG – 2% KCl solution was prepared and sheared in the flow loop and the DR behavior was compared to 600 wppm XG solution prepared in deionized water (Fig. 43). It was observed that presence of 2% KCl in XG solution, slightly decreased the DR efficiency for fresh solutions (from 38% to 33%). DR behavior and shear resistance of both solutions were similar and at the end of the shearing period the difference in the DR efficiency remained identical to the DR before shearing. These

results indicated that XG molecules showed higher resistance to the presence of salt ions than HPAM molecules.

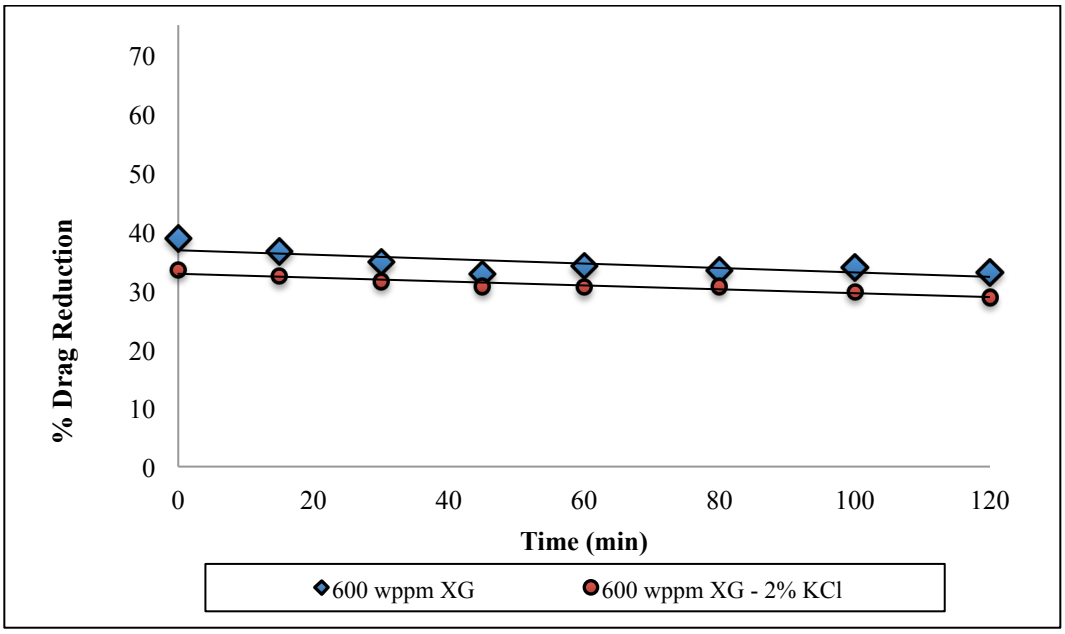

Fig. 43. Effect of salt on the drag reduction efficiency of 600 wppm XG – 2% KCl at 30 GPM (113.56 l/min)

In order to improve the DR efficiency of HPAM solutions in the presence of salt ions, binary HPAM/XG solution were prepared by dissolving polymer powders in 2% KCl solution. The concentrations of the studied binary solution were 150 wppm HPAM+ 300 wppm XG – 2% KCL and 150 wppm HPAM+ 500 wppm XG – 2% KCl, which were similar to the polymer solutions that were verified in section 3.3.6. The DR behavior of the binary solution is displayed in Fig. 44 and compared with 1000 wppm HPAM – 2% KCl solution. Both binary solutions exhibited greater DR efficiencies than the HPAM solution during the entire shearing period. It was found that the presence of XG in the solutions reduced the negative effect of salt ions on HPAM molecules. Addition of salt to 1000 wppm HPAM solution resulted in 58% reduction in DR efficiency, whereas for binary solutions DR declines were 25% (150 wppm HPAM+ 300 wppm XG) and 17% (150 wppm HPAM+ 500 wppm XG). Comparison of the binary solutions suggested that 150 wppm HPAM+500 wppm XG – 2% KCl solution induced greater drag

reduction efficiency, indicating that increasing XG concentration in the solution would result in greater DR efficiency. Both binary solutions exhibited excellent mechanical resistance during the shearing period. The decline in the DR efficiency of both solutions was only 2%.

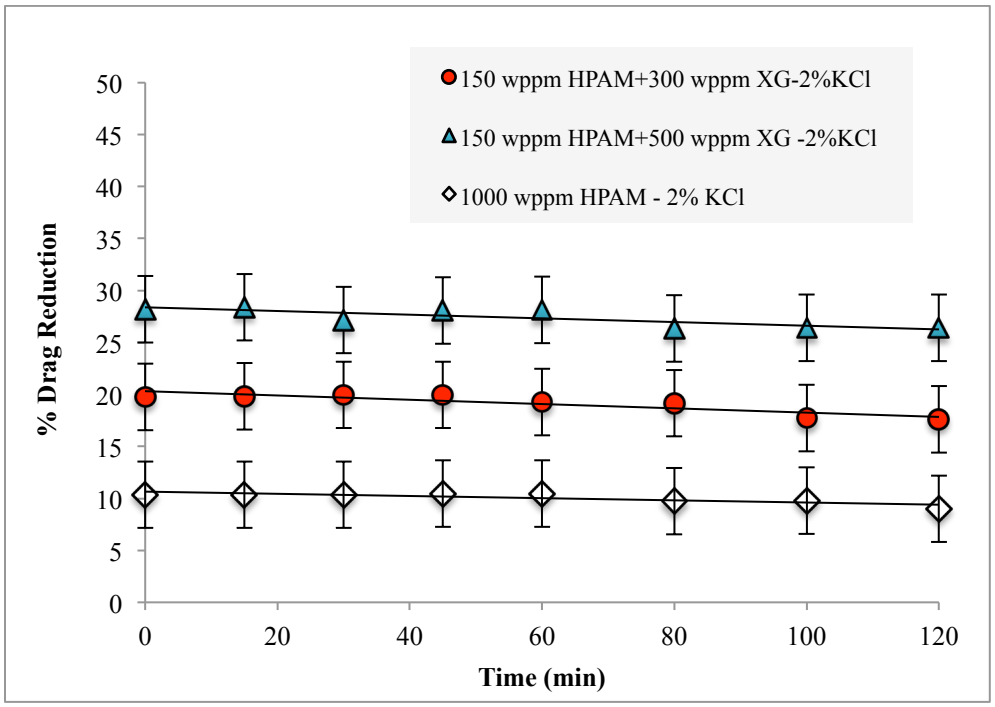

Fig. 44. Effect of salt on the drag reduction efficiency of HPAM/XG binary solutions at 30 GPM (113.56 l/min)

CHAPTER IV

CONCLUSIONS

In this study rheological behavior and drag reduction efficiency of various polymer solutions were investigated. The studied polymer solutions included anionic polyacrylamide, xanthan gum, guar gum and binary polyacrylamide/polysaccharide mixtures. Polyacrylamide is a long-chain flexible molecule that is utilized in various drag reduction applications including transfer pipelines, field irrigation, and hydraulic fracturing treatment. Polyacrylamide is an efficient drag reducer and small quantities of polyacrylamide in the solution can reduce drag up to 70%. But, polyacrylamide suffers from mechanical degradation and chain scission, when exposed to turbulent flow conditions. Mechanical degradation results in significant loss of drag reduction efficiency. Biopolymers such as polysaccharides are largely used in industrial applications. Some of the polysaccharides such xanthan gum and guar gum are important components of hydraulic fracturing fluids and are used as viscosifiers. Both guar gum and xanthan gum are known to exhibit drag reduction characteristics and high resistance to shear degradation. Another advantage associated with biopolymers is their biodegradability. Previous studies (Sohn et al. [51]; Kim et al. [34]; Berman et al. [52]) suggested that drag reduction induced by XG and other biopolymers depended on concentration and molar mass of the polymer. According to the literature, binary polymer solutions give rise to DR efficiency and shear stability. Recently Sandoval and Soares verified the DR behavior of PAM/XG and PEO/XG binary solutions in a pressure driven flow loop. The authors reported clear synergism between polymers. They concluded that the improvement observed in the mixed solutions was related to the change of the

polymeric conformation from coiled to elongated [58].

Sensitivity to the presence of salt ions and free radicals in the solution is the second drawback associated with polyacrylamide – based friction reducers [19]. It is believed that addition of salt results in reduction in the size of polyacrylamide macromolecules and consequently viscosity of the solution [66]. Kim et al. observed that biopolymers maintained a good level of drag reduction in the presences of salt ions at concentrations above 50 ppm. Wyatt et al. [20] suggested that salinity of the solution did not alter the drag reduction capability of XG at concentrations above its second critical concentration, C**. But in dilute concentrations (C < C*), presence of salt negatively affected the drag reduction capability of XG solutions.

The main objective of this work was to improve the mechanical resistance of polyacrylamide solutions by mixing with shear resistant biopolymers such as xanthan gum and guar gum. Verification of the salt tolerance and the improving the drag reduction behavior of polyacrylamide molecules in saline environment were the other objective of this research.

The project was divided into two parts. In the first part the rheological behavior of various concentrations of HPAM, XG, and GG solutions were verified. Rheological characterization included steady shear and dynamic oscillatory tests, where the viscosity profiles of the polymer solutions were obtained and viscous and elastic behavior of the solutions were determined. Also, using viscosity models the rheological parameters were developed for various polymer concentrations. In the second part, the rheological behavior of polymer solutions was verified in a closed flow loop. First the effect of concentration on DR efficiency of single polymer solutions was determined and then the synergism in the DR efficiency and shear resistance of HPAM/XG and HPAM/GG solutions were studied. Investigation of the DR behavior of the polymer solutions also included the verification of DR models in correlating the DR data. Finally, the DR behaviors of HPAM and HPAM/XG solutions in the presence salt ions were studied.

The conclusions are summarized as below:

According to the rheological characterization experiments all of the HPAM solutions exhibited shear thinning behavior and both the zero and infinite shear plateau were detectable. It was found that the concentration of the HPAM in the solution had a direct influence on the viscosity of the solutions. Using both Carreau-Yasuda and power-law models the rheological parameters were calculated and concentration regimes were determined for HPAM solutions. The calculated critical overlap concentrations, C* and C** were 160 and 4950 wppm, respectively.

Similar to HPAM solutions, shear-thinning behavior was observed for XG solutions (except for C < 160 wppm) and viscosity of the solutions were directly affected by the XG concentration. Infinite shear viscosity was only observed for C > 600 wppm solutions. Concentration regimes were determined using the parameters calculated from Carreau-Yasida model and the calculated C* and C** were 260 and 3400 wppm, respectively.

Like other polymer solutions, GG solutions exhibited shear thinning behavior and viscosity of the solutions were proportional to polymer concentration. GG solutions were less viscous than both XG and HPAM solutions and the solutions began to behave like Newtonian fluids at C < 600 wppm. Calculated critical overlap concentrations of GG solutions were C* = 720 wppm and C** = 2400 wppm.

Among the three polymer solutions, the smallest C* vales belonged to HPAM solutions, indicating that HPAM polymer chains began to interact at lower concentration than XG and GG molecules. The reason for this phenomenon is attributed to the large molecular weight of HPAM molecule. The second critical overlap concentration was in HPAM > XG > GG order, indicating that the second jump in the viscosity of HPAM solutions occurred at a higher concentration than XG and GG. This kind of behavior could occur as a result of high flexibility of HPAM molecules.

In order to verify the viscoelastic behavior of polymer solutions, dynamic oscillatory experiments were carried out. The results showed that by increasing HPAM concentration the resistance of the solution to deformation (G*) increased. The relative magnitude of G" to G' (or tan δ) decreased with increasing concentration suggesting that increasing polymer concentration increased the elasticity of the solutions. It was also observed that at high frequencies ($\omega > 10$ rad/s) the viscous behavior of the solutions dominated the elastic behavior.

Similar to HPAM, both G' and G" increased by increasing XG and GG concentrations in the solution, indicating that the resistance of the solutions to deformation increased by increasing polymer concentration. Both G' and G" were dependent on frequency suggesting that (the at the studied concentrations) solutions were not structured (were fluid-like). According to the dynamic oscillatory results the order of resistance of the polymer solutions (at the same concentration) to deformation was HPAM > XG > GG, indicating that the degree of elasticity for HPAM solutions was greater than XG and GG solutions.

Drag reduction (DR) measurements were performed in a closed flow loop. For HPAM solutions, the extent of DR increased from 30% to 67% with increasing HPAM concentration from 100 to 1000 wppm. The highest drag reduction efficiency and the lowest decline in DR% belonged to 1000 wppm HPAM solution. All the HPAM solutions suffered from mechanical degradation and loss of DR efficiency over the shearing period. Results indicated that the resistance to shear degradation increased with increasing polymer concentration.

It was observed that, for fresh XG solutions (t = 0), the extent of DR increased from 26% to 45% by increasing XG concentration from 100 wppm to 1000 wppm. DR results also showed that at the studied concentrations, the DR efficiencies were well below the MDR. It was observed that all XG solutions exhibited high shear resistance to mechanical degradation. At the end of the shearing period (t = 120 min), $DR_{t=120}/DR_{max}$ values for 300, 600, and 1000 wppm solutions were

0.85, 087, and 0.97, respectively. These values were higher than the values obtained for HPAM solutions ($DR_{t=120}/DR_{max}$= 0.72 for 1000 wppm HPAM), indicating that XG solutions were more resistant to shear degradation.

The extents of DR for GG solutions were much lower than HPAM and XG solutions. At concentrations below 1000 wppm, the solutions behaved like Newtonian fluids and the DR efficiency was negligible (DR < 1% for 500 wppm GG). As mentioned earlier GG is not a flexible molecule and the extent of drag reduction depends only on concentration and molecular weight of the polymer and drag reduction occurs as a result of the interactions of polymer networks with turbulent flow [34, 51, 52]. The first critical overlap concentration for GG solution was measured to be 720 wppm, which is much greater than the critical concentrations of XG and HPAM (240 and 50 wppm, respectively). This implied that in order for GG to be an effective friction reducer, the required polymer concentration should be greater than the concentration required for XG or HPAM.

Due to small molar mass and low flexibility, GG did not exhibit good drag reduction properties (contrary to XG and HPAM), therefore, the presence of GG did not improve the DR behavior of the HPAM/GG binary solutions.

Mixed HPAM/XG solutions (C < 300 wppm) initially exhibited greater DR (40% and 55%) compared to XG, but due to shear degradation, DR% declined for HPAM/XG solutions. Compared to 200 wppm HPAM solution, addition of XG did not improve the drag reduction efficiency of HPAM/XG mixed solutions. Though, XG slightly improved the resistance against mechanical degradation in HPAM/XG mixed polymer solutions. But in concentrated HPAM/XG solutions (C > 300 wppm), where concentration of XG was above critical overlap concentration, addition of XG significantly improved DR efficiency. It was found that the binary solutions demonstrated greater DR efficiency than either 600 wppm XG or 150 wppm HPAM solutions

(identical polymer concentration). According to the results, binary HPAM/XG solutions exhibited relatively high shear resistance. The $DR_{t=120}/DR_{max}$ values for binary HPAM/XG solutions were 0.88 and 0.82, which were close to 0.85 for 600 wppm XG solution. The greatest shear resistance belonged to 150 wppm HPAM+500 wppm XG ($DR_{t=120}/DR_{max}$ = 0.88) among the studied polymer solutions. Although the concentrations of XG in HPAM/XG solutions were smaller than in 600 wppm XG solution, both binary solutions exhibited similar or even better shear resistances.

Effect of salinity on the DR behavior of polymer solutions was investigated. It was observed that as a result of repulsive forces exerted by salt ions, the DR reduction efficiency of HPAM solutions were suppressed drastically. It was also found that increasing HPAM concentration (up to 1000 wppm) did not improve the extent of DR. Investigation of the DR behavior of XG in saline solutions showed that presence of salt did not have as significant effect as it had on HPAM molecules. Therefore, binary HPAM/XG/salt solutions were prepared and the extent of DR was measured. It was found that binary HPAM/XG/salt solutions exhibited greater DR efficiencies than 1000 wppm HPAM/salt solution, indicating that presence of XG in the solution reduced the negative effect of salt ions on charged HPAM molecules.

REFERENCES

[1] K.L. Larch, K. Aminian, S. Ameri, The Impact of Multistage Fracturing on the Production Performance of the Horizontal Wells in Shale Formations, Society of Petroleum Engineers, 2012.
[2] R. Khan, A.R. Al-nakhli, An Overview of Emerging Technologies and Innovations for Tight Gas Reservoir Development, Society of Petroleum Engineers, 2012.
[3] B.R. Meyer, L.W. Bazan, R.H. Jacot, M.G. Lattibeaudiere, Optimization of Multiple Transverse Hydraulic Fractures in Horizontal Wellbores, Society of Petroleum Engineers, 2010.
[4] T.T. Palisch, M. Vincent, P.J. Handren, Slickwater Fracturing: Food for Thought, (2010).
[5] R. Barati, J.-T. Liang, A review of fracturing fluid systems used for hydraulic fracturing of oil and gas wells, Journal of Applied Polymer Science 131(16) (2014) n/a-n/a.
[6] D. Loveless, J. Holtsclaw, J.D. Weaver, J.W. Ogle, R.K. Saini, Multifunctional Boronic Acid Crosslinker for Fracturing Fluids, International Petroleum Technology Conference, 2014.
[7] Q. Wu, Y. Sun, H. Zhang, Y. Ma, B. Bai, M. Wei, Experimental Study of Friction Reducer Flows in Microfracture during Slickwater Fracturing, Society of Petroleum Engineers, 2013.
[8] K. Wutherich, K.J. Walker, Designing Completions in Horizontal Shale Gas Wells: Perforation Strategies, Society of Petroleum Engineers, 2012.
[9] L.E. Pendleton, Horizontal Drilling Review, Society of Petroleum Engineers, 1991.
[10] S.N. Shah, M.C. Vincent, R.X. Rodriquez, T.T. Palisch, Fracture Orientation And Proppant Selection For Optimizing Production In Horizontal Wells, Society of Petroleum Engineers, 2010.
[11] R.A. Kalgaonkar, P.R. Patil, Performance Enhancements in Metal-Crosslinked Fracturing Fluids, Society of Petroleum Engineers, 2012.
[12] B.C. Ames, A. Bunger, Role of Turbulent Flow in Generating Short Hydraulic Fractures With High Net Pressure in Slickwater Treatments, Society of Petroleum Engineers, 2015.
[13] H. Sun, B. Wood, R.F. Stevens, J. Cutler, Q. Qu, M. Lu, A Nondamaging Friction Reducer for Slickwater Frac Applications, Society of Petroleum Engineers, 2011.
[14] P.B. Kaufman, G.S. Penny, J. Paktinat, Critical Evaluation of Additives Used in Shale Slickwater Fracs, Society of Petroleum Engineers, 2008.
[15] A.S. Pereira, R.M. Andrade, E.J. Soares, Drag reduction induced by flexible and rigid molecules in a turbulent flow into a rotating cylindrical double gap device: Comparison between Poly (ethylene oxide), Polyacrylamide, and Xanthan Gum, Journal of Non-Newtonian Fluid Mechanics 202(0) (2013) 72-87.
[16] H.A. Abdulbari, A. Shabirin, H. Abdurrahman, Bio-polymers for improving liquid flow in pipelines—A review and future work opportunities, Journal of Industrial and Engineering Chemistry 20(4) (2014) 1157-1170.
[17] B.A. Toms, Some observations on the flow of linear polymer solutions through straight tubes at large Reynolds numbers, Proceedings of the 1st International Congress on Rheology, 1948, pp. 135-141.
[18] W. Brostow, Drag reduction in flow: Review of applications, mechanism and prediction, Journal of Industrial and Engineering Chemistry 14(4) (2008) 409-416.
[19] D. Kulmatova, Turbulent drag reduction by additives, Phys. Rev. Lett 84 (2013) 4765-4768.
[20] N.B. Wyatt, C.M. Gunther, M.W. Liberatore, Drag reduction effectiveness of dilute and entangled xanthan in turbulent pipe flow, Journal of Non-Newtonian Fluid Mechanics 166(1–2) (2011) 25-31.

[21] A. Skelland, X. Meng, The critical concentration at which interaction between polymer molecules begins in dilute solutions, Polymer—Plastics Technology and Engineering 35(6) (1996) 935-945.
[22] S. Sasaki, Drag Reduction Effect of Rod-Like Polymer Solutions. III. Molecular Weight Dependence, Journal of the Physical Society of Japan 61(6) (1992) 1960-1963.
[23] T. Lim, J.T. Uhl, Prud, apos, R.K. homme, Rheology of Self-Associating Concentrated Xanthan Solutions, Journal of Rheology (1978-present) 28(4) (1984) 367-379.
[24] P.-e. Jansson, L. Kenne, B. Lindberg, Structure of the extracellular polysaccharide from xanthomonas campestris, Carbohydrate research 45(1) (1975) 275-282.
[25] M. Milas, W.F. Reed, S. Printz, Conformations and flexibility of native and re-natured xanthan in aqueous solutions, International journal of biological macromolecules 18(3) (1996) 211-221.
[26] L. Bezemer, J.B. Ubbink, J.A. de Kooker, M.E. Kuil, J.C. Leyte, On the conformational transitions of native xanthan, Macromolecules 26(24) (1993) 6436-6446.
[27] G. Holzwarth, Conformation of the extracellular polysaccharide of Xanthomonas campestris, Biochemistry 15(19) (1976) 4333-4339.
[28] K.S. Parvathy, N.S. Susheelamma, R.N. Tharanathan, Hydration characteristics of guar gum samples and their fractions, Food Hydrocolloids 21(4) (2007) 630-637.
[29] E. Yaseen, T. Herald, F. Aramouni, S. Alavi, Rheological properties of selected gum solutions, Food Research International 38(2) (2005) 111-119.
[30] P.L. Cunha, R.R. Castro, F.A. Rocha, R.C. de Paula, J.P. Feitosa, Low viscosity hydrogel of guar gum: preparation and physicochemical characterization, International journal of biological macromolecules 37(1-2) (2005) 99-104.
[31] M.R. Gittings, L. Cipelletti, V. Trappe, D.A. Weitz, M. In, J. Lal, The Effect of Solvent and Ions on the Structure and Rheological Properties of Guar Solutions, The Journal of Physical Chemistry A 105(40) (2001) 9310-9315.
[32] W.R. Sharman, E.L. Richards, G.N. Malcolm, Hydrodynamic properties of aqueous solutions of galactomannans, Biopolymers 17(12) (1978) 2817-2833.
[33] C.A. Kim, S.T. Lim, H.J. Choi, J.I. Sohn, M.S. Jhon, Characterization of drag reducing guar gum in a rotating disk flow, Journal of Applied Polymer Science 83(13) (2002) 2938-2944.
[34] C.A. Kim, H.J. Choi, C.B. Kim, M.S. Jhon, Drag reduction characteristics of polysaccharide xanthan gum, Macromolecular Rapid Communications 19(8) (1998) 419-422.
[35] P.R. Kenis, Turbulent flow friction reduction effectiveness and hydrodynamic degradation of polysaccharides and synthetic polymers, Journal of Applied Polymer Science 15(3) (1971) 607-618.
[36] C.M. White, M.G. Mungal, Mechanics and prediction of turbulent drag reduction with polymer additives, Annu. Rev. Fluid Mech. 40 (2008) 235-256.
[37] P. Virk, H. Baher, The effect of polymer concentration on drag reduction, Chemical Engineering Science 25(7) (1970) 1183-1189.
[38] P.S. Virk, Drag reduction fundamentals, AIChE Journal 21(4) (1975) 625-656.
[39] P.S. Omrani, R. Delfos, B. Boersma, Polymer Induced Drag Reduction in a Turbulent Pipe Flow Subjected to a Coriolis Force, Flow, turbulence and combustion 89(4) (2012) 589-599.
[40] P. Ptasinski, B. Boersma, F. Nieuwstadt, M. Hulsen, B. Van den Brule, J. Hunt, Turbulent channel flow near maximum drag reduction: simulations, experiments and mechanisms, Journal of Fluid Mechanics 490 (2003) 251-291.
[41] I. Zadrazil, A. Bismarck, G.F. Hewitt, C.N. Markides, Shear layers in the turbulent pipe flow of drag reducing polymer solutions, Chemical Engineering Science 72(0) (2012) 142-154.
[42] B.R. Elbing, M.J. Solomon, M. Perlin, D.R. Dowling, S.L. Ceccio, Flow-induced degradation of drag-reducing polymer solutions within a high-Reynolds-number turbulent boundary layer, Journal of Fluid Mechanics 670 (2011) 337-364.

[43] N.-J. Kim, S. Kim, S.H. Lim, K. Chen, W. Chun, Measurement of drag reduction in polymer added turbulent flow, International Communications in Heat and Mass Transfer 36(10) (2009) 1014-1019.
[44] H.C. Hershey, J.L. Zakin, A molecular approach to predicting the onset of drag reduction in the turbulent flow of dilute polymer solutions, Chemical Engineering Science 22(12) (1967) 1847-1857.
[45] E.J. Hinch, Mechanical models of dilute polymer solutions in strong flows, Physics of Fluids 20(10) (1977) S22-S30.
[46] J.L. Lumley, Drag reduction in turbulent flow by polymer additives, Journal of Polymer Science: Macromolecular Reviews 7(1) (1973) 263-290.
[47] M. Tabor, P.G.d. Gennes, A Cascade Theory of Drag Reduction, EPL (Europhysics Letters) 2(7) (1986) 519.
[48] D. Joseph, Fluid dynamics of viscoelastic fluids, Applied Mathematical Sciences 28 (1990).
[49] A. Japper-Jaafar, M. Escudier, R. Poole, Turbulent pipe flow of a drag-reducing rigid "rod-like" polymer solution, Journal of Non-Newtonian Fluid Mechanics 161(1) (2009) 86-93.
[50] A. Zaitoun, P. Makakou, N. Blin, R.S. Al-Maamari, A.-A.R. Al-Hashmi, M. Abdel Goad, H.H. Al-Sharji, Shear Stability of EOR Polymers, Society of Petroleum Engineers, 2012.
[51] J.I. Sohn, C.A. Kim, H.J. Choi, M.S. Jhon, Drag-reduction effectiveness of xanthan gum in a rotating disk apparatus, Carbohydrate Polymers 45(1) (2001) 61-68.
[52] N.S. Berman, Drag reduction by polymers, Annual Review of Fluid Mechanics 10(1) (1978) 47-64.
[53] M.P. Escudier, F. Presti, S. Smith, Drag reduction in the turbulent pipe flow of polymers, Journal of Non-Newtonian Fluid Mechanics 81(3) (1999) 197-213.
[54] G. Dingilian, E. Ruckenstein, Positive and negative deviations from additivity in drag reduction of binary dilute polymer solutions, AIChE Journal 20(6) (1974) 1222-1224.
[55] E. Dschagarowa, T. Bochossian, Drag reduction in polymer mixtures, Rheol Acta 17(4) (1978) 426-432.
[56] J. Malhotra, P. Chaturvedi, R. Singh, Drag reduction by polymer–polymer mixtures, Journal of applied polymer science 36(4) (1988) 837-858.
[57] G. Reddy, R. Singh, Drag reduction effectiveness and shear stability of polymer-polymer and polymer-fibre mixtures in recirculatory turbulent flow of water, Rheol Acta 24(3) (1985) 296-311.
[58] G.A. Sandoval, E.J. Soares, Effect of combined polymers on the loss of efficiency caused by mechanical degradation in drag reducing flows through straight tubes, Rheol Acta (2016) 1-11.
[59] C. Montgomery, Fracturing Fluids, International Society for Rock Mechanics.
[60] M.W. Liberatore, E.J. Pollauf, A.J. McHugh, Shear-induced structure formation in solutions of drag reducing polymers, Journal of non-newtonian fluid mechanics 113(2) (2003) 193-208.
[61] M.S. Khan, Aggregate formation in poly(ethylene oxide) solutions, Journal of Applied Polymer Science 102(3) (2006) 2578-2583.
[62] K. Kim, M.T. Islam, X. Shen, A.I. Sirviente, M.J. Solomon, Effect of macromolecular polymer structures on drag reduction in a turbulent channel flow, Physics of Fluids 16(11) (2004) 4150-4162.
[63] W. Brostow, Drag reduction and mechanical degradation in polymer solutions in flow, Polymer 24(5) (1983) 631-638.
[64] H.J. Choi, C.A. Kim, J.-I. Sohn, M.S. Jhon, An exponential decay function for polymer degradation in turbulent drag reduction, Polymer Degradation and Stability 69(3) (2000) 341-346.
[65] J. Paktinat, apos, B.J. Neil, M.G. Tulissi, Case Studies: Improved Performance of High Brine Friction Reducers in Fracturing Shale Reservoirs, Society of Petroleum Engineers, 2011.
[66] M.T. Ghannam, Rheological properties of aqueous polyacrylamide/NaCl solutions, Journal of applied polymer science 72(14) (1999) 1905-1912.
[67] P.-G. De Gennes, Scaling concepts in polymer physics, Cornell university press1979.

[68] N.B. Wyatt, M.W. Liberatore, The effect of counterion size and valency on the increase in viscosity in polyelectrolyte solutions, Soft Matter 6(14) (2010) 3346-3352.
[69] N.B. Wyatt, M.W. Liberatore, Rheology and viscosity scaling of the polyelectrolyte xanthan gum, Journal of Applied Polymer Science 114(6) (2009) 4076-4084.
[70] J.-I. Sohn, C. Kim, H. Choi, M. Jhon, Drag-reduction effectiveness of xanthan gum in a rotating disk apparatus, Carbohydrate Polymers 45(1) (2001) 61-68.
[71] C.W. Macosko, R.G. Larson, Rheology: principles, measurements, and applications, (1994).
[72] M.M. Cross, Analysis of flow data on molten polymers, European Polymer Journal 2(3) (1966) 299-307.
[73] K. Yasuda, R.C. Armstrong, R.E. Cohen, Shear flow properties of concentrated solutions of linear and star branched polystyrenes, Rheol Acta 20(2) (1981) 163-178.
[74] A. Franck, Understanding rheology of structured fluids, Book of TA instruments (2004) 1-17.
[75] S. Knoll, R. Prud'homme, Interpretation of Dynamic Oscillatory Measurements for Characterization of Well Completion Fluids, SPE International Symposium on Oilfield Chemistry, Society of Petroleum Engineers, 1987.
[76] C. Tiu, T. Moussa, P.J. Carreau, Steady and dynamic shear properties of non-aqueous drag-reducing polymer solutions, Rheol Acta 34(6) (1995) 586-600.
[77] M.W. Liberatore, S. Baik, A.J. McHugh, T.J. Hanratty, Turbulent drag reduction of polyacrylamide solutions: effect of degradation on molecular weight distribution, Journal of non-newtonian fluid mechanics 123(2) (2004) 175-183.
[78] J.B. Bello, A.J. Müller, A.E. Sáez, Effect of intermolecular cross links on drag reduction by polymer solutions, Polymer Bulletin 36(1) (1996) 111-118.
[79] S. Lim, H. Choi, S. Lee, J. So, C. Chan, λ-DNA induced turbulent drag reduction and its characteristics, Macromolecules 36(14) (2003) 5348-5354.
[80] E.J. Soares, G.A. Sandoval, L. Silveira, A.S. Pereira, R. Trevelin, F. Thomaz, Loss of efficiency of polymeric drag reducers induced by high Reynolds number flows in tubes with imposed pressure, Physics of Fluids (1994-present) 27(12) (2015) 125-105.

APPENDICES

The shear stress versus shear rate profiles of HPAM solutions is displayed in Fig a.

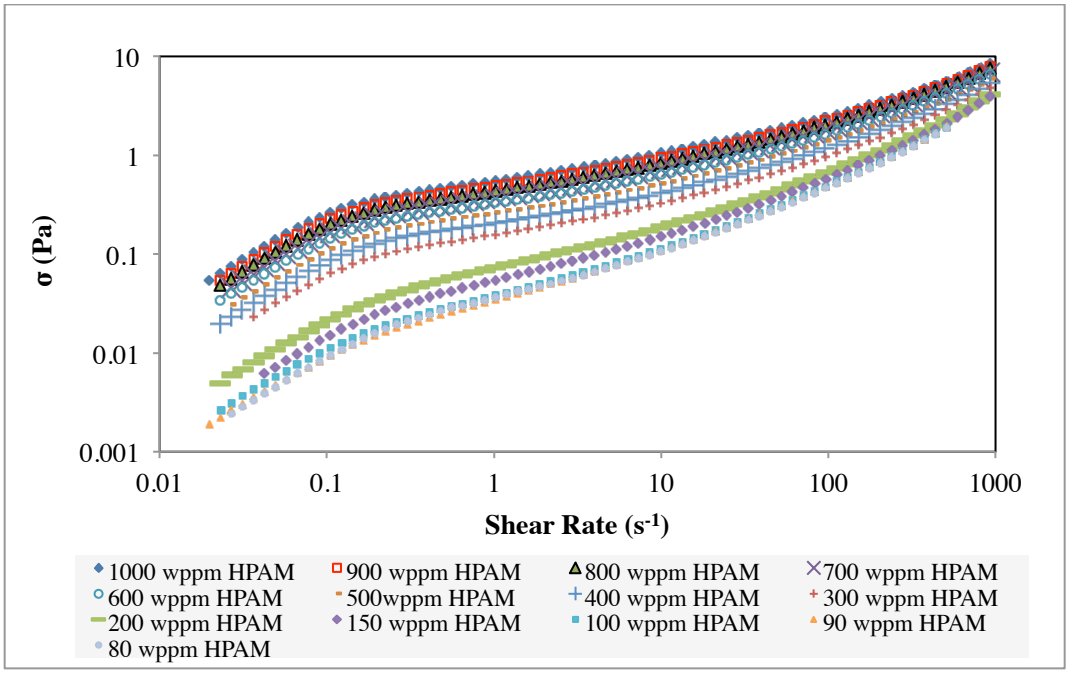

Fig a. Shear stress vs. shear rate profiles of HPAM solutions

Shear stress profiles of various concentrations of XG solutions are displayed in Fig b.

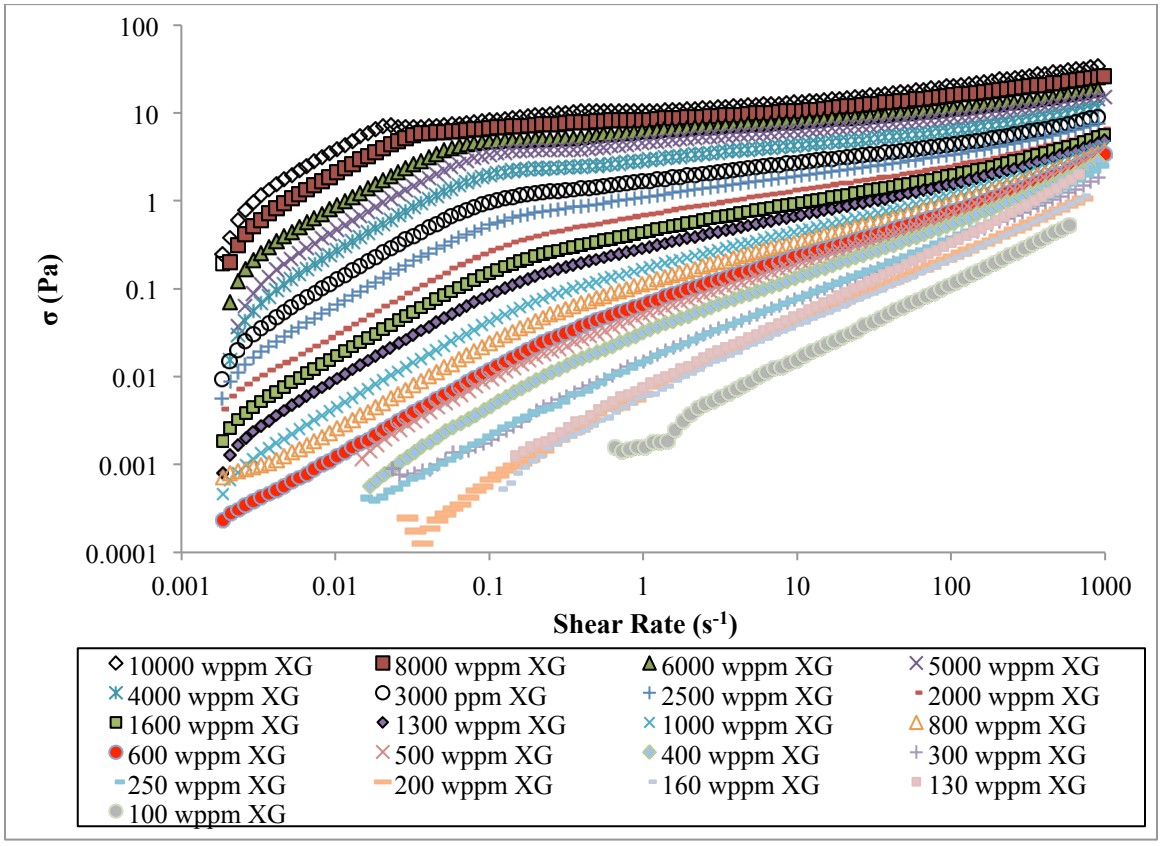

Fig b. Shear stress vs. shear rate profiles of XG solutions

Shear stress profiles of various concentrations of GG solutions are displayed in Fig c.

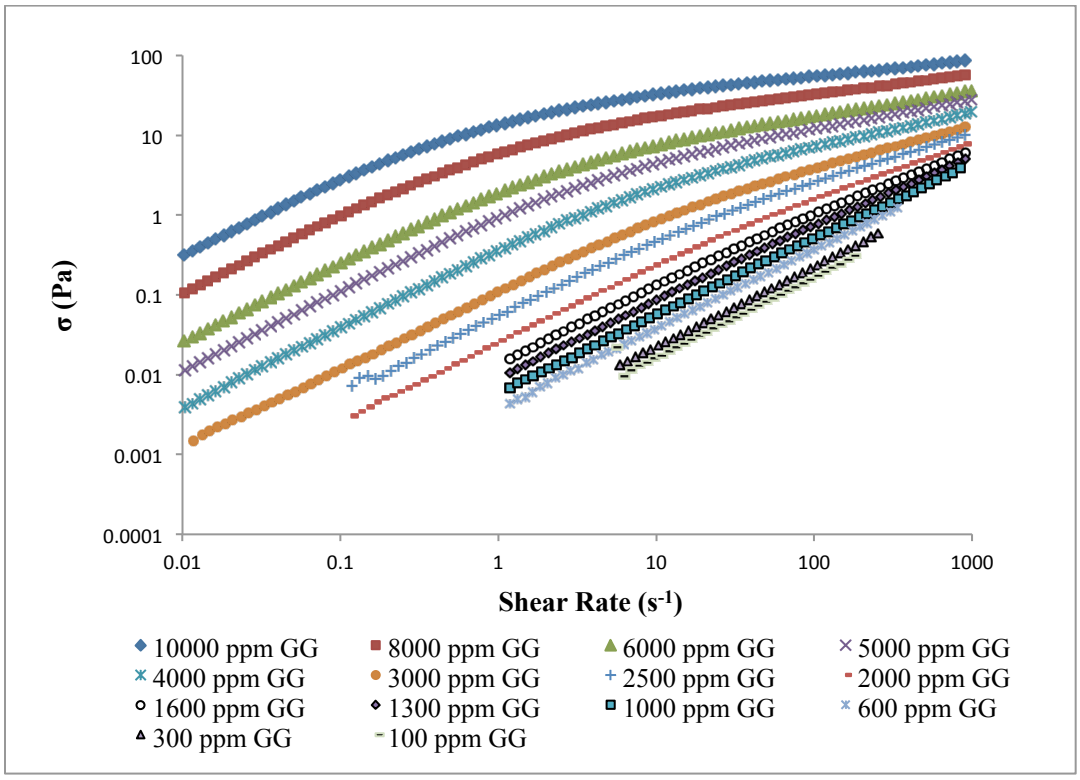

Fig c. Shear stress vs. shear rate profiles of GG solutions

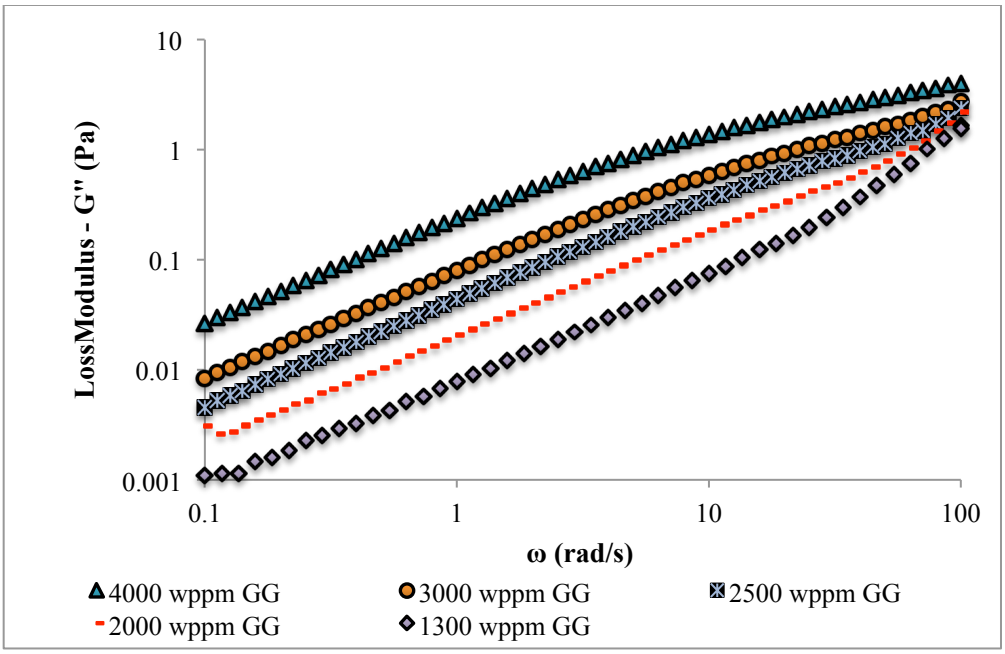

Fig d. Loss modulus (G") for various concentrations of GG solutions

VITA

Mehdi Habibpour Rezaabadi

Candidate for the Degree of

Doctor of Philosophy/Education

Thesis: INVESTIGATION OF THE DRAG REDUCTION BEHAVIOR OF POLYACRYLAMIDE/POLYSACCHARIDE BINARY POLYMER SOLUTIONS

Major Field: Chemical Engineering

Biographical:

Education:

- Completed the requirements for the Doctor of Philosophy in chemical engineering at Oklahoma State University, Stillwater, Oklahoma in May, 2017.
- Completed the requirements for the Master of Science in chemical engineering at University of Science & Technology, Tehran/Iran in 2009.
- Completed the requirements for the Bachelor of Science in chemical engineering at University of Science & Technology, Tehran/Iran in 2006.

Experience:

Oklahoma State University (January 2013 – May 2017)

- Designed a closed flow loop for drag reduction measurements
- Characterized polymer solutions utilized in drag reduction applications
- Modeling the drag reduction behavior and mechanical degradation of various non-Newtonian fluids
- Preparation and characterization of mono-sized emulsions
- Mentored "reservoir engineering" and "production engineering" courses

IRANDELCO (October 2007 – September 2012)

- Established a catalyst characterization lab; equipment purchase, installation, test procedure development, personnel training, implementation of ISO/IEC 17025:2005
- experiments including various characterization and activity test techniques
- Researched TWC catalyst formulations with a focus on precious metal loading reduction
- Participated in several R&D projects such as improving TWC resistance to poisoning, aging, developing new formulations for new car engines